March 2017

Gold Nanoparticle Biodistributions and Stability in Vivo from Mass Spectrometric Imaging

SUKRU GOKHAN ELCI
University of Massachusetts - Amherst

GOLD NANOPARTICLE BIODISTRIBUTIONS AND STABILITY *IN VIVO* FROM MASS SPECTROMETRIC IMAGING

A Dissertation Presented

by

SUKRU GOKHAN ELCI

Submitted to the Graduate School of the
University of Massachusetts Amherst in partial fulfillment
of the requirements for the degree of

DOCTOR OF PHILOSOPHY

February 2017

Chemistry

GOLD NANOPARTICLE BIODISTRIBUTIONS AND STABILITY *IN VIVO* FROM MASS SPECTROMETRIC IMAGING

A Dissertation Presented

by

SUKRU GOKHAN ELCI

Approved as to style and content by:

_____
Richard W. Vachet, Chair

_____
Edward G. Voigtman, Member

_____
Michael J. Knapp, Member

_____
Baoshan Xing, Member

_____
Craig T, Martin, Department Head
Department of Chemistry

“Our true mentor in life is science”

“Hayatta en hakiki mürşit ilimdir”

- Mustafa Kemal ATATÜRK

DEDICATION

To my beloved family

To all of my friends

ACKNOWLEDGMENTS

I would like to express my gratitude to my research advisor Prof. Richard W. Vachet for his enormous guidance, intellectual discussion, encouragement and patience throughout my study. He has been an excellent role model for me as a brilliant researcher, patient mentor and responsible academic advisor. It has been a great privilege for me to conduct research with all the support he provided. I have been shaped by his ambition and influence throughout my studies and I hope to pass along this beautiful gaining into my future career.

I would like to thank my dissertation committee members, Prof. Edward G. Voigtman, Prof. Michael J. Knapp and Prof. Baoshan Xing. I appreciate their time and effort advising and helping me.

I would like to express my gratitude to Prof. Julian F. Tyson, for his friendly welcoming, guidance and friendship.

Thank you to all the lovely and friendly both past and present members of the Vachet lab. Without their help and support, I could not have finished this dissertation work. They have significantly contributed to my learning process and I enjoyed every moment I have spent with these amazing people. I acknowledge all the contributions that Bo Yan, Alyssa Marsico, Laura Castellanos, Kristen Sikora, Tyler Marcinko, Gunnar Klemmer, Liam Jackson, Alicia Cruz, Gulen Yesilbag Tonga, Ying Jiang, Daniel Moyano, Brian Creran, Bradley Duncan, Sung Tae Kim, Chang Soo Kim and Krishnendu Saha have made in this dissertation work. I would also like to thank both the Department of Chemistry for admitting me and supporting me thereafter, and the Universitry of Massachusetts Amherst, which provided numerous great opportunities and activities for my personal and professional development.

Thank you to all of my close friends from Turkey. Especially, Ayberk Altiok, Mert Keskin, Eray Aydogdu, Caglar Kiraz, Gozde Otcu and Aysin Gencer for their endless support, great memories and their endless friendship. I appreciated their patience towards my anger and rage throughout my studies.

Thank you to all of my close friends in Amherst. Especially, Jill Graham and Alyssa Marsico for their help on everything, enjoyable moments in lab and outside the lab, and experiences that we had.

Most of all, the biggest thank goes to my great family. Especially to my dad and my mom. I thank my dad for being my secret research advisor and guiding me throughout my life and my studies. He is the biggest role model in my life. I specifically thank my mom for her support in every aspect of my studies and life and being there in the moments that I needed her the most. I also want to thank my sister for her support with everything. Last but not least, I would like to thank my lovely nephew for his energy and fun.

Finally, I thank all of the people who love me, care about me, and who have touched my life. I am extremely grateful about their presence, support and encouragements. I could not have finished my PhD study without their love and support.

ABSTRACT

GOLD NANOPARTICLE BIODISTRIBUTIONS AND STABILITY IN VIVO FROM MASS SPECTROMETRIC IMAGING

FEBRUARY 2017

SUKRU GOKHAN ELCI

B.S., IZMIR INSTITUTE OF TECHNOLOGY

Ph.D., UNIVERSITY OF MASSACHUSETTS AMHERST

Directed by: Professor Richard W. Vachet

Their smaller size, inherent non-toxicity and tunable properties of gold nanoparticles (AuNPs) attract researchers for their use in biological applications such as drug delivery, imaging and therapeutics. Understanding the *in vivo* fate of these AuNPs are essential for their potential effects in both the environment and the body. In this dissertation, mass spectrometric imaging methods using laser ablation inductively-coupled plasma mass spectrometry (LA-ICP-MS) and laser desorption/ionization (LDI-MS) have been investigated to monitor the *in vivo* fate of AuNPs. AuNP injected mouse tissue samples can be obtained and readily imaged to track the injected AuNPs using these methods. A first-ever imaging of 2 nm monolayer protected AuNPs *in vivo* using LA-ICP-MS is described. In addition, sub-organ biodistribution of AuNPs using LA-ICP-MS has been investigated. An alternative quantification strategy that can be used for LA-ICP-MS is expressed. A dual mode imaging method that can be used to monitor the stability of AuNPs by combining LA-ICP-MS and LDI-MS is reported.

TABLE OF CONTENTS

Page

LIST OF TABLES

Table Page

LIST OF FIGURES

Figure Page

LIST OF SCHEMES

Scheme Page

CHAPTER 1

INTRODUCTION

1.1. Gold nanoparticles in history

Gold is a precious metal that has a characteristic beautiful and bright golden yellow color with an Earth abundance of only 5 part per billion (ppb).[1,2] In the global market, 50% of Au is used in jewelry, 40% in investments and 10% in other industries.[3] Its relative scarcity makes Au one of the most precious metals in the world and is the reason why it was used as a currency over centuries. The malleable properties of Au allow it to be processed and easily formed into different shapes. It can even be hammered into very thin sheets or stretched into fine threads.[4] In ancient times, goldsmiths knew how to hammer Au into very thin leafs (500 atoms thick, i.e., 144 nm). These thin leafs contributed to the development of modern science, providing one of the critical components (Au foil bombarded by α particles) for the Rutherford backscattering experiment that led to the establishment of the atomic nucleus model.

Further developments allowed processing of Au into sub-100 nm structures with unique properties distinct from bulk Au. One of the most famous examples of nanoscale Au is found in the Lycurgus Cup, which displays green or red color based on how it is exposed to light (Figure 1.1).[5] After the Lycurgus Cup, Au flakes were widely used in stained glass to produce church windows of various colors, noticeably the ruby red color.[6] These examples represent the early use of manmade nanomaterials. Although nanoscale

Au was used at the time, the nature of it was not well known due to the lack of analytical tools to characterize such minuscule structures.

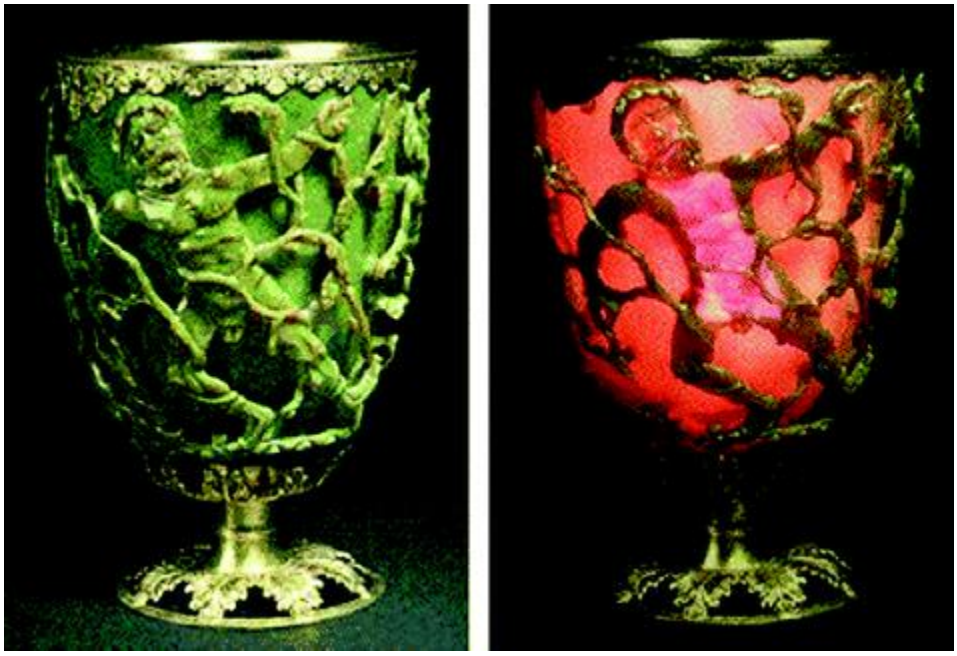

Figure 1.1. Lycurgus cup under different light exposures (Reproduced from Ref 6)

The first known example of gold nanoparticles was reported in 1857 by Michael Faraday.[7] In his work, he discovered "fine particles" by reacting aqueous $HAuCl_4$ with phosphorous dissolved in CS_2. The "fine particles" suspension showed a ruby red color, completely distinct from bulk Au's golden yellow color, but at the time, there was no theory that could explain this observation. Other studies conducted within the last few decades have demonstrated an entire spectrum of varying colors of Au "fine particles." After Faraday's discovery, researchers, including Richard Zsimondy and Theodor Svedberg, investigated these "fine particles" and identified them as nanoscale structures made of Au.[8]

1.2. Gold nanoparticles in biological applications

Besides the optical features of Au nanomaterials, Au has a variety of inherent properties that make it attractive to researchers for its use in biological applications. Gold is known to be the least reactive metal and can be stored for years without any oxidation.[9] This non-reactive and bioinert nature of Au makes it an excellent candidate for *in vitro* and *in vivo* applications. The low toxicity of Au nanomaterials has been reported in *in vitro* studies, and preliminary results indicate biocompatibility *in vivo* and in clinical studies.[10,11]

In addition to the bio-inert nature of Au nanoparticles, Au has the well-known ability to form strong bonds with compounds containing thiol (-SH) or disulfide (S-S) groups.[12] Using thiol chemistry, a wide range of self-assembled monolayers (SAM), which are mostly long alkanethiol or alkyl disulfides, can be attached onto the Au surface (Figure 1.2).[13] These self-assembled monolayers have been further engineered to give functionality, solubility in water, biocompatibility and stability to the particles.[14-16] Figure 1.3 represents the schematic structure of the monolayer attached on the Au nanoparticles used in this dissertation.

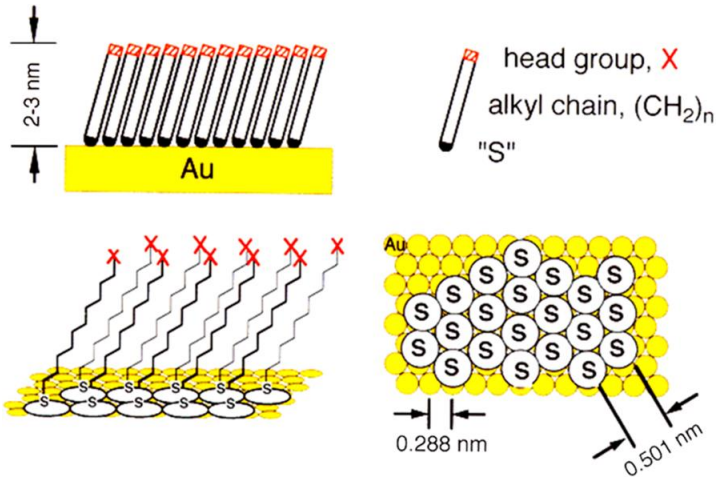

Figure 1.2. Schematic illustrations of a self-assembled monolayer (SAM) of alkanethiolate formed on the surface of a Au substrate. (Reproduced from Ref 13)

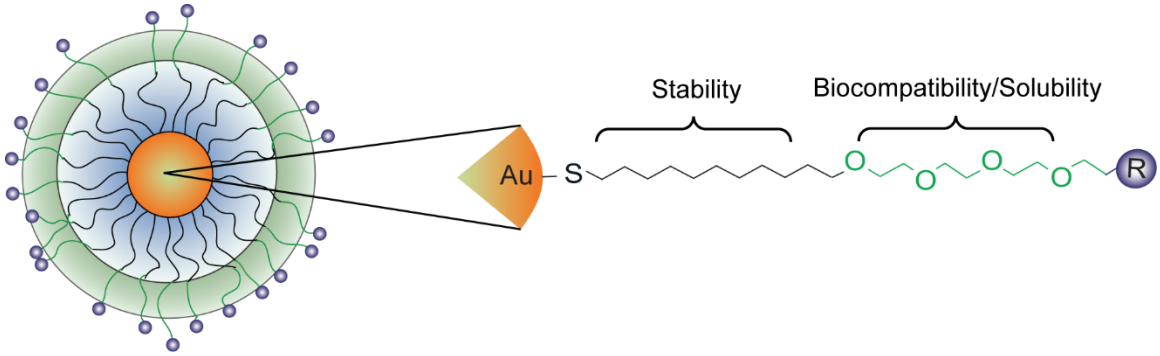

Figure 1.3. Schematic representation of monolayer structure

The unique properties and development of monolayer structures open up many biomedical applications such as drug delivery,[17,18] imaging,[19] sensors[20] and therapeutics.[21]

1.3. Characterization of monolayer protected AuNPs

The need for development of better analytical tools to characterize, detect, map and quantify nanomaterials has increased significantly in the 21st century. For the quality control purposes of the nanomaterials, their characterization is essential for defining physical properties such as size, shape and surface chemistry.

Different techniques have been applied to characterize the physical properties of nanoparticles (NPs). For the measurement of the core size and shape, atomic force microscopy (AFM),[22] transmission electron microscopy (TEM),[23] and scanning tunneling microscopy (STM)[24] are most commonly used. Although these techniques are capable of measuring core sizes of NPs, they cannot characterize SAMs attached on the surface of the NPs. In addition to the above mentioned techniques, X-ray diffraction (XRD),[25] and small

angle X-ray scattering (SAXS),[26] have been utilized for characterization of NPs. Even in using these techniques, the characterization of SAMs on NPs remains challenging. It is essential to investigate new approaches for the characterization of SAMs to better understand the interactions of SAMs with biological molecules.[27,28]

Thermogravimetric analysis (TGA)[29] and nuclear magnetic resonance (NMR)[30] are used to obtain information from SAMs. TGA provides ligand-to-core mass ratio of the NPs, but it cannot characterize the structure of the SAM. NMR, on the other hand, can be used to get structural information of the SAMs; however, peak broadening and the large sample size required for NMR are major drawbacks of this method. Alternatively, Fourier transform infrared spectroscopy (FT-IR) and UV-Vis are capable of approximate identification of the surface monolayers.

1.4. Mass spectrometric characterization of AuNPs

Used universally as a measurement tool for the characterization of various compounds, mass spectrometry (MS) is a promising tool for the characterization of AuNPs. Laser desorption/ionization (LDI),[31,32] matrix-assisted laser desorption/ionization (MALDI),[33] electrospray ionization (ESI),[34] and ion-mobility (IM) MS[35] have previously been applied for characterization of NPs.

The first examples of LDI-MS analysis of Au nanoparticles provided information for intact Au clusters but very little information was obtained for the SAMs.[31] Further analysis was performed on AuNPs with LDI-MS and MALDI-MS.[36] In those reports, signals from the alkanethiol monolayer and its fragments were detected. Until recently, these studies were limited to only certain types of AuNPs with certain number of gold atoms and SAMs. A wide range of core sizes have been successfully detected by MALDI-

MS,[33,37] but intact analysis of AuNPs has still been limited to NPs with certain types of monolayers and core sizes.

AuNPs with intact SAMs have also been investigated by other MS techniques such as ESI[34] and IM-MS.[35] ESI-MS has been shown to provide information for intact Au cores with the surface monolayer attached.[38] It is able to provide information on the exact composition of the AuNPs, but, NPs that are detectable by ESI-MS are only limited to certain number of core metal atoms and types of ligands attached. Ligand segregation information provided by IM-MS have been shown to be useful for quantifying surface components of NPs.[39] The application of IM-MS to characterize the monolayers in complex matrices such as cells or tissues are undoubtedly will be challenging.

1.5. Detection of AuNPs

Besides being able to characterize AuNPs for different applications, detecting them in a sensitive and selective way is crucial for understanding their biodistribution and environmental fate.[40-43] Previously, AuNPs were monitored in complex systems such as bacteria,[44] plants,[45] cells[46] and animal[47] for understating their fate. Detection of NPs in complex biological systems requires analytical techniques that have a high tolerance to biomolecules and good selectivity. Given the complexity of biological systems, the techniques described above for characterization of NPs may not be suitable in order to analyze AuNPs in biological systems. Besides their applicability in biological systems to obtain quantitative information are challenging.

Optical methods, such as confocal microscopy,[48] can be used to monitor nanoparticles in biological systems. These techniques often require specialized optical equipment, though, and accurate quantitative information is typically not obtainable.

Alternatively, NPs can be labeled to allow their detection in biological systems.[49,50] Although this technique overcomes the challenge caused by the complexity of the biological system, the additional labeling may cause changes in the behavior of the NPs. Also, design of numerous labels for various applications are challenging.

Elemental analysis methods like inductively-coupled plasma mass spectrometry are widely used for detection of AuNPs in complex biological samples.[51,52] For example, using ICP-MS, the effect of surface properties on biodistribution of AuNPs was investigated in cells,[53] fish[54] and plants.[55] Both the effect of surface charge and size on the cellular uptake of AuNPs have been investigated.[56] In this particular work, four different AuNPs with different sizes and surface charges were prepared and uptake efficiencies were measured with ICP-MS. The quantitative Au amounts revealed the changes in the uptake of AuNPs with different core sizes and surface charges (Figure 1.4). Although this method provides total Au amounts present in the biosystem, there is no information obtained from the SAMs present on the AuNPs.

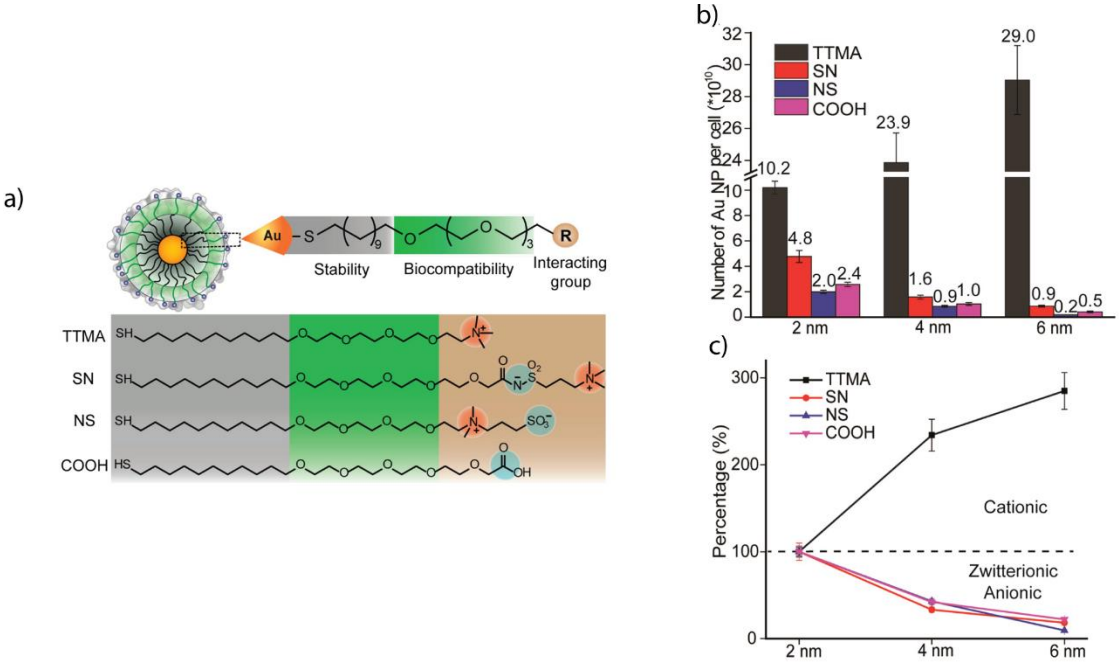

Figure 1.4. a) Structure of the AuNPs investigated in this study with cationic, zwitterionic and anionic headgroups b) Cellular uptake of AuNPs with different core size by HeLa cells after 3 h incubation in serum-free media. ICP-MS used for determination of gold per cell amounts and values are indicated in the histogram. c) Uptake trend of AuNPs with different sizes. Efficiency of the uptake of 4 and 6 nm NP was normalized to that of 2 nm NP with the same surface charge. Mean values ± standard deviation, n = 3. (Reproduced from Ref 56)

Several other mass spectrometric methods, such as LDI, MALDI, ESI and IM have been investigated for the detection of monolayers in pure samples. Although successful detection of monolayers have been shown with these methods, applicability of them in biological matrices are challenging. During analysis of the AuNPs in biosystems with MALDI-MS and ESI-MS, ionization of biomolecules can cause interferences that could prevent detection of the monolayers.[57,58] LDI-MS is the most promising method in terms of obtaining interference-free information from the intact monolayers on the AuNPs.[59] It can also provide multiplexed detection of monolayer simultaneously in complex biosystems.[59,32]

In LDI-MS, a laser irradiates the sample and the energy provided from the laser is absorbed by the NP core.[60,61] This absorbed energy is then transferred to the monolayer on the NP surface, which then desorbs/ionizes. Using this method, characterization of a wide range of NPs with various NP core materials can be achieved since most core materials bound to the monolayer on the NPs surface can efficiently absorb at wavelengths such as 337 and 355 nm, which are the laser wavelengths commonly used in commercial mass spectrometers. For example, alkanethiol compounds attached to the AuNPs surface can be

detected using this method because the Au core can readily absorb the laser energy and transfer it to cleave the Au-S bond to desorb/ionize the monolayer.[62] This localized energy transfer between the NP core and the monolayer allows us to obtain interference-free signals from the monolayer attached to the NP core and very high selectivity. These advantages of LDI-MS enable its use in biological applications. Previously, our group demonstrated the detection of AuNPs in biological samples such as cells[32] and tissues[59]. In addition, other researchers have also utilized this selective ionization process for various applications including use of AuNPs as MALDI matrices.[63,64]

1.6. Imaging of AuNPs using mass spectrometry

Monolayer protected AuNPs are widely investigated in biological applications because they provide desired functionalities, protection and biocompatibility for these applications.[65,66] The environmental exposure of these AuNPs and their biodistribution is a growing concern. For this reason, there is an urge for development of new methods that could track AuNPs in complex biosystems.[67] Different approaches, such as magnetic resonance imaging (MRI),[68] Raman spectroscopy,[69,70] surface plasmon resonance (SPR),[71,72] and fluorescence microscopy[73,74] have been used to obtain site-specific information of nanomaterials. However, each of these techniques require specific properties to allow the detection of the NPs. Another method known as the radionuclide-labeling also has similar limitations as described.[75] Although these techniques are capable of providing useful information about NPs distribution in biological systems, it is very challenging to obtain site-specific quantitative measurements. In addition, simultaneous monitoring of multiple NPs is not easy with these methods. To overcome the described

challenges of monitoring NPs with quantitative information, alternative tools are necessary.

A most common method for obtaining biodistribution information for AuNPs is ICP-MS. Quantitative information from the core material of any metal NP can be obtained with high sensitivity using ICP-MS. Since every species transforms into an atomic form in the plasma, any metallic NP in any biological matrix can be monitored after sample digestion. While, the total amounts of the NPs can be detected in any matrices, any site-specific information is lost due to sample digestion. In addition, the sample preparation is time-consuming and it is unclear whether the NPs are still intact *in vivo* or not.

In the last decade mass spectrometric imaging techniques allowed researches to monitor biomolecules such as proteins,[76,77] peptides,[78] lipids,[79] and other biomolecules[80,81] in tissue samples. Besides biomolecules, hyphenated sample introduction systems [i.e. laser ablation (LA)] with ICP-MS allowed monitoring the biodistribution of metals present in tissue samples.[82,83] The applicability of LA-ICP-MS for NPs has been also demonstrated in biosystems such as cells,[53,84] tissues[85,86] and plants.[87] Although LA-ICP-MS can successfully monitor the NPs *in vivo*, it still cannot identify if the NPs are still intact in the tissues. It is also challenging to obtain multiplexed information for the NPs with same core material. On the other hand, LDI-MS can provide the desired information for the monolayer of the NPs, even in complex biosystems such as cells[32] and tissues.[59] This technique can also monitor the NPs in a multiplexed fashion to obtain site-specific information of the biodistribution of the NPs. Quantitative imaging of these nanomaterials are possible with the appropriate standards.

While LA-ICP-MS has been used to detect NPs in biological systems, it has not been used to measure very small NPs that are commonly used in biomedical applications. Much of the work described in this dissertation will demonstrate the first examples of quantitative imaging of 2 nm monolayer protected AuNPs using LA-ICP-MS in mouse tissues. Previously, LA-ICP-MS have been used to monitor biodistribution of NPs *in vivo* with sizes up to 13 nm.[82] Most of the previous works revealed the overall biodistributions of the NPs in tissue. To better understand *in vivo* fate of the NPs, the research described here will show sub-organ biodistribution information for AuNPs in tissues. Furthermore, using a combination of both elemental and molecular mass spectrometric imaging methods, it will be shown if the NPs are still intact or not in mouse tissues.

1.7. Dissertation overview

LA-ICP-MS has been shown to monitor AuNPs in complex biological systems such as cells[53,80] and tissues.[81,82] This method is based on ablation of solid materials with a laser and transfer of the ablated material *via* a carrier gas into the plasma of the ICP-MS. Highly sensitive detection of NPs are achieved with this method and quantitative information for the biodistribution of NPs is obtained with appropriate standards.[88,89] Information regarding whether or not the AuNPs are intact *in vivo* is provided with LDI-MS imaging.[59] Similar to LA-ICP-MS, this method is based on selective desorption/ionization of the monolayer on the NPs surface with laser irradiation. Use of mass barcodes instead of any other labeling strategies allows monitoring the biological fate of NPs on their uptake and monolayer stability.[90] For effective use of NPs, their biodistribution needs to be monitored in order to modulate their potential environmental, health and safety effects. Currently, there are limited analytical tools for tracking, quantifying, and imaging NPs in biological

and environmental systems. In this dissertation quantitative biodistribution of AuNPs and their stability in mouse tissues will be revealed by mass spectrometric imaging techniques.

In Chapter 2, the first-ever imaging of 2 nm monolayer protected AuNPs *in vivo* using LA-ICP-MS will be described. How LA-ICP-MS imaging can be used to quantify and monitor 2 nm monolayer protected AuNPs *in vivo* will be demonstrated. Three different AuNPs with varying surface charges (positive, negative, neutral) have been investigated. The findings show that to obtain accurate quantitative information for AuNPs *in vivo*, it is critical to choose a matrix that is well matched with the tissue of interest. In addition, initial observation showed that the surface charge affected the biodistribution of the AuNPs.

In Chapter 3, an alternative quantification method that could be used for LA-ICP-MS imaging will be described. Matrix-matched quantification methods require time-consuming sample preparation and the matrix choice is critical for accurate quantification. Inkjet printing is explored as an alternative and is used to obtain standard samples that could be used for quantification of AuNPs *in vivo*. It will be demonstrated how inkjet printing can be used to print that standard samples and how that can be used for quantification of AuNPs in tissue samples.

The initial differences observed on the biodistribution of AuNPs will be further investigated using LA-ICP-MS in Chapter 4. Four different AuNPs with varying surface charge were investigated. In three different mouse tissues, our observations show that the surface charge dictates the biodistribution of the AuNPs. In addition, using the Hematoxylin and Eosin Y (H&E) staining, sub-organ regions of the tissue were identified and quantitative information about the biodistribution of AuNPs were determined.

Finally, to better understand the in vivo fate of the AuNPs, a dual-mode imaging method that can monitor the stability of AuNPs in a site specific manner will be investigated. Three different parameters that can affect the stability of the particles (time, organ, NP surface chemistry) were investigated. Time dependent results indicate that the stability of the particles are lost over time. It was also discovered that organ bio-composition dramatically affects the stability of the particle. The NP surface chemistry design is also important to obtain stability within same tissue environment.

1.8. References

[1] Gray, T.; Mann, N. *The Elements: A Visual Exploration of Every Known Atom in the Universe*; Black Dog & Leventhal Publishers, Inc.: New York, 2012.

[2] Tilling, R. I.; Gottfried, D.; Rowe, J. J. *Econ. Geol. Bull. Soc. Econ. Geol.* **1973**, *68*, 168-186.

[3] Savage, N. *Nature* **2013**, *495*, S2-S3.

[4] Nutting, J.; Nuttall, J. L. *Gold Bull.* **1977**, *10*, 2-8.

[5] Ulf Leonhardt *Nature Photonics* **2007**, *1*, 207-208.

[6] http://www.vam.ac.uk/.

[7] Faraday, M. *Philos. Trans. R. Soc. London* **1857**, *147*, 145-181.

[8] Mappes, T.; Jahr, N.; Csaki, A.; Vogler, N.; Popp, J.; Fritzsche, W. *Angew. Chem. Int. Ed.* **2012**, *51*, 11208-11212.

[9] Puddephatt, R. J. *The Chemistry of Gold*; Elsevier Scientific:Amsterdam, 1978.

[10] Cobley, C. M.; Chen, J.; Cho, E. C.; Wang, L. V.; Xia, Y. *Chem. Soc. Rev.* **2011**, *40*, 44-56.

[11] Dreaden, E. C.; Alkilany, A. M.; Huang, X.; Murphy, C. J.; El-Sayed, M. A. *Chem. Soc. Rev.* **2012**, *41*, 2740-2779.

[12] Love, J. C.; Estroff, L. A.; Kriebel, J. K.; Nuzzo, R. G.; Whitesides, G. M. *Chem. Rev.* **2005**, *105*, 1103-1169.

[13] Whitesides, G. M.; Laibinis, P. E. *Langmuir* **1990**, *6*, 87-96.

[14] De, M.; Ghosh, P. S.; Rotello, V. M. *Adv. Mater.* **2008**, *20*, 4225-4241.

[15] Daniel, M. C.; Astruc, D. *Chem. Rev.* **2004**, *104*, 293-346.

[16] Boisselier, E.; Astruc, D. *Chem. Soc. Rev.* **2009**, *38*, 1759-1782.

[17] Duncan, B.; Kim, C.; Rotello, V. M. *J. Control. Release* **2010**, *148*, 122-127.

[18] Veiseh, O.; Gunn, J. W.; Zhang, M. Q. *Adv. Drug Deliv. Rev.* **2010**, *62*, 284-304.

[19] Mahmoudi, M.; Hosseinkhani, H.; Hosseinkhani, M.; Boutry, S.; Simchi, A.; Journeay, W. S.; Subramani, K.; Laurent, S. *Chem. Rev.* **2011**, *111*, 253-280.

[20] You, C. C.; Miranda, O. R.; Gider, B.; Ghosh, P. S.; Kim, I. B.; Erdogan, B.; Krovi, S. A.; Bunz, U. H. F.; Rotello, V. M. *Nat. Nanotechnol.* **2007**, *2*, 318-323.

[21] Li, Z.; Barnes, J. C.; Bosoy, A.; Stoddart, J. F.; Zink, J. I. *Chem. Soc. Rev.* **2012**, *41*, 2590-2605.

[22] Jensen, T. R.; Malinsky, M. D.; Haynes, C. L.; Van Duyne, R. P. *J. Phys. Chem. B* **2000**, *104*, 10549-10556.

[23] Nie, S.; Emory, S. R. *Science* **1997**, *275*, 1102-1106.

[24] Jackson, A. M.; Hu, Y.; Silva, P. J.; Stellacci, F. *J. Am. Chem. Soc.* **2006**, *128*, 11135-11149.

[25] Sun, S.; Murray, C. B.; Weller, D.; Folks, L.; Moser, A. *Science* **2000**, *287*, 1989-1992.

[26] Heaven, M. W.; Dass, A.; White, P. S.; Holt, K. M.; Murray, R. W. *J. Am. Chem. Soc.* **2008**, *130*, 3754-3755.

[27] Zhu, Z. J.; Posati, T.; Moyano, D. F.; Tang, R.; Yan, B.; Vachet, R. W.; Rotello, V. M. *Small* **2012**, *8*, 2659-2663.

[28] Arvizo, R. R.; Miranda, O. R.; Thompson, M. A.; Pabelick, C. M.; Bhattacharya, R.; Robertson, J. D.; Rotello, V. M.; Prakash, Y. S.; Mukherjee, P. *Nano Lett.* **2010**, *10*, 2543-2548.

[29] Hostetler, M. J.; Wingate, J. E.; Zhong, C.-J.; Harris, J. E.; Vachet, R. W.; Clark, M. R.; Londono, J. D.; Green, S. J.; Stokes, J. J.; Wignall, G. D.; Glish, G. L.; Porter, M. D.; Evans, N. D.; Murray, R. W. *Langmuir* **1998**, *14*, 17-30.

[30] Polito, L.; Colombo, M.; Monti, D.; Melato, S.; Caneva, E.; Prosperi, D. *J. Am. Chem. Soc.* **2008**, *130*, 12712-12724.

[31] Whetten, R. L.; Khoury, J. T.; Alvarez, M. M.; Murthy, S.; Vezmar, I.; Wang, Z. L.; Stephens, P. W.; Cleveland, C. L.; Luedtke, W. D.; Landman, U. *Adv. Mater.* **1996**, *8*, 428-433.

[32] Zhu, Z. J.; Ghosh, P. S.; Miranda, O. R.; Vachet, R. W.; Rotello, V. M. *J. Am. Chem. Soc.* **2008**, *130*, 14139-14143.

[33] Dass, A.; Stevenson, A.; Dubay, G. R.; Tracy, J. B.; Murray, R. W. *J. Am. Chem. Soc.* **2008**, *130*, 5940-5946.

[34] Tracy, J. B.; Crowe, M. C.; Parker, J. F.; Hampe, O.; Fields-Zinna, C. A.; Dass, A.; Murray, R. W. *J. Am. Chem. Soc.* **2007**, *129*, 16209-16215.

[35] Angel, L. A.; Majors, L. T.; Dharmaratne, A. C.; Dass, A. *ACS Nano* **2010**, *4*, 4691-4700.

[36] Schaaff, T. G. *Anal. Chem.* **2004**, *76*, 6187-6196.

[37] Dass, A.; Holt, K.; Parker, J. F.; Feldberg, S. W.; Murray, R. W. *J. Phys. Chem. C* **2008**, *112*, 20276-20283.

[38] Tracy, J. B.; Kalyuzhny, G.; Crowe, M. C.; Balasubramanian, R.; Choi, J. P.; Murray, R. W. *J. Am. Chem. Soc.* **2007**, *129*, 6706-6707.

[39] Harkness, K. M.; Fenn, L. S.; Cliffel, D. E.; McLean, J. A. *Anal. Chem.* **2010**, *82*, 3061-3066.

[40] Service, R. F. *Science* **2005**, *310*, 1609.

[41] Maynard, A. D.; Aitken, R. J.; Butz, T.; Colvin, V.; Donaldson, K.; Oberdorster, G.; Philbert, M. A.; Ryan, J.; Seaton, A.; Stone, V.; Tinkle, S. S.; Tran, L.; Walker, N. J.; Warheit, D. B. *Nature* **2006**, *444*, 267-269.

[42] Wiesner, M. R.; Lowry, G. V.; Alvarez, P.; Dionysiou, D.; Biswas, P. *Environ. Sci. Technol.* **2006**, *40*, 4336-4345.

[43] Colvin, V. L. *Nat. Biotechnol.* **2003**, *21*, 1166-1170.

[44] Kang, S.; Mauter, M. S.; Elimelech, M. *Environ. Sci. Technol.* **2009**, *43*, 2648-2653.

[45] Lin, S.; Reppert, J.; Hu, Q.; Hudson, J. S.; Reid, M. L.; Ratnikova, T. A.; Rao, A. M.; Luo, H.; Ke, P. C. *Small* **2009**, *5*, 1128-1132.

[46] Drescher, D.; Giesen, C.; Traub, H.; Panne, U.; Kneipp, J.; Jakubowski, N. *Anal. Chem.*, **2012**, *84*, 9684-9688.

[47] Harper, S.; Usenko, C.; Hutchison, J. E.; Maddux, B. L. S.; Tanguay, R. L. *J. Exp. Nanosci.* **2008**, *3*, 195-206.

[48] Lindfors, K.; Kalkbrenner, T.; Stoller, P.; Sandoghdar, V. *Phys. Rev. Lett.* **2004**, *93*, 037401.

[49] Li, Z.-P.; Wang, Y.-C.; Liu, C.-H.; Li, Y.-K. *Anal. Chim. Acta* **2005**, *551*, 85-89.

[50] Trisha, E.; James, F. L. *Int. J. Nanomed.* **2012**, *7*, 5625-5639.

[51] Allabashi, R.; Stach, W.; De La Escosura-Muñiz, A.; Liste-Calleja, L.; Merkoçi, A. *J. Nanopart. Res.* **2009**, *11*, 2003-2011.

[52] Wang, L.; Li, Y.-F.; Zhou, L.; Liu, Y.; Meng, L.; Zhang, K.; Wu, X.; Zhang, L.; Li, B.; Chen, C. *Anal. Bioanal. Chem.* **2010**, *396*, 1105-1114.

[53] Dykman, L. A.; Khlebtsov, N. G. *Chem. Rev.* **2014**, *114*, 1258-1288.

[54] Zhu, Z. J.; Carboni, R.; Quercio, M. J.; Yan, B.; Miranda, O. R.; Anderton, D. L.; Arcaro, K. F.; Rotello, V. M.; Vachet, R. W. *Small* **2010**, *6*, 2261-2265.

[55] Zhu, Z. J.; Wang, H. H.; Yan, B.; Zheng, H.; Jiang, Y.; Miranda, O. R.; Rotello, V. M.; Xing, B. S.; Vachet, R. W. *Environ. Sci. Technol.* **2012**, *46*, 12391-12398.

[56] Jiang, Y.; Huo, S.; Mizuhara, T.; Das, R.; Lee, Y.-W.; Hou, S.; Moyano, D. F.; Duncan, B.; Liang, X.-J.; Rotello, V. M. *ACS Nano*, **2015**, *9*, 9986-9993.

[57] Wu, Z. W.; Gayathri, C.; Gil, R. R.; Jin, R. C. *J. Am. Chem. Soc.* **2009**, *131*, 6535-6542.

[58] Fields-Zinna, C. A.; Sardar, R.; Beasley, C. A.; Murray, R. W. *J. Am. Chem. Soc.* **2009**, *131*, 16266-16271.

[59] Yan, B.; Kim, S. T.; Kim, C. S.; Saha, K.; Moyano, D. F.; Xing, Y.; Jiang, Y.; Roberts, A. L.; Alfonso, F. S.; Rotello, V. M.; Vachet, R. W. *J. Am. Chem. Soc.* **2013**, *135*, 12564-12567.

[60] McLean, J. A.; Stumpo, K. A.; Russell, D. H. *J. Am. Chem. Soc.* **2005**, *127*, 5304-5305.

[61] Castellana, E. T.; Russell, D. H. *Nano Lett.* **2007**, *7*, 3023-3025.

[62] Gong, W.; Elitzin, V. I.; Janardhanam, S.; Wilkins, C. L.; Fritsch, I. *J. Am. Chem. Soc.* **2001**, *123*, 769-770.

[63] Pilolli, R.; Palmisano, F.; Cioffi, N. *Anal. Bioanal. Chem.* **2012**, *402*, 601-623.

[64] Ocsoy, I.; Gulbakan, B.; Shukoor, M. I.; Xiong, X.; Chen, T.; Powell, D. H.; Tan, W. *ACS Nano* **2013**, *7*, 417-427.

[65] Dwivedi, A. D.; Dubey, S. P.; Sillanpää, M.; Kwon, Y.-N.; Lee, C.; Varma, R. S. *Coord. Chem. Rev.* **2015**, *287*, 64-78.

[66] Yang, X.; Yang, M.; Pang, B.; Vara, M.; Xia, Y. *Chem. Rev.* **2015**, *115*, 10410-10488.

[67] Behra, R.; Krug, H. *Nat. Nanotechnol.* **2008**, *3*, 253-254.

[68] Lee, J. H.; Huh, Y. M.; Jun, Y.; Seo, J.; Jang, J.; Song, H. T.; Kim, S.; Cho, E. J.; Yoon, H. G.; Suh, J. S.; Cheon, J. *Nat. Med.* **2007**, *13*, 95-99.

[69] Qian, X. M.; Nie, S. M. *Chem. Soc. Rev.* **2008**, *37*, 912-920.

[70] Verma, A.; Stellacci, F. *Small* **2010**, *6*, 12-21.

[71] Sendroiu, I. E.; Gifford, L. K.; Luptak, A.; Corn, R. M. *J. Am. Chem. Soc.* **2011**, *133*, 4271-4273.

[72] Paul, S.; Paul, D.; Fern, G. R.; Ray, A. K. *J. R. Soc. Interface* **2011**, *8*, 1204-1211.

[73] Medintz, I. L.; Uyeda, H. T.; Goldman, E. R.; Mattoussi, H. *Nat. Mater.* **2005**, *4*, 435-446.

[74] Cheng, Y.; Meyers, J. D.; Broome, A. M.; Kenney, M. E.; Basilion, J. P.; Burda, C. *J. Am. Chem. Soc.* **2011**, *133*, 2583-2591.

[75] Rojas, S.; Gispert, J. D.; Martin, R.; Abad, S.; Menchon, C.; Pareto, D.; Victor, V. M.; Alvaro, M.; Garcia, H.; Herance, J. R. *ACS Nano* **2011**, *5*, 5552-5559.

[76] Hardesty, W. M.; Caprioli, R. M. *Anal. Bioanal. Chem.* **2008**, *391*, 899-903.

[77] Reyzer, M. L.; Caprioli, R. M. *Int. J. Biol. Marker* **2007**, *22*, 56.

[78] Minerva, L.; Boonen, K.; Menschaert, G.; Landuyt, B.; Baggerman, G.; Arckens, L. *Anal. Chem.* **2011**, *83*, 7682-7688.

[79] Berry, K. A. Z.; Li, B. L.; Reynolds, S. D.; Barkley, R. M.; Gijon, M. A.; Hankin, J. A.; Henson, P. M.; Murphy, R. C. *J. Lipid Res.* **2011**, *52*, 1551-1560.

[80] Cha, S. W.; Song, Z. H.; Nikolau, B. J.; Yeung, E. S. *Anal. Chem.* **2009**, *81*, 2991-3000.

[81] Zimmerman, T. A.; Rubakhin, S. S.; Romanova, E. V.; Tucker, K. R.; Sweedler, J. V. *Anal. Chem.* **2009**, *81*, 9402-9409.

[82] Becker, J. S.; Matusch, A.; Wu, B. *Anal. Chim. Acta* **2014**, *835*, 1-18.

[83] Becker, J. S. *Biomed. Spectrosc. Imaging*, **2012**, *1*, 187-204.

[84] Wang, M.; Zheng, L.; Wang, B.; Chen, H.-Q.; Zhao, Y.-L.; Chai, Z.-F.; Reid, H. J.; Sharp, B. L.; Feng, W. *Anal. Chem.*, **2014**, *86*, 10252-10256.

[85] Hsieh, Y.-K.; Hsieh, H.-A.; Hsieh, H.-F.; Wang, T.-H.; Ho, C.-C.; Lin, P.-P.; Wang, C.-F. *J. Anal. At. Spec.* **2013**, *28*, 1396-1401.

[86] Wang, T.; Hsieh, H.; Hsieh, Y.; Chiang, C.; Sun, Y.; Wang, C. *Anal. Bioanal. Chem.* **2012**, *404*, 3025-3036.

[87] Koelmel, J.; Leland, T.; Wang, H.; Amarasiriwardena, D.; Xing, B. *Environ. Pollut.* **2013**, *174*, 222-228.

[88] Hare, D. J.; Lear, J.; Bishop, D.; Beavis, A.; Doble, P. A. *Anal. Methods*, **2013**, *5*, 1915-1921.

[89] Hare, D.; Austin, C.; Doble, P. *Analyst*, **2012**, *137*, 1527-1537.

[90] Zhu, Z.-J.; Tang, R.; Yeh, Y.-C.; Miranda, O. R.; Rotello, V. M.; Vachet, R. W.; *Anal. Chem.*, **2012**, *84*, 4321-4326.

CHAPTER 2

QUANTITATIVE IMAGING OF 2 nm MONOLAYER PROTECTED GOLD NANOPARTICLE DISTRIBUTION USING LASER ABLATION INDUCTIVELY-COUPLED PLASMA MASS SPECTROMETRY (LA-ICP-MS)

This chapter is adapted from a paper published as: Elci, S. G.; Yan, B.; Kim, S. T.; Saha, K.; Jiang, Y.; Klemmer, G. A.; Moyano, D. F.; Yesilbag Tonga, G.; Rotello V. M.; Vachet, R. W. *Analyst* **2016**, *141*, 2418-2425.

2.1 Introduction

Nanomaterials are widely used in biomedical applications such as drug delivery, therapeutics, sensors and other nanodevices.[1-3] Functionalized nanoparticles (NPs) have tailorable sizes and surface properties that allow them to be tuned for a wide range of biomedical applications. For example, NP surface chemistry can be designed to influence their absorption, distribution, metabolism, excretion, and toxicity.[4,5] Gold NPs (AuNPs), in particular, have been widely studied because they possess unique qualities that make them appealing for biomedical applications. Especially, gold's inherent non-toxicity is the main property for its selection on biological applications. Besides, AuNPs can be readily synthesized to have a range of sizes, and their surface properties can be easily modified by taking advantage of gold-thiol chemistry.[6,7] In recent years, there has been a rapid increase in the use of AuNPs in drug delivery,[8] sensing,[3] cancer diagnosis and therapy,[9] and even environmental studies.[10,11]

Several approaches have been applied to understand the fate of the AuNPs *in vivo*. A commonly used approach is surface-enhanced Raman spectroscopy (SERS), which relies on the plasmonic properties of AuNPs and how these properties change during interactions with each other and with biological systems.[12-15] The use of SERS for quantitation, however, has been very limited. Electron microscopy is commonly used to image NPs in biological samples. This technique is typically low throughput, though, and does not broadly lend itself to reliable quantitative information, despite some recent nanopipette-based approaches to address this issue.[16] X-ray spectroscopies have also been used to image AuNPs[17,18] and other NPs,[19,20] but these techniques require difficult to access instrumentation such as synchrotron sources.

Laser ablation inductively coupled plasma mass spectrometry (LA-ICP-MS) is an emerging method for imaging NP distributions in biological systems[21-23] This technique has high sensitivity, multi-element detection capability, and spatial resolutions in the 25-50 μm range that make it suitable for tissue analyses. In addition, quantitative images can be obtained when using the appropriate standardization approaches.[24-26] To date, several reports have described the imaging of nanomaterials in cells,[27-29] tissues[30-32] and plants.[33] A few of these studies have involved AuNPs, yet all but one[33] have measured AuNPs with core sizes between 13 and 50 nm. AuNPs with smaller core sizes (< 5 nm) are biomedically interesting because these systems have high payload to carrier ratios. Also, together with their monolayer coatings these NPs are just large enough to avoid being cleared by the kidney but small enough to have sufficient circulation times for therapeutic applications.[34] The challenge of detecting and imaging these smaller AuNPs, however, is the fact that they

contain much less gold than their larger counterparts. For example, a AuNP with a 2 nm core diameter has 1000 times less gold than a AuNP with a 20 nm core.

In this chapter, quantitative imaging of functionalized AuNPs with 2 nm cores will be demonstrated. It is demonstrated that LA-ICP-MS imaging provides sub-tissue biodistribution information that is valuable for understanding the biological fate of AuNPs *in vivo*. Moreover, we find that the AuNPs remain intact *in vivo* as different surface monolayers cause distinct sub-tissue distributions. Overall, these measurements open the door for studying how surface chemistry influences AuNP biodistributions, with important implications for the design of NP-based therapeutics.

2.2 Results and Discussion

Three different AuNPs (Figure 2.1, AuNPs 1-3) were selected to investigate the ability of LA-ICP-MS to image AuNPs in mouse tissues. The AuNPs consist of a 2 nm Au core (Figure 2.10) and monolayers attached to the core *via* a thiol group (Figure 2.1). The design of the monolayer structure provides biocompatibility, solubility in water and stability for these AuNPs.[8] Indeed, previous studies have shown that this NP design is biocompatible in fish and mice[35-37] and that this design allows the NPs to remain intact *in vivo*.[37] Spleen, liver, lung, and kidney tissues were selected for imaging because separate ICP-MS experiments on tissue homogenates indicated that these tissues were the main sites of Au accumulation after NP injection (Table 2.1). Moreover, these organs represent a range of tissue types with various sub-tissue features.

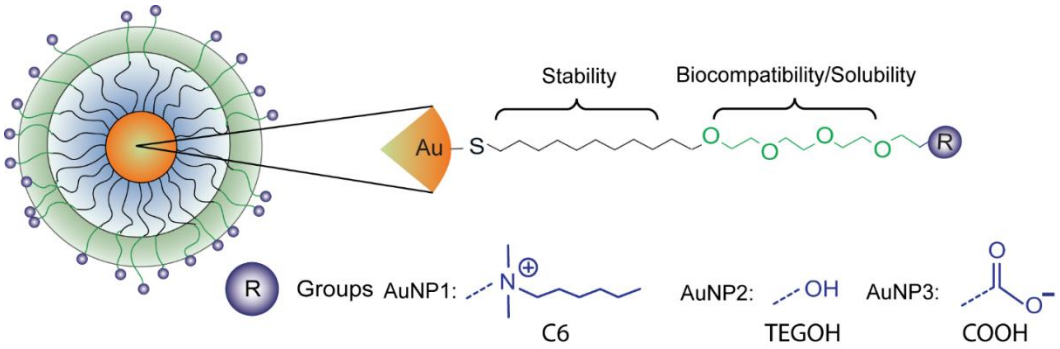

Figure 2.1. Structures of AuNPs used in this study.

Table 2.1. Summary of ICP-MS quantification of homogenized tissue samples from mice injected with AuNPs.

	ICP-MS (ng/g)[a]			
Mouse Tissue	**AuNP 1**	**AuNP 2**	**AuNP 3[b]**	**Control**
Spleen	6000 ± 400	600 ± 100	1200 ± 300	8 ± 1
Liver	3400 ± 400	1000 ± 200	2600 ± 500	2 ± 1
Lung	700 ± 100	110 ± 40	40 ± 5	3 ± 2
Kidney	60 ± 30	55 ± 10	60 ± 5	2 ± 1

[a] The standard deviations (n = 3) are obtained by averaging the ICP-MS results obtained from three different mice injected with the indicated NP.

[b] The standard deviations (n = 2) are obtained by averaging the ICP-MS results obtained from two different mice injected with the indicated NP (Three mouse used for injection initially but the injection on one of the mouse was not successful, to avoid more mouse sacrifice, two of the successfully injected mouse were used).

To arrive at the optimal parameters for quantitative laser ablation analysis of the AuNPs, we deposited AuNPs on glass slide using an inkjet printer in a manner similar to that described previously.[38] Laser energy, frequency, scan rate, and spot size were investigated, and laser energy and scan rate were found to be particularly important for obtaining homogeneous Au signals for images with optimal resolution (Figure 2.2). We found that the best images were obtained with a laser energy of 3.34 J (40% power) and a scan rate of 10 µm/sec, which is slower than most LA-ICP-MS imaging applications that typically use a scan rate above 30 µm/sec.

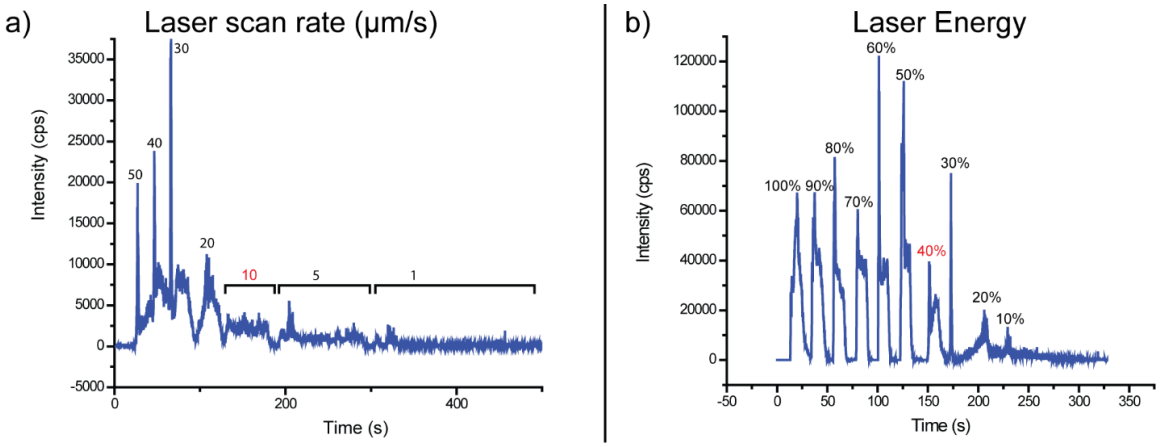

Figure 2.2. Identification of laser ablation condition for optimal resolution. a) Optimization of the laser scan rate showing the homogeneous ablation at 10 µm/s. b) Optimization of the laser energy showing homogeneous signal at a laser energy percentage of 40%, which corresponds to 3.34 J. Optimal values were identified by finding conditions that lead to relatively constant signals over a 500 µm space of inkjet-printed AuNPs.

Upon identifying optimal imaging conditions, we first examined spleen tissues because its distinct histological regions (i.e. red pulp and white pulp) particularly reveal

the value of LA-ICP-MS imaging (Figure 2.3 and Figure 2.4). From Figure 2.3, it is clear that Au accumulates in the red pulp region (i.e. red/orange color in optical image of Figure 2.3a) but not in the white pulp region (i.e. white circles in optical image of Figure 2.3a and pale red regions in the ^{57}Fe images in Figure 2.3c) of the tissue after injection of AuNP 1. The role of the red pulp is to remove antigens, microorganisms and dead erythrocytes from the blood, while the white pulp contains different lymphocytes that are important in immune responses. These images suggest that AuNP 1 is filtered from circulation but is not taken up by the lymphocytes that comprise the white pulp.

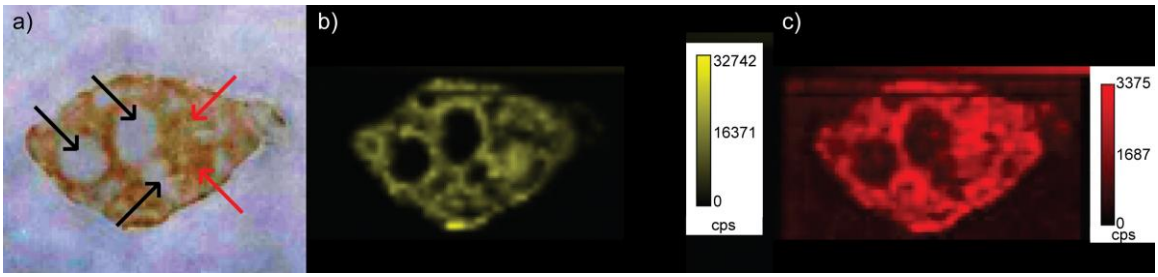

Figure 2.3. a) Optical image of a spleen tissue taken from a mouse injected with AuNP 1. The red pulp is red/orange in color, whereas the white pulp is white and can be challenging to distinguish from the area surrounding the organ in this image. Selected red pulp regions are indicated with red arrows, whereas selected white pulp regions are indicated with black arrows. b) LA-ICP-MS image of the same spleen showing the distribution of gold. c) LA-ICP-MS image of the same spleen showing the distribution of the iron. (cps=counts per second)

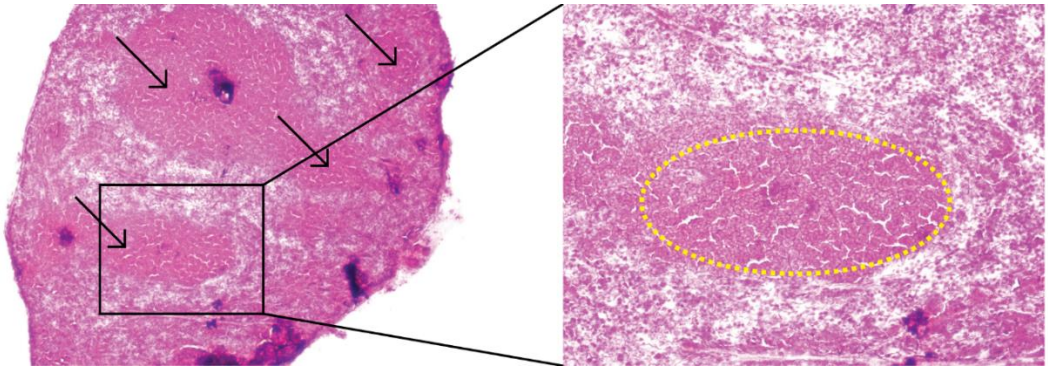

Figure 2.4. H&E staining images of the spleen tissue (black arrows illustrating the white pulp regions and the rectangle zoom in region gives a closer look to the white pulp region in the yellow dashed line).

LA-ICP-MS images of spleens taken from mice injected with AuNPs 2 and 3 are also readily obtained (Figure 2.5), even though these AuNPs accumulate in the spleen to a much lesser extent than AuNP 1 (Table 2.1). The images in Figure 2.5 illustrate that the red pulp is the primary site of accumulation for both NPs; however, AuNP 2 clearly distributes to some extent in the white pulp as well. This observation is in stark contrast to the behavior of AuNPs 1 and 3, indicating that NP surface chemistry influences how the NPs distribute internally. Importantly, because the different AuNPs show different distributions, the NPs very likely remain intact *in vivo*, highlighting the fact that our measurements are reporting on the AuNP distributions and not just total gold. Previously, we have investigated the particles with tetra ethylene glycol (TEG) and without TEG group on C_{11} chain particles. The particle with TEG showed high stability in cell and imaging them in spleen tissue with LDI-MS showed that the particles were still intact.[39,47]

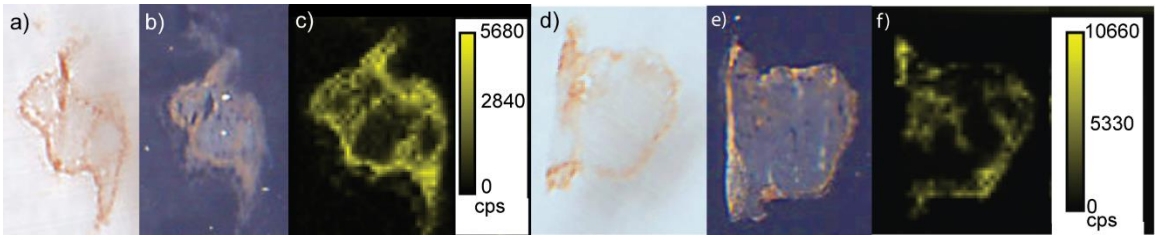

Figure 2.5. a) Optical image of a spleen tissue taken from a mouse injected with AuNP 2. b) False color optical image of a spleen tissue taken from a mouse injected with AuNP 2. c) LA-ICP-MS image of the same spleen tissue showing the distribution of gold. The light gray regions indicate the white pulp. d) Optical image of a spleen tissue taken from a mouse injected with AuNP 3. e) False color optical image of a spleen tissue taken from a mouse injected with AuNP 3. The light gray regions indicate the white pulp. f) LA-ICP-MS image of the same spleen tissue showing the distribution of gold. (cps=counts per second)

We were also able to obtain valuable images from liver, kidney, and lung tissues (Figure 2.6). The liver, which typically accumulates the second highest level of AuNPs in our experiments (Table 2.1), is responsible for removing toxic substances from circulation by storing or detoxifying them. In general, the liver shows a more homogeneous distribution of AuNPs than the spleen; however, we do find that AuNP 1 accumulates more in liver tissue surrounding the blood vessels rather than in the blood vessels themselves (Figure 2.6b). This observation can be confirmed by comparing the images of the Au distributions with the images of ^{57}Fe distributions (Figure 2.6c). Fe is more homogeneously distributed throughout the liver tissue, including in the blood vessels. Significant levels of Au are not found in the blood vessels, suggesting rapid uptake of AuNP 1 into the surrounding tissue and clearance from circulation. Interestingly, AuNPs 2 and 3 show a broader distribution throughout the liver, including in the blood vessels (Figure 2.7). The

fact that AuNPs with different surface chemistries distribute differently highlights the fact these images are revealing AuNP distributions and not just bulk gold distributions.

Somewhat surprisingly we also find AuNPs in lung tissue, even though the NPs were injected intravenously (Figure 2.6d and e). Gold measurement in this tissue is likely due to the large amount of blood circulating through the lungs to remove gaseous molecules. Presumably, the AuNPs are taken up by the tissue surrounding the alveolar spaces, which are seen as black in the optical image of Figure 2.6d. Lastly, we have also obtained images of kidney tissues (Figure 2.6f and g), which is remarkable in that these tissues typically accumulated less than 100 ppb of Au as determined from the tissue homogenate samples (Table 2.1). While the Au levels were low in the kidney, it is clear that Au is distributed throughout the kidney with certain regions having higher concentrations. In addition, removal of particle that are greater than 5 nm size is not possible from kidney[40] and as a result of that the particles might be accumulating in the spleen and liver at a higher extent. The full implications of these distributions are not clear.

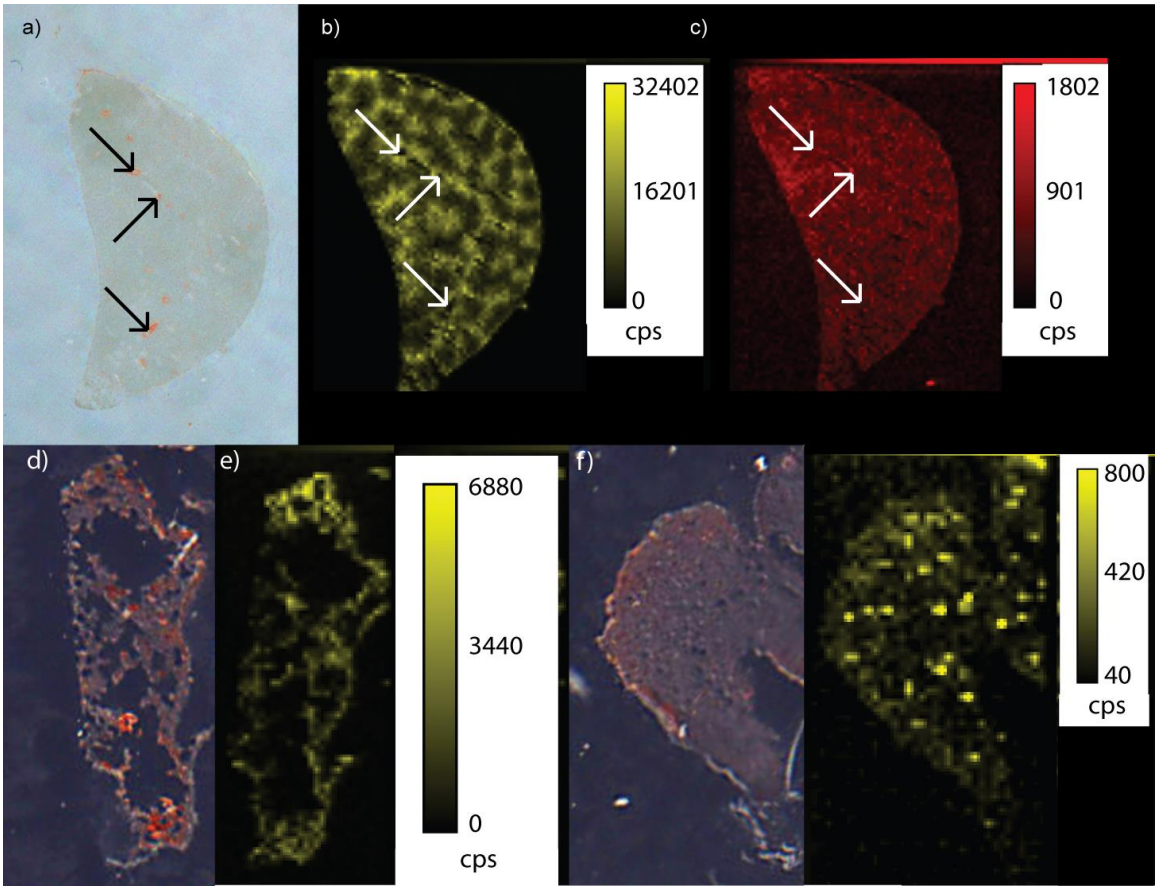

Figure 2.6. a) Optical image of a liver tissue taken from a mouse injected with AuNP 1. The red spots in the optical image represent the blood vessels that traverse through the liver (black arrows indicate the portal veins present. b) LA-ICP-MS image of the same liver showing the distribution of gold. c) LA-ICP-MS image of the liver showing the distribution of Fe. d) Optical image of a lung tissue taken from a mouse injected with AuNP 1. e) LA-ICP-MS image of the same lung tissue showing the distribution of gold. f) Optical image of a kidney tissue taken from a mouse injected with AuNP 1. g) LA-ICP-MS image of the same kidney tissue showing the distribution of gold. (cps=counts per second)

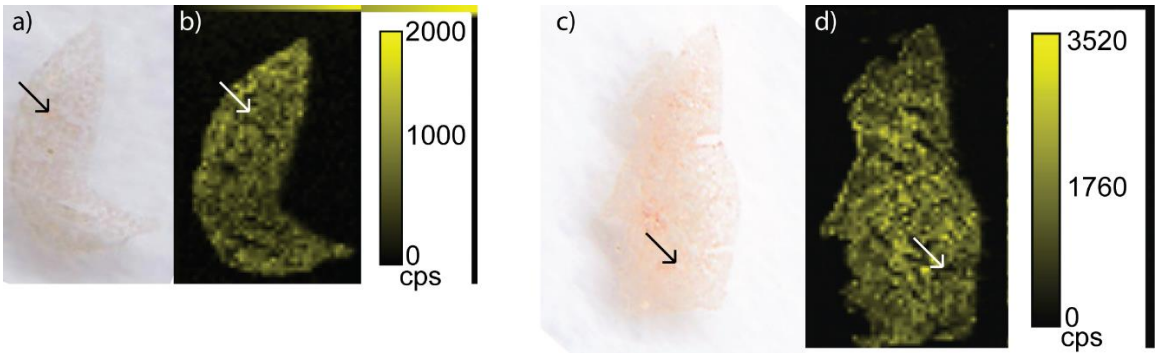

Figure 2.7. a) Optical image of a liver tissue taken from a mouse injected with AuNP 2. b) LA-ICP-MS image of the same liver tissue showing the distribution of gold. c) Optical image of a liver tissue taken from a mouse injected with AuNP 3. d) LA-ICP-MS image of the same liver tissue showing the distribution of gold. (cps=counts per second)

Having established that LA-ICP-MS can indicate the distributions of functionalized 2 nm AuNPs in mouse tissues, we next investigated the possibility of generating quantitative images. To achieve this quantitation, we investigated a matrix-matching approach in which we spiked known concentrations of AuNPs into sets of tissue homogenates (Scheme 2.1). Ideally, appropriate mouse tissues would be used as the matrix for the organs of interest, but the small size of mouse organs and the unnecessary sacrifice of mice caused us to study more readily available tissues. We investigated chicken breast and beef liver as tissue phantoms for matrix matching and found that chicken breast worked well as a matrix match for the spleen, kidney and lung, whereas beef liver was more appropriate for liver tissues.

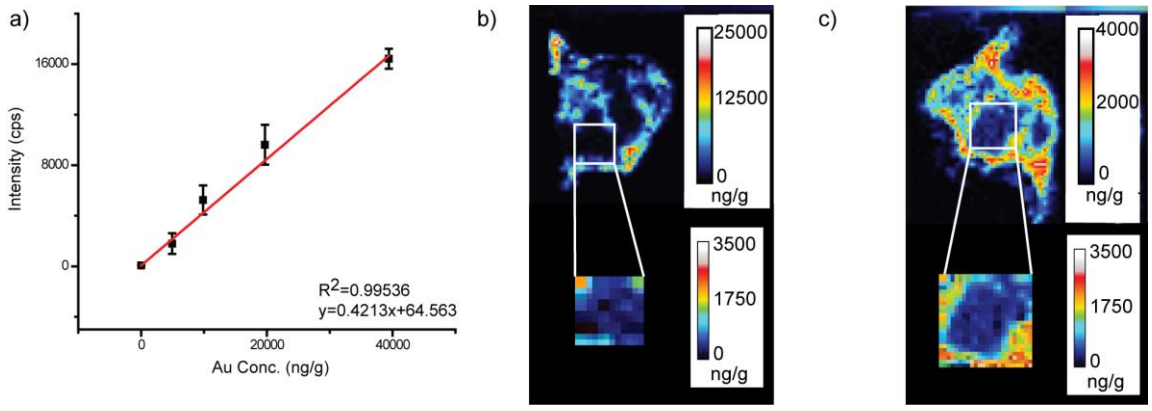

Figure 2.8. a) Example calibration curve obtained for AuNP 3 using chicken breast homogenate as the matrix. b) Quantitative LA-ICP-MS image of a spleen taken from a mouse injected with AuNP 3 with the zoomed in region of the white pulp. c) Quantitative LA-ICP-MS image of a spleen taken from a mouse injected with AuNP 2 with the zoomed in region of the white pulp.

Using the matrix-matching strategy we were able to quantify AuNP distributions in tissues. Figure 2.8 shows the data for spleen tissue from a mouse that was injected with AuNP 3. Using chicken breast homogenate, we obtained the calibration curve for the spleen tissue using five different NP concentrations (Figure 2.8a). The calibration curve was obtained by averaging the Au signal from the entire tissue homogenate slice, and then this curve was used to obtain quantitative images for the spleen (Figure 2.8b). As was seen in Figure 2.8b, AuNP 3 is distributed solely in the red pulp, but now AuNP amounts at specific locations are apparent. Site-specific quantitation is particularly valuable for spleen images of AuNP 2 (Figure 2.8c), which show significant levels of Au in the white pulp regions. The quantitative images indicate that 50 ± 25 ppb (or about 10%) of the NPs is found in the white pulp regions, whereas 300 ± 80 ppb (or about 60%) is found in the red pulp and a remarkable 150 ± 50 (or about 30%) is found in the one pixel-wide regions that surrounds

each white pulp region. This latter narrow (~ 40 μm) region around the white pulp is known as the marginal zone and is the location where the spleen's immune response is initiated.[41] The full implications of these results are beyond the scope of this work and will be investigated in future work.

To help validate these data, we compared the average quantity obtained across this entire spleen slice to a part of the same spleen tissue that had been homogenized and analyzed by ICP-MS. In doing so, we find that the average Au amount in the tissue slice is within a factor of 2 of the tissue homogenates (Table 2.2). This level of agreement is excellent, given that the tissue slice represents only a very small fraction of this heterogeneous tissue, whereas the ICP-MS results were obtained from approximately one half of the entire spleen tissue.

Quantitative images were also obtained for several other tissues and NPs. For the spleen, lung, and kidney we find good agreement between the LA-ICP-MS data and the ICP-MS results from the tissue homogenates when chicken breast is used as the calibration matrix (Table 2.2). For liver tissues, chicken breast was not found to be a reliable matrix for quantification, as the LA-ICP-MS and ICP-MS results usually did not compare well (Tables 2.1 and 2.2). Instead, beef liver homogenates were found to be a more reliable matrix, allowing for a more reasonable comparison between the LA-ICP-MS and ICP-MS results (Tables 2.1 and 2.2). Upon applying the appropriate calibration curves for each tissue, we are able to estimate detection limits for this LA-ICP-MS imaging method. Gold amounts around 10 ng/g (i.e. 10 ppb) or higher in tissue sections provide useful quantitative information, as is evident in the images of kidney tissue (Figure 2.9 and Table 2.1). This

concentration is similar to the detection range seen in previous LA-ICP-MS of transition metals, which were found to be detectable in the 10 – 300 ng/g (i.e. 10 – 300 ppb) range.[21]

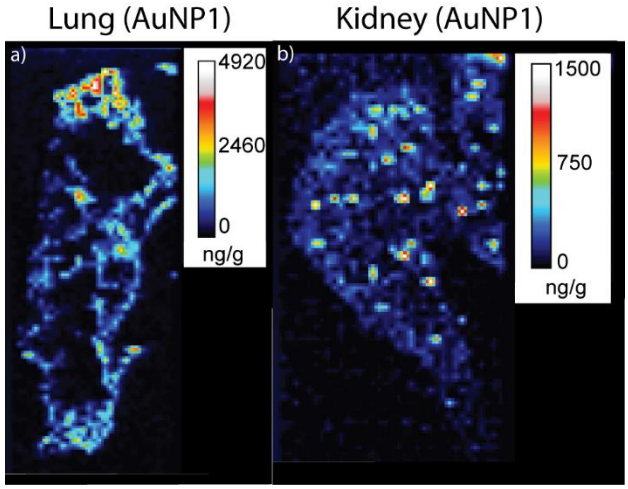

Figure 2.9. Quantitative LA-ICP-MS images of a lung (a) and a kidney (b) taken from a mouse injected with AuNP1.

Table 2.2. Summary of LA-ICP-MS quantification results of tissues slices from mice injected with AuNPs.

Mouse Tissue	**LA-ICP-MS (ng/g)[a]**
Spleen (AuNP1)	9000±2000*
Spleen (AuNP2)	500±150**
Spleen (AuNP3)	6000±4000**
Liver (AuNP1-liver homogenate)	10000
Liver (AuNP2-chicken breast homogenate)	11000
Liver (AuNP2-liver homogenate)	450
Liver (AuNP3-liver homogenate)	3700

Lung (AuNP1)	300
Kidney (AuNP1)	80

[a] The LA-ICP-MS quantitative data obtained by summing the data obtained for each pixel. *n=2, **n=3

2.3. Conclusion

In this work, we demonstrate that LA-ICP-MS can be used to quantitatively image the biodistributions of monolayer-protected AuNPs with 2 nm cores. To our knowledge, this is the first report on quantification of < 10 nm core AuNPs in animal tissues using LA-ICP-MS. We achieve excellent sensitivity and spatial resolution in these imaging experiments, allowing us to determine how AuNPs with different monolayer coatings distribute *in vivo*. Thus, our approach provides useful insight into not only how NPs distribute but also how they are processed *in vivo*. This latter information is accessible from the sub-organ NP distributions in tissues such as the spleen and liver. We also find that the proper choice of matrix for the calibration standards is essential for obtaining quantitative images. Taken together, this imaging approach will provide important tissue/organ distribution data that will greatly facilitate the design and study of nanomaterials for biomedical applications.

2.4. Experimental

2.4.1. Synthesis of 2 nm AuNPs

The AuNPs used in this study (Figure 2.1) were synthesized by the Brust-Schiffrin two-phase method, and were post-functionalized using the Murray place exchange reaction.[42,43] The details of the synthetic procedure for the NPs used in this study are

reported in previous work.[44-46] After synthesis, the AuNPs were dialyzed for 72 h against MilliQ water using Spectra/Por Dialysis Membranes (molecular weight cutoff of 1,000 Da) to separate the free ligands from the AuNPs. The core sizes of the NPs were then measured by transmission electron microscopy (TEM) on a JEOL100S electron microscope and were found to have core diameters that are 2.0 ± 0.1 nm, 1.8 ± 0.2 nm and 2.0 ± 0.4 nm for AuNP 1, 2, and 3, respectively (Figure 2.10). They were also characterized by laser-desorption/ionization mass spectrometry to confirm the monolayer coating.[47]

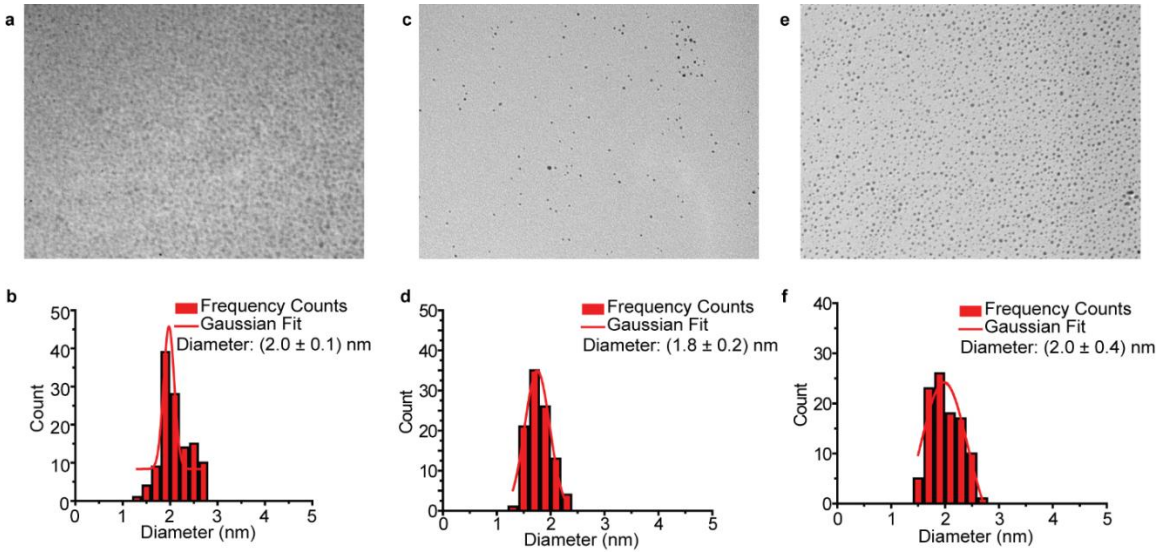

Figure 2.10. a) TEM image and b) core size distribution of AuNP 1, c) TEM image and d) core size distribution of AuNP 2, e) TEM image and f) core size distribution of AuNP 3.

2.4.2. Animal Experiments

Animal care: All animal experiments were conducted in accordance with the guidelines of Institutional Animal Care and Use Committee (IACUC) at University of Massachusetts Amherst. Female Balb/c mice were purchased from Jackson Laboratory (Bar Harbor, ME). Food and water intake were assessed daily.

***Intravenous injection of AuNPs*:** 50 μL of each AuNP at a concentration of 2 μM was administered intravenously to the Balb/c mice. Because the average NP core sizes are about 2 nm, the total gold amount of injected in case was approximately 4000 ng, which is expected given that around 200 gold atoms are present in each AuNP.[48] After 24 h, the mice were sacrificed by the inhalation of carbon dioxide and cervical dislocation. The organ samples were then harvested for analysis. Following sacrifice, organs were collected and cut into two parts, except the kidneys and lungs of which each mouse has two. One part or one of the duplicate organs (in the case of the lung and kidney) was homogenized and analyzed by ICP-MS for total gold, while the other was used for LA-ICP-MS imaging.

***Tissue preparation for imaging*:** Using a LEICA CM1850 cryostat, tissue samples were sliced to a thickness of 12 μm (for spleen and liver) or 20 μm (for kidney and lung) at -20 °C. Then, the sliced tissues were attached to regular glass slides.

2.4.3. ICP-MS sample preparation and measurements

Using a 3:1 (v:v) mixture of HNO_3 (68%) and H_2O_2 (30%), each organ was digested overnight. The next day 0.5 mL of aqua regia was added, and the sample was then diluted to 10 mL using de-ionized water. (**Aqua regia is highly corrosive and must be handled with extreme caution.**) Au standard solutions (gold concentrations: 20, 10, 5, 2, 1, 0.5, 0.2 and 0 ppb) were prepared prior to each experiment. A Perkin Elmer NEXION 300X ICP mass spectrometer was used for the analysis of samples. Prior to the analysis, daily performance measurements were done to ensure the instrument was operating under optimum conditions. Using the standard mode, ^{197}Au signals were obtained. The RF power

for the ICP was 1.6 kW, and the nebulizer gas flow rate was within a range of 0.9-1 L/min. The plasma gas flow rate and auxiliary gas flow rate were 16.5 L/min and 1.4 L/min, respectively. The analog stage voltage and pulse stage for the detector were -1600 V and 950 V, respectively. The deflector voltage was set to -12 V, and 50 ms was selected for the dwell time during the operation of the ICP-MS.

2.4.4. LA-ICP-MS measurement conditions and imaging

For imaging of the tissue samples, a CETAC LSX-213 G2 laser ablation system (Photon Machines, Omaha, NE, USA) attached *via* a 2 m length of tubing to the ICP mass spectrometer was used. Optimization of the laser ablation conditions was first performed using pure AuNP samples on glass slides. As described in the results and discussion, the optimal conditions were found to be: a laser energy of 3.34 J, a spot size of 50 µm, a scan rate of 10 µm/sec, and laser shot frequency of 10 Hz. The energy value obtained directly from the instrument's indicator of the laser parameter where it shows the laser energy. Laser scanning was done in the line scan mode. Transfer of the ablated material from the ablation chamber to the plasma was accomplished using a 600 mL/min flow of He gas and a 10 sec shutter delay. The mass spectrometer was operated using the kinetic energy discrimination mode, which was especially important for measurements of ^{57}Fe.

2.4.5. Data analysis and image generation

ICP-MS data were analyzed using Excel and Origin 9.0 (from OriginLab, Northampton, MA, USA). Using Excel, each of the line data collected were processed to obtain the pixel size of 50 µm x 50 µm. This is achieved by summing up 5 seconds of the data collected (10 µm/s scan rate x 5 second leads to 50 µm length) and used as the single

individual pixels.[49] Images of the LA-ICP-MS data were generated using the software ImageJ. Optical images of the tissues were processed with Adobe Photoshop.

2.4.6. Matrix-matched standard preparation for LA-ICP-MS

***Homogenate preparation*:** Chicken breast and beef liver were purchased from a local market and used as the matrix-matched standards. Small pieces of these tissues were cut and placed in 15 mL plastic tubes. Water was added to the tubes, and the tissues were homogenized using a PowerGen 125 homogenizer (Fisher Scientific). Homogenized tissues were transferred into 1.5 mL centrifuge tubes and were centrifuged at 12000 rpm for 10 minutes. Using a pipette, excess water in the supernatant was removed from each centrifuge tubes, and 50 mg homogenates were weighed and transferred into 0.5 mL tubes. 50 µL of 2 µM AuNP solutions were then mixed with the 50 mg homogenates. The AuNP-homogenates mixtures were then placed into a homemade sample holder and frozen prior to slicing at the desired thickness on the cryostat.

***Sample holder preparation*:** To prepare the sample holder for matrix matched standards, a 50 mL centrifuge tube was cut at the 35 mL line and the top part of the tube with the cap was used. The tube was then filled with optical cutting temperature (OCT) solution. Five Edvotek 0.5-10 µL ultra pipet tips were attached to a piece of tape and slowly placed into the OCT solution. The resulting set up was placed in a freezer until the OCT solution was completely frozen. The embedded tips were then removed with tweezers, and the gold nanoparticle-tissue homogenate mixture was deposited into the five spaces that remained in the frozen OCT.

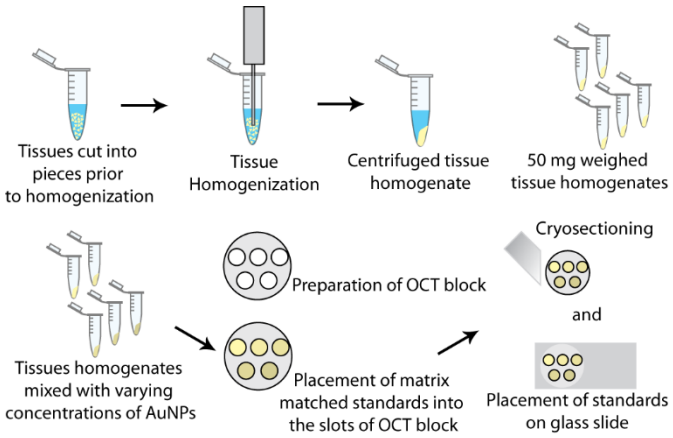

Scheme 2.1. Illustration of matrix-matched standard preparation.

2.5. References

[1] Sun, T.; Zhang, Y.S.; Pang, B.; Hyun, D. C.; Yang, M.; Xia, Y. *Angew. Chem. Int. Ed.* **2014**, *53*, 12320-12364.

[2] Lee, D.-E.; Koo, H.; Sun, I-C.; Ryu, J. H.; Kim, K.; Kwon, I.C. *Chem. Soc. Rev.* **2012**, *41*, 2656-2672.

[3] Saha, K.; Agasti, S. S.; Kim, C.; Li, X.; Rotello, V. M. *Chem. Rev.* **2012**, *112*, 2739-2779.

[4] Zolnik, B. S.; Sadrieh, N. *Adv. Drug Deliver. Rev.* **2009**, *61*, 422-427.

[5] Kim, S. T.; Saha, K.; Kim, C.; Rotello, V. M. *Acc. Chem. Res.* **2013**, *46*, 681-691.

[6] Boisselier, E.; Astruc, D. *Chem. Soc. Rev.* **2009**, *38*, 1759-1782.

[7] Yeh, Y.-C.; Creran, B.; Rotello, V. M. *Nanoscale* **2012**, *4*, 1871-1880.

[8] Rana, S.; Bajaj, A.; Mout, R.; Rotello, V. M. *Adv. Drug Deliver. Rev.* **2012**, *64*, 200-216.

[9] Yesilbag Tonga, G.; Moyano, D. F.; Kim, C. S.; Rotello, V. M. *Curr. Opin. Colloid Interface Sci.* **2014**, *19*, 49-55.

[10] Farre, M.; Sanchis, J.; Barcelo, D. *Trend. Anal. Chem.* **2011**, *30*, 517-527.

[11] Zhu, Z.-J.; Wang, H.; Yan, B.; Zheng, H.; Jiang, Y.; Miranda, O.R.; Rotello, V. M.; Xing, B.; Vachet, R. W. *Environ. Sci. Technol.* **2012**, *46*, 12391-12398.

[12] Drescher, D.; Kneipp, J. *Chem. Soc. Rev.* **2012**, *41*, 5780-5799.

[13] Ando, J.; Fujita, K.; Smith, N.I.; Kawata, S. *Nano Lett.* **2011**, *11*, 5344-5348.

[14] Qian X.M.; Nie, S. M. *Chem. Soc. Rev.* **2008**, *37*, 912-920.

[15] Jain, P. K.; Huang, X.; El-Sayed, I. H.; El-Sayed, M. A. *Accounts Chem. Res.* **2008**, *41*, 1578-1586.

[16] Tai, L.-A.; Kang, Y.-T.; Chen, Y.-C.; Wang, Y.-C.; Wang, Y.-J.; Wu, Y.-T.; Liu, K.-L.; Wang, C.-Y.; Ko, Y.-F.; Chen, C.-Y.; Huang, N.-C.; Chen, J.-K.; Hsieh, Y.-F.; Yew, T.-R.; Yang, C.-S. *Anal. Chem.* **2012**, *84*, 6312-6316.

[17] Xiang Li, X.; Anton, N.; Zuber, G.; Vandamme, T. *Adv. Drug Deliver. Rev.* **2014**, *76*, 116-133.

[18] Ricketts, K.; Guazzoni, C.; Castoldi, A.; Gibson, A.P.; Royle, G.J. *Phys. Med. Biol.* **2013**, *58*, 7841-7855.

[19] Hernandez-Viezcasa, J. A.; Castillo-Michel, H.; Servin, A.D.; Peralta-Videa, J. R.; Gardea-Torresdey, J. L. *Chem. Eng. J.* **2011**, *170*, 346-352.

[20] Priester, J. H.; Ge, Y.; Mielke, R. E.; Horst, A. M.; Cole Moritz, S.; Espinosa, K.; Gelb, J.; Walker, S. L.; Nisbet, R. M.; An, Y.-J.; Schimel, J. P.; Palmer, R. G.; Hernandez-Viezcas, J. A.; Zhao, L.; Gardea-Torresdey, J. L.; Holden, P. A. *Proc. Natl. Acad. Sci.* **2012**, *109*, 2451-2456.

[21] Becker, J. S.; Becker, J. S. *Biomed. Spectrosc. Imaging* **2012**, *1*, 187-204.

[22] Becker, J. S. *Int. J. Mass Spectrom.* **2010**, *289*, 65-75.

[23] Becker, J. S.; Matusch, A.; Wu, B. *Anal. Chim. Acta* **2014**, 835, 1-18.

[24] Hare, D.; Austin, C.; Doble, P. *Analyst* **2012**, *137*, 1527-1537.

[25] Konz, I.; Fernández, B.; Fernández, M. L.; Pereiro, R.; Sanz-Medel, A. *Anal. Bioanal. Chem.* **2012**, *403*, 2113-2125.

[26] Hare, D. J.; Lear, J.; Bishop, D.; Beavis, A.; Doble, P. A. *Anal. Methods* 2013, **5,** 1915-1921.

[27] Wang, M.; Zheng, L.-N.; Wang, B.; Chen, H.-Q.; Zhao, Y.-L.; Chai, Z.-F.; Reid, H. J.; Sharp, B. L.; Feng, W.-Y. *Anal. Chem.* **2014**, *86*, 10252-10256.

[28] Drescher, D.; Giesen, C.; Traub, H.; Panne, U.; Kneipp, J.; Jakubowski, N. *Anal. Chem.* **2012**, *84*, 9684-9688.

[29] Büchner, T.; Drescher, D.; Traub, H.; Schrade, P.; Bachmann, S.; Jakubowski, N.; Kneipp, J. *Anal. Bioanal. Chem.* **2014**, *406*, 7003-7014.

[30] Wang, T.; Hsieh, H.; Hsieh, Y.; Chiang, C.; Sun, Y.; Wang, C. *Anal. Bioanal. Chem.* **2012**, *404*, 3025-3036.

[31] Hsieh, Y.-K.; Hsieh, H.-A.; Hsieh, H.-F.; Wang, T.-H.; Ho, C.-C.; Lin, P.-P.; Wang, C.-F. *J. Anal. At. Spectrom.* **2013**, *28*, 1396-1401.

[32] Kamaly, N.; Pugh, J. A.; Kalber, T. L.; Bunch, J.; Miller, A. D.; McLeod, C. W.; Bell, J. D. *Mol. Imaging Biol.* **2010**, *12*, 361-366.

[33] Koelmel, J.; Leland, T.; Wang, H.; Amarasiriwardena, D.; Xing, B. *Environ. Pollut.* **2013**, *174*, 222-228.

[34] Petros, R.; DeSimone, J. *Nat. Rev. Drug Discovery* **2010**, *9*, 615-627.

[35] Zhu, Z.-J.; Carboni, R.; Quercio, M. J.; Yan, B.; Miranda, O. R.; Anderton, D. L.; Arcaro, K.F.; Rotello, V. M.; Vachet, R. W. *Small* **2010**, *6*, 2261-2265.

[36] Arvizo, R. R.; Miranda, O. R.; Moyano, D. F.; Walden, C. A.; Giri, K.; Bhattacharya, R.; Robertson, J. D.; Rotello, V. M.; Reid, J. M.; Mukherjee, P. *PLoS One* **2011**, *6*, e24374.

[37] Yan, B.; Kim, S. T.; Kim, C. S.; Saha, K.; Moyano, D. F.; Xing, Y.; Jiang, Y.; Roberts, A. L.; Alfonso, F. S.; Rotello, V. M.; Vachet, R.W. *J. Am. Chem. Soc.* **2013**, *135*, 12564-12567.

[38] Creran, B.; Yan, B.; Moyano, D. F.; Gilbert, M. M.; Vachet, R. W.; Rotello, V. M. *Chem. Comm.* **2012**, *48*, 4543-4545.

[39] Zhu, Z. -J.; Tang, R.; Yeh, Y.-C.; Miranda, O. R.; Rotello, V. M.; Vachet, R. W. *Anal. Chem.* **2012**, *8*, 4321-4326.

[40] Choi, H. S.; Liu, W.; Misra, P.; Tanaka, E.; Zimmer, J. P.; Ipe, B I.; Bawendi, M. G.; Frangioni, J. V. *Nature Biotechnol.* **2007**, *25*, 1165-1170.

[41] Mebius, R. E.; Kraal, G. *Nat. Rev. Immunol.* **2005**, 5, 606-616.

[42] Brust, M.; Walker, M.; Bethell, D.; Schiffrin, D. J.; Whyman, R.J. *Chem. Soc. Chem. Comm.* **1994**, 801-802.

[43] Templeton, A. C.; Wuelfing, M. P.; Murray, R. W. *Acc. Chem. Res.* **2000**, *33*, 27-36.

[44] Miranda, O. R.; Li, X. N.; Garcia-Gonzalez, L.; Zhu, Z. J.; Yan, B.; Bunz, U. H. F.; Rotello, V. M. *J. Am. Chem. Soc.* **2011**, *133*, 9650-9653.

[45] Miranda, O. R.; Chen, H.-T.; You, C.-C.; Mortenson, D. E.; Yang, X.-C.; Bunz, U. H. F.; Rotello, V. M. *J. Am. Chem. Soc.* **2010**, *132*, 5285-5289.

[46] Hong, R.; Emrick, T.; Rotello, V. M. *J. Am. Chem. Soc.* **2004**, *126*, 13572-13573.

[47] Yan, B.; Zhu, Z. J.; Miranda, O. R.; Chompoosor, A.; Rotello, V. M.; Vachet, R. W.; *Anal. Bioanal. Chem.* **2010**, *396*, 1025-1035.

[48] Liu, X.; Atwater, M.; Wang, J.; Huo, Q. *Colloids Surf., B* **2007**, *58*, 3-7.

[49] Köppen, C.; Reifschneider, O.; Castanheira, I.; Sperling, M.; Karst, U.; Ciarimboli, G. *Metallomics* **2015**, *7*, 1595-1603.

CHAPTER 3

QUANTITATIVE IMAGING OF GOLD NANOPARTICLES IN TISSUES USING INKJET-PRINTED STANDARDS

3.1. Introduction

Several approaches have been applied to understand the fate of the AuNPs *in vivo*, including laser ablation inductively coupled plasma mass spectrometry (LA-ICP-MS) imaging.[1-4] Although most of these techniques are capable of generating biodistribution maps for the AuNPs *in vivo*, they lack of quantitative abilities. In this sense, LA-ICP-MS imaging is a promising tool with available quantification methods.[5,6]

The most commonly used quantification strategy for LA-ICP-MS imaging is to use matrix-matched calibration standards.[7] In this approach, calibration standards are prepared from materials that are as similar to the sample that is analyzed.[8] Although, this procedure is widely applied in LA-ICP-MS imaging, the laborious sample preparation, heterogeneous distribution of standards, and the difficulty of matching with the original sample's composition are the major drawbacks of the method. Several other approaches, such as spin coating,[9] internal and external calibration,[6,10] and certified reference materials (CRMs),[6] have also been applied for quantitative LA-ICP-MS imaging to overcome the drawbacks of matrix matched calibration standards. Although these methods provide successful quantification for some samples, in many cases they still do not adequately match with the matrix of the original sample. For this reason, developing alternative strategies for quantification are required for further improvement.

Inkjet printing is a convenient way to deposit controlled amounts of material in a spatially defined way. The homogeneous printout, easy sample preparation and cheap instrumentation makes it a potentially promising approach for creating standards for LA-ICP-MS imaging. Previously, inkjet printing has been used for internal standardization to improve signal reproducibility in LA-ICP-MS imaging,[11,12] but there are a few reports on its use for calibration standards for quantitative imaging.[13]

In this chapter, we describe the use of inkjet printing as an alternative approach for quantitative LA-ICP-MS imaging of AuNPs *in vivo*. We have explored whether inkjet-printed standards can be added as internal standards to tissues of interest in a standard addition-type approach. By adding the standards to the tissue that is being imaged, we surmised that 'matrix-matching' would be ideal.

3.2. Results and Discussion

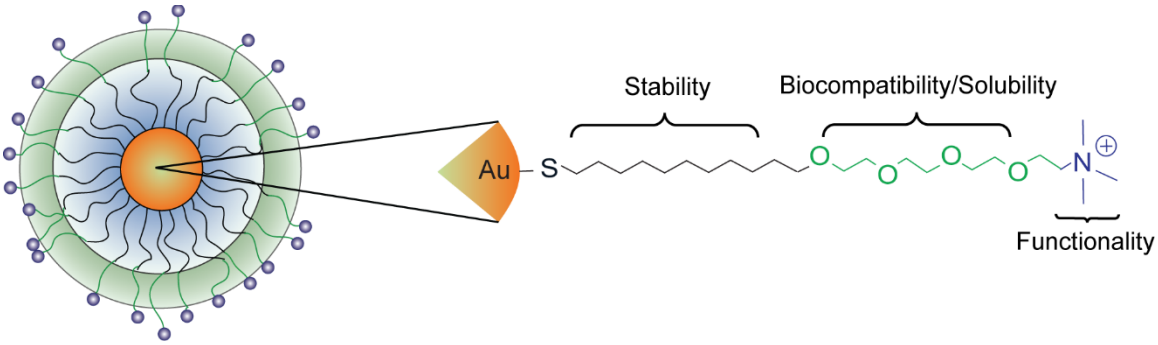

Figure 3.1 Structure of the AuNP used in the study

Positively charged AuNPs with tetraalkylammonium head group (referred to as TTMA throughout the chapter) were selected for preparation of inkjet-printed standards. The AuNP consists of a 2 nm core and monolayer attached to the core *via* thiol group

(Figure 3.1). The TTMA AuNP solution was prepared by dissolving the NPs in an ink formulation, that consisted of 69% water, 20% glycerol, 10% 1,2 hexanediol, 1% triethanolamine.[14] This formulation was found to be critical for obtaining successful printouts from the printer.

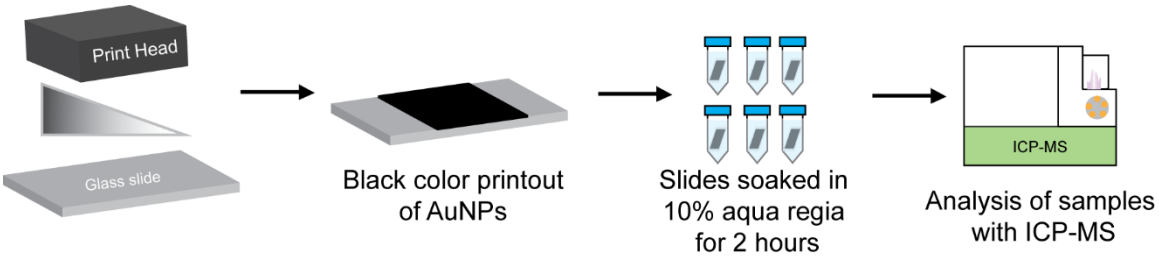

Figure 3.2. Illustration of quantification of the printed Au amounts.

Using the CD printing software (Print CD) provided with the printer, different printing conditions were investigated in order to find the amounts of Au printed on the glass surface. Different black percentages (100, 95, 90, 85, 80, 66, 60, 47, 33, 0 %) were selected and printed onto glass surfaces (Figure 3.2). The slides were washed with 10 % aqua regia to dissolve the printed gold amounts and soaked for 2 hours prior to the analysis with ICP-MS. Quantitative recoveries were obtained from washing the glass slides with this method, and the obtained results were plotted in order to generate calibration curves for the amounts of Au printed as a function of the % black that was used (Figure 3.3). The results indicate that below 60 % black values no amounts of Au are detected. Using % black values of 66 % to 100 % allowed a linear calibration curve to be achieved with an r^2=0.99951 (Figure 3).

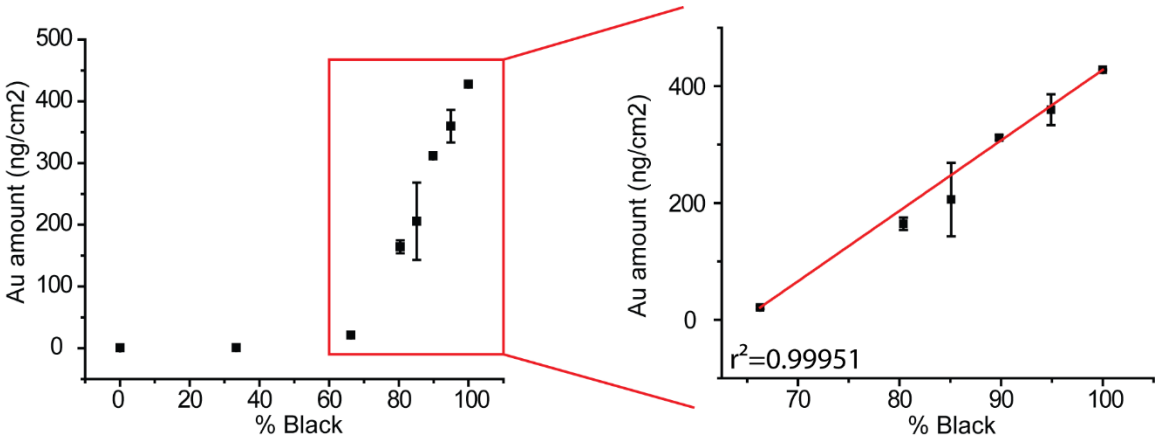

Figure 3.3. Quantification results of printed amounts of AuNP at different black percentage values.

Day-to-day variation is one of the major concern for the inkjet-printed standard preparation.[13] In order to investigate the variability of the printouts from different days, calibration curves were generated for selected black percentage values on two different days (Figure 3.4). The results indicate that the variation from day-to-day printouts was insignificant.

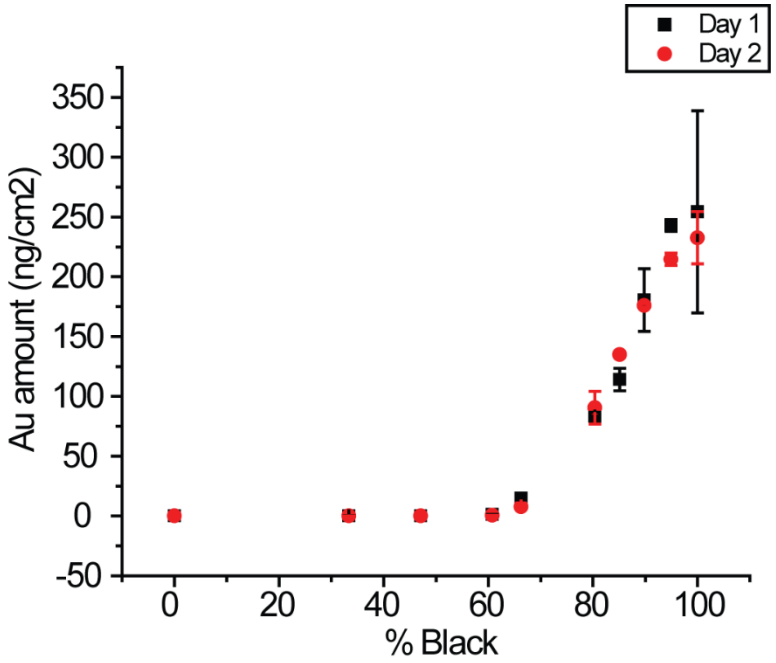

Figure 3.4. Day-to-day variation comparison of the printouts obtained from printer

Following successful quantification of printed Au amounts, the feasibility of inkjet-printed standards for LA-ICP-MS imaging was investigated. In chapter 2, a quantitative LA-ICP-MS imaging method for 2 nm monolayer protected AuNPs using matrix-matched standards was developed.[15] Optimum instrumental parameters obtained in chapter 2 with the matrix-matched standards were also used in this work. Selected black percentages were printed as line patterns onto glass slides and a blank control mouse liver tissue sliced was placed on top of the printed standards (Figure 3.5).

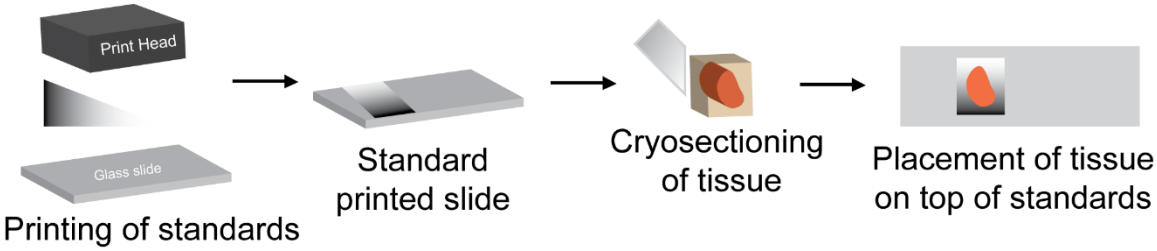

Figure 3.5. An illustration of the sample preparation procedure for quantitative LA-ICP-MS imaging with inkjet-printed standards.

Upon placement of the control mouse tissue, the sample was imaged using LA-ICP-MS. ^{57}Fe signals were used to locate the tissue and generate an image of it as Fe is located throughout the tissue. At the same time, ^{197}Au signals were obtained to generate images of the inkjet-printed samples. The results obtained from inkjet-printed standards were then used to plot calibration curves. Linear calibration curves with r^2=0.99296 were obtained from the inkjet-printed standards in LA-ICP-MS imaging (Figure 3.6).

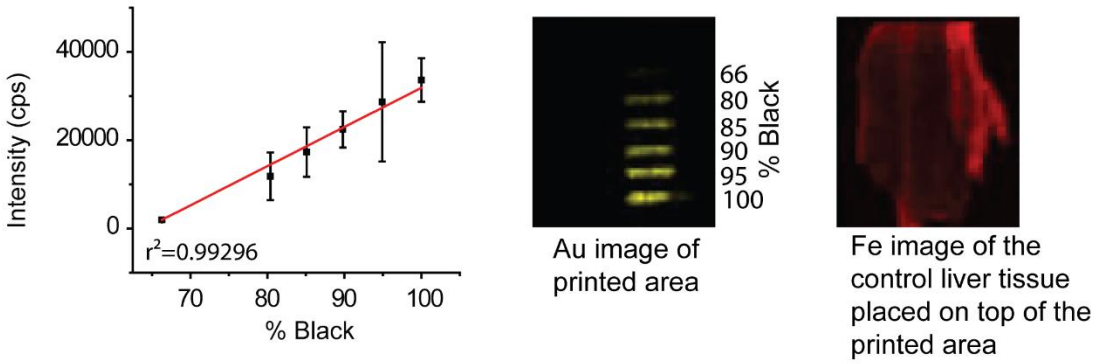

Figure 3.6. Quantification results obtained from a control mouse tissue placed on top of the inkjet-printed standards.

3.3. Future direction

Initial experiments allow us to quantify the printed amounts of the AuNPs from different black percentages. Using this information, we can select 6 different black percentages to be used for inkjet-printed standards. With the selected inkjet-printed standards, a calibration curve can be plotted and linear calibration curves can be achieved from these samples with the blank mouse tissue. Overall, these results are promising to move forward to use inkjet-printed standards for exact matrix matching with tissues of interest. This could be achieved by placing only small part of the tissue on the edge of the inkjet-printed standards (Figure 3.7). The inkjet-printed standards and the tissue could be imaged simultaneously with the LA-ICP-MS system, and the obtained data could be further processed to generate calibration curves.

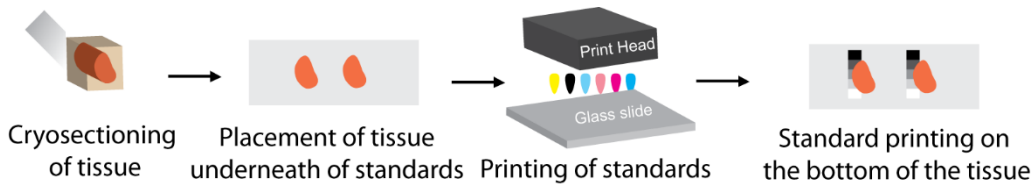

Figure 3.7. An illustration of the usage of the inkjet-printed standards for quantification of AuNPs in tissue samples from mice injected with AuNPs.

Data analysis of the samples could be done by generating histogram bins for each of the printed lines. The results could then be extracted to separate the signals coming from the tissue samples and the inkjet-printed standards. The obtained averages from the histogram bins could be used to generate the calibration curve for the quantification of Au amounts in the tissue (Figure 3.8).

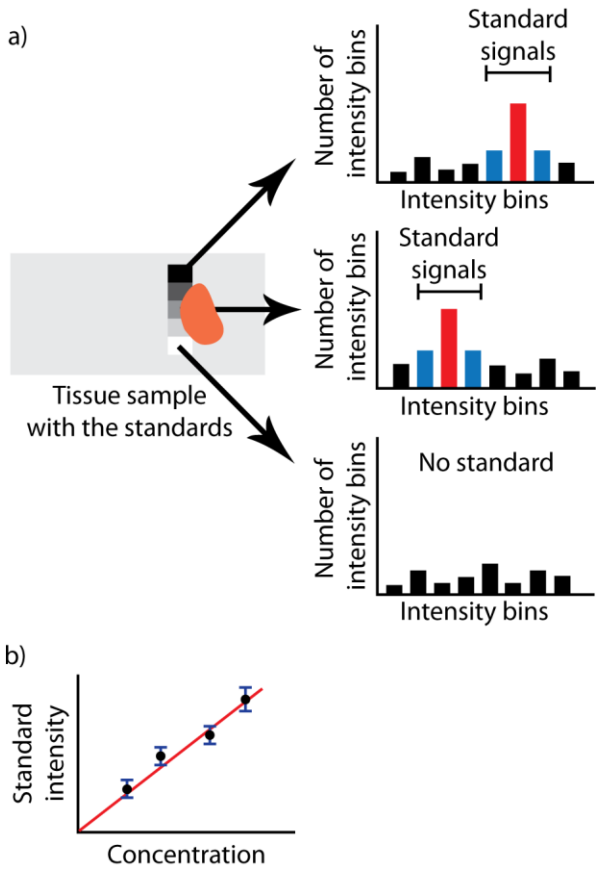

Figure 3.8. a) Illustration of histogram calculation for generation of calibration curve from inkjet-printed standards. b) Calibration curve plotted using the average values of the intensity bins obtained from inkjet-printed standards.

3.4. Conclusion

In conclusion, the inkjet-printed standards could possibly be used as an alternative strategy for LA-ICP-MS imaging. Quantitative recoveries obtained from the different printed AuNP amounts and negligible day-to-day variation suggest that it is a potentially promising approach for LA-ICP-MS quantification. Linear calibration curves were also obtained from the experiments with blank mouse liver tissue. With the application towards AuNP injected mouse tissues, this method might be used for better matrix matching and thus better quantitative imaging.

3.5. Experimental

3.5.1. Instrumentation

For all printing experiments, an Epson Artisan 50 inkjet printer was used. It was selected over other brands and types due to its piezoelectric print head that does not cause any issues with the experimental materials. For example, some brands uses heat-based print heads that can affect to the composition of the materials and the quality of the printouts obtained.

3.5.2. Synthesis of AuNP

The AuNP used in this study were synthesized using Brust-Schiffrin two-phase method.[16] Using Murray place exchange reaction, the AuNPs were functionalized with the

desired monolayer.[17] The details of the synthetic procedure for the synthesis of the monolayer can be found in Chapter 2. Following place exchange reaction, AuNPs were dialyzed for 72 hours against MilliQ water using Spectra/Por Dialysis Membranes (molecular weight cutoff of 1000 Da) to remove excess free ligand.

3.5.3. Inkjet printing formulation

For successful printouts from a piezoelectric print head, the formulation viscosity was optimized. As previously noted, we used an organic solvent system that is known to enable reliable printouts. The formulation consisted of 69% water, 20% glycerol, 10% 1,2 hexanediol, and 1% triethanolamine that was then mixed with 1:1 ratio of the AuNPs solution. 10 mL of this mixture was then placed into an empty black ink cartridge (obtained from Inksupply.com) to be printed.

3.5.4. Printing of inkjet-printed standards

Using the CD printing software, a rectangular shape and a 6 line pattern was created for obtaining quantification of AuNPs amount and inkjet-printed standards, respectively. Rectangular shapes were drawn using the shape tool in the Print CD software. Using font size of 4 and the letter "I" in horizontal orientation, 6 lines of the selected black percentages were also printed out. The printed sample were dried overnight and a blank control mouse tissue was placed on top of the printed samples prior to their analysis with LA-ICP-MS.

3.5.5. Quantification of Au amounts printed

Using the CD printing software (Print CD) provided with the Epson Artisan 50 printer, we printed different black percentages (100, 95, 90, 85, 80, 66, 60, 47, 33, 0 %).

Glass slides (from Fisher Scientific) were placed onto the CD printing tray and rectangular regions of the different black percentages were printed out. Two rectangular regions (approximately 3.5x1.7 cm) were printed onto the same glass slide and the slides were cut into half. Each half was placed into a different 50 mL centrifuge tube and they were washed with 1 mL aqua regia **(Aqua regia is highly corrosive and must be handled with extreme caution.)**. After washing the slides with aqua regia, samples were diluted to 10 mL and slides were soaked for 2 hours. Following digestion of the samples, the glass slides were removed from the solution and the samples were analyzed with ICP-MS. The parameters used for ICP-MS analysis were described in Chapter 2. Au standard solution were prepared prior to the each experiment (20, 10, 5, 2, 1, 0.5, 0.2, 0 ppb).

3.6. References

[1] Drescher, D.; Kneipp, J. *J. Chem. Soc. Rev*. **2012**, *41*, 5780-5799.

[2] Qian, X. M.; Nie, S. M. *Chem. Soc. Rev*. **2008**, *37*, 912-920.

[3] Xiang Li, X.; Anton, N.; Zuber, G.; Vandamme, T. *Adv. Drug Delivery Rev*. **2014**, *76*, 116-133.

[4] Priester, J. H.; Ge, Y.; Mielke, R. E.; Horst, A. M.; Cole Moritz, S.; Espinosa, K.; Gelb, J.; Walker, S. L.; Nisbet, R. M.; An, Y.-J.; Schimel, J. P.; Palmer, R. G.; Hernandez-Viezcas, J. A.; Zhao, L.; Gardea-Torresdey, J. L.; Holden, P. A. *Proc. Natl. Acad. Sci. U. S. A.* **2012**, *109*, 2451-2456.

[5] Becker, J. S.; Becker, J. S. *Biomed. Spectrosc. Imaging* **2012**, *1*, 187-204.

[6] Limbeck, A.; Galler, P.; Bonta, M.; Bauer, G.; Nischkauer, W.; Vanhaecke, F. *Anal. Bioanal. Chem.* **2015**, *407*, 6593-6617.

[7] Becker, J. S.; Zoriy, M. V.; Pickhardt, C.; Palomero-Gallagher, N.; Zilles, K. *Anal. Chem.* **2005**, *77*, 3208-3216.

[8] Hare, D. J.; Lear, J.; Bishop, D.; Beavis, A.; Doble, P. A. *Anal. Methods* **2013**, *5*, 1915-1921.

[9] Claverie, F.; Malherbe, J.; Bier, N.; Molloy, J. L.; Long, S. E. *Anal. Chem.* **2013**. *85*, 3584-3591.

[10] Hare, D.; Austin, C.; Doble, P. *Analyst* **2012**, *137*, 1527-37.

[11] Moraleja, I.; Esteban-Fernández, D.; Lázaro, A.; Humanes, B.; Neumann, B.; Tejedor, A.; Luz Mena, M.; Jakubowski, N.; Gómez-Gómez, M. M. *Anal. Bioanal. Chem.* **2016**, 408, 2309-2318.

[12] Hoesl, S.; Neumann, B.; Techritz, S.; Sauter, G.; Simon, R.; Schluter, H.; Michael W.; Linscheid, M.W.; Theuring, F.; Jakubowskia, N.; Muellera, L. *J. Anal. At. Spectrom*. **2016**, *31*, 801-808.

[13] Bonta, M.; Lohninger, H.; Marchetti-Deschmanna, M.; Limbeck, A. *Analyst* **2014**, *139*, 1521-1531.

[14] Marsico, A. L. M.; Creran, B.; Duncan, B.; Elci, S. G.; Jiang, Y.; Onasch, T. B.; Wormhoudt, J.; Rotello, V. M.; Vachet R. W. *J. Am. Soc. Mass Spectrom.* **2015**, *26*, 1931-1937.

[15] Elci, S. G.; Yan, B.; Kim, S. T.; Saha, K.; Jiang, Y.; Klemmer, G. A.; Moyano, D. F.; Yesilbag Tonga, G.; Rotello V. M.; Vachet, R. W. *Analyst* **2016**, *141*, 2418-2425.

[16] Brust, M.; Walker, M.; Bethell, D.; Schiffrin, D.J.; Whyman, R.J. *Chem. Soc. Chem. Comm.* **1994**, 801-802.

[17] Templeton, A. C.; Wuelfing, M. P.; Murray, R. W. *Acc. Chem. Res.* **2000**, *33*, 27-36.

CHAPTER 4

SURFACE CHARGE CONTROLS THE SUB-ORGAN BIODISTRIBUTION OF GOLD NANOPARTICLES

This chapter is adapted from a paper published as: Elci, S. G.; Jiang, Y.; Yan, B.; Kim, S. T.; Saha, K.; Moyano, D. F.; Yesilbag Tonga, G.; Jackson, L. C.; Rotello, V. M.; Vachet, R. W. *ACS Nano* **2016**, *10*, 5536-5542.

4.1. Introduction

Recent advances in the synthesis and functionalization of nanoparticles (NPs) has led to an increasing number of applications in imaging,[1,2] drug delivery[3,4] and therapeutics.[5] Effective use of nanomaterials as drug delivery vehicles requires them to overcome biological barriers, accumulate in specific tissue and sub-tissue regions, and resist rapid clearance.[6,7] For both active and passive targeted drug delivery applications, it is therefore important to understand the effect of NP surface functionality on biological distributions.[8] Several studies have investigated the *in vivo* biodistributions of differently sized NPs[9,10] but relatively few report the effect of surface functionality of the NPs *in vivo*.[11,12] NP size influences how NPs are cleared or stored in the reticulo-endothelial system organs (*e.g.* liver, spleen, *etc.*) after their uptake by the mononuclear phagocyte system in blood stream.[13,14] While smaller NPs (< 5 nm) are excreted from the body by renal clearance, larger particles (> 100 nm) are filtered by the spleen and sequestered by the liver.[15] Particles with sizes between these two extremes (5 - 100 nm) typically have longer circulation

times.[16,17] In this size range the fate of NPs *in vivo* is likely to be influenced by a range of factors, including NP shape and surface chemistry.

Surface chemistry is a particularly important determinant, influencing cellular uptake,[18-20] immune system activation,[21] and the composition of the protein 'corona' that develops around NPs *in vivo*.[22,23] To date, most *in vivo* applications of nanomaterials have involved PEG-functionalized NPs to minimize protein corona formation and concomitant rapid NP removal from circulation *via* opsonization,[13,24-26] although binding to plasma proteins is still possible, including interactions with IgG and fibrinogen.[27] A few studies have explored how modification to PEG surface coatings, such as the introduction of charged moieties, influences protein corona formation and subsequent interactions with components in the blood and uptake by macrophages.[12,28-33] Not surprisingly, surface chemistry can influence protein adsorption, [31,32] but it also affects uptake by macrophages[28-30,33] and perhaps even plays a more important role than size in NP-cell interactions.[12,27,29,33] Overall, existing work indicates that the influence of NP surface chemistry on the fate of the NPs *in vivo* is complex. Quantitative information about the effect of surface chemistry on NP biodistributions will improve our understanding of NP fate in biological systems. Moreover, site-specific quantitative information about nanomaterial sub-organ distributions, which is, with a few exceptions,[34,35] lacking in nanomaterial studies *in vivo*, will yield a deeper understanding of how NP surface chemistry influence biological pathways inside organisms.

In this chapter, we investigate the sub-organ biodistribution of AuNPs with different surface charge that have been intravenously injected into mice. We focus on the distributions of these AuNPs in the kidney, liver and spleen, as these organs not only tend

to accumulate the highest levels of NPs, but they also have distinct cell types that are involved in different biological functions, including clearance and immune responses. We use laser ablation inductively-coupled plasma imaging (LA-ICP-MS) to quantitatively track the sub-organ distributions. Compared to common imaging techniques, such as TEM, confocal microscopy, and AFM, the biggest advantage of LA-ICP-MS imaging is the ability to provide quantitative information about distributions. Moreover, the technique does not require any specific physical property, such as fluorescence, for detection. Our studies here show that surface charge influences the sub-organ biodistributions of the AuNPs, and the imaging results clearly reveal that surface charge affects the response of the immune system to the injected NPs.

4.2. Results and Discussion

Functionalized AuNPs with 2 nm cores were injected into mice to explore how surface chemistry influences NP sub-organ distribution. Each of the AuNPs has the same hydrophobic interior to confer stability, and a tetra(ethyleneglycol) layer to provide compatibility and solubility (Figure 4.1). The surface chemistry was varied *via* the headgroup of the attached ligand, giving rise to NPs that differ in charge (Figure 4.1). AuNPs 1 and 2 also differ in hydrophobicity. Our previous work showed that the presence of serum influences the uptake of these NPs to different extents, making it edifying to study their difference *in vivo*.[36] As was observed previously with similar AuNPs,[14] differences in surface chemistry can have a dramatic effect on the biodistributions of these NPs in the mice, as indicated by the total amount of gold accumulated in each organ (Figure 4.2). In most cases, the positively-charged AuNPs (AuNPs 1 and 2) accumulate to the greatest extent in each organ. Moreover, the liver and spleen accumulate the highest concentrations

of the NPs, which is similar to previous observations for cells and tissues.[37,38] This biodistribution profile likely arises because the reticuloendothelial system plays a dominant role in NP clearance.[19,39] The liver and spleen are major detoxifying and filtering organs in mammals. With a high proportionate blood-flow to these organs together with the propensity of positively-charged NPs to been readily taken up into cells,[14] it is perhaps not surprising that AuNPs 1 and 2 are found most extensively in these organs.

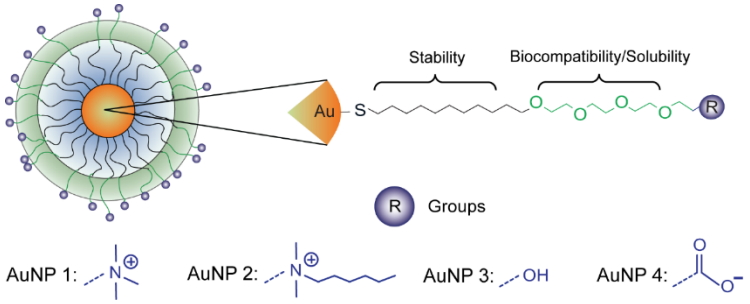

Figure 4.1. Design and structure of the AuNPs used in the study

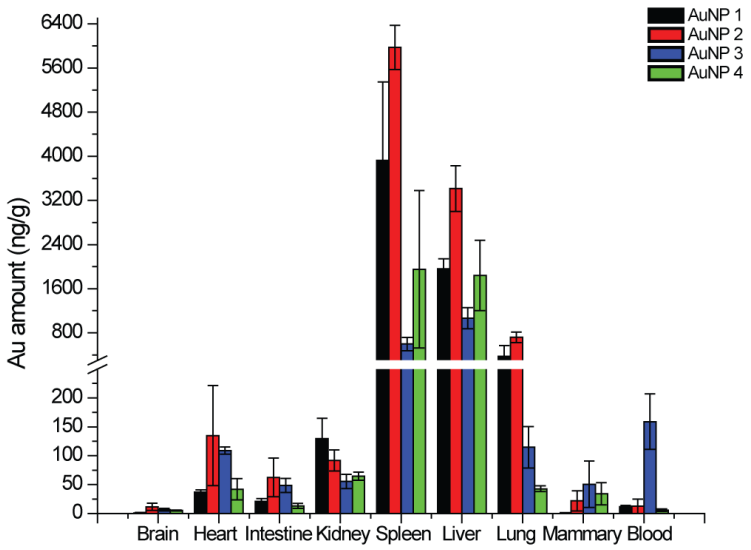

Figure 4.2. AuNP concentrations in different organs after 24 hours of injection as determined by ICP-MS. The AuNP concentrations were calculated by the gold amount (ng) divided by organ weight (g). The error bars correspond to the standard error of the mean from measurements of organs from 4 mice.

Beyond organ-by-organ distributions, we were interested in understanding whether surface chemistry influences NP distributions within the different structures of the kidney, lung, spleen, and liver. To address this question, we used LA-ICP-MS to quantitatively image the NP biodistributions in these organs. Strictly speaking, LA-ICP-MS is an element specific technique and thus reports on total gold concentrations, but previous work from our groups has shown that AuNPs with the same design remain intact *in vivo*.[40] Moreover, the NP surface coating has a noticeable influence on the distribution of these NPs, indicating that the technique is probing the locations of the AuNPs.

The lung and kidney contain relatively low concentrations of AuNPs as compared to the liver and spleen, but AuNP distributions in these organs can be readily obtained using LA-ICP-MS imaging. The lung tissues are somewhat difficult to image because of the fragile nature of this organ. As a result the images do not reveal much beyond the fact that all four AuNPs are absent in the alveolar spaces of the lung (Figure 4.3). This observation is not surprising given that the alveolar space is a gas-filled region in the lungs.

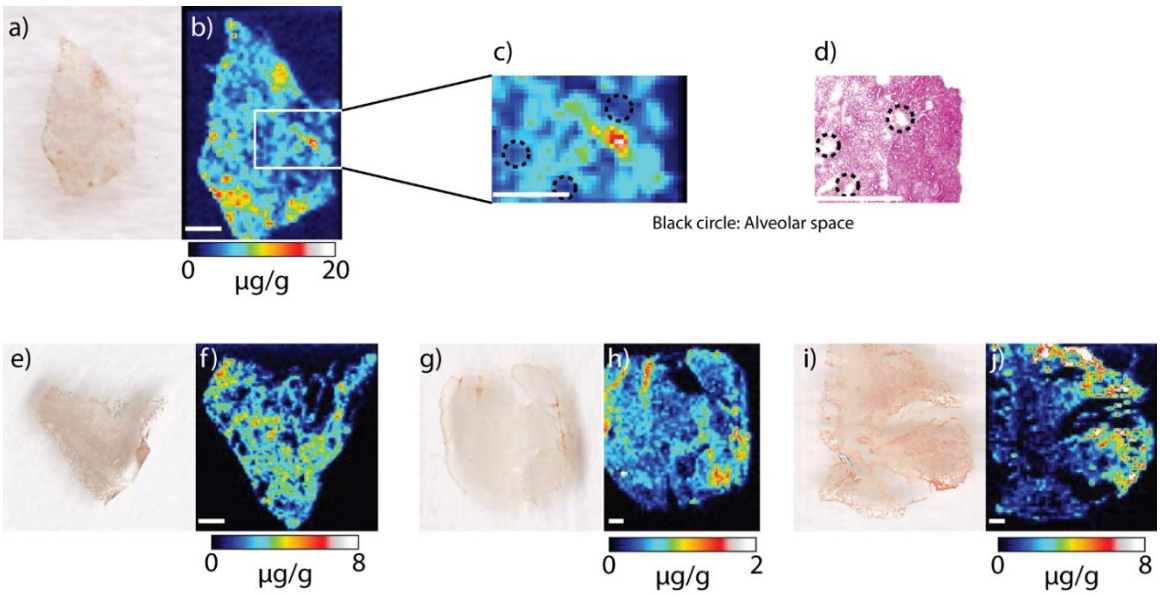

Figure 4.3. Imaging results for the lung tissues. (a) optical and (b) quantitative LA-ICP-MS images of AuNP 1; c) zoomed-in area illustrating the amount of AuNP 1 in a selected area of the lung tissue with various alveolar spaces indicated in black dotted lines; (d) optical image after H&E staining of the same region shown in (c), indicating the alveolar spaces in black dotted lines. (e) optical and (f) quantitative LA-ICP-MS images of AuNP 2; (g) optical and (h) quantitative LA-ICP-MS images of AuNP 3 (i) optical and (j) quantitative LA-ICP-MS images of AuNP 4. All scale bars correspond to 0.5 mm.

More provocative is the finding that the AuNPs are distributed in a surface charge-dependent fashion in the kidney. Images of this organ from mice injected with the positively-charged AuNPs 1 and 2 have a more punctate appearance than the images from mice injected with AuNPs 3 and 4 (Figure 4.4). Comparing the LA-ICP-MS images with H&E stains of the kidney (Figure 4.4c and d) indicate that AuNPs 1 and 2 accumulate in the glomeruli (the initial step in filtration in the nephron) of the kidney, whereas AuNP 3 and 4 do not selectively accumulate in these regions of the kidney. Indeed, AuNP 3

accumulates extensively in the arteries that transport blood into the kidney, and AuNP 4 is more homogeneously distributed in the organ. Another interesting observation is that AuNPs 1, 2, and 4 do not appear to accumulate in the arteries.

The concentration of the positively-charged AuNPs in the glomeruli of the kidney suggests that surface charge influences how these AuNPs are filtered by the kidney. Glomeruli are part of the initial stage of filtering by the kidney, playing an important role in a process that eventually ends with the excretion of materials from the blood into urine.[41] Glomeruli have pores that are less than 10 nm in diameter, and their membranes are negatively-charged, which might explain why the positively-charged AuNPs preferentially accumulate in this region of the kidney. Filtering of intact NPs by the kidney is expected to be slow because particles larger than 5 nm in hydrodynamic size are not excreted efficiently by this organ.[42] Quite likely the accumulation of AuNPs 1 and 2 in the glomeruli influences the rate at which these particular NPs are excreted relative to AuNPs 3 and 4. Future work will investigate this possibility *via* a more thorough study of the metabolism and excretion characteristics of these materials. Clearly, though, surface charge influences NP distributions, and LA-ICP-MS images reveal valuable information for better understanding biological responses to injected NPs.

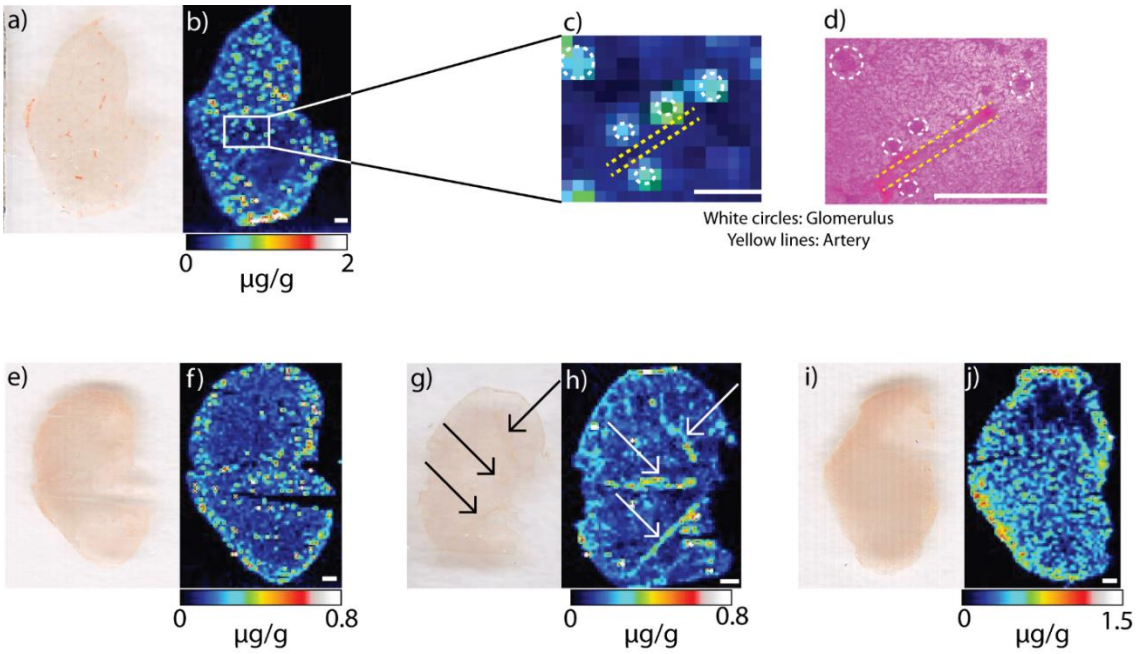

Figure 4.4. Imaging results for the kidney tissues. (a) optical and (b) quantitative LA-ICP-MS images of AuNP 1; c) zoomed-in area illustrating the amount of AuNP 1 in a selected area of the kidney tissue with an artery vein and glomeruli indicated in yellow and white dotted lines, respectively; (d) optical image after H&E staining of the same region shown in (c), indicating the artery vein and glomeruli indicated in yellow and white dotted lines. (e) optical and (f) quantitative LA-ICP-MS images of AuNP 2; (g) optical image showing the artery veins indicated in black arrows and (h) quantitative LA-ICP-MS images of AuNP 3 and (i) optical and (j) quantitative LA-ICP-MS images of AuNP 4. All scale bars correspond to 0.5 mm.

Upon imaging spleen tissues by LA-ICP-MS, we found that the AuNPs are heterogeneously distributed in this organ (Figure 4.5). All four AuNPs accumulate to a significant extent in the red pulp region of the spleen, but AuNP 3 (Figure 4.5h) and to a lesser extent AuNP 4 (Figure 4.5j) accumulate in the white pulp and the marginal zone

between the red and white pulp (Figure 4.5h and Table 4.1). The positively-charged AuNPs (*i.e.* AuNP 1 and AuNP 2) accumulate very little in the white pulp and marginal zone (Table 1). In fact, in most images, no statistically significant levels of the positively-charged NPs are found in the white pulp.

The observed AuNP distributions provide interesting insight into how surface chemistry affects NP fate *in vivo*, especially in light of the physiological role of the spleen. The primary role of the red pulp is to clean the blood of particulate matter, antigens, and dead blood cells, whereas the white pulp acts as part of the immune system. The marginal zone is the exchange or sieving region between the white and red pulp, and much of the immune response generated by the spleen starts in this region.[43,44] Consequently, the observation that the neutral AuNP 3 is found to the greatest extent in the marginal zone and white pulp suggests that this NP may have elicited an immune response to a greater extent than the others. It is known that antigen exposure in the marginal zone of the spleen can cause the transport of bacteria from the marginal zone to the periarteriolar lymphoid sheath of the white pulp.[45] It is possible that AuNP 3 is being transported in an analogous way, giving rise to its accumulation in this region of the spleen.

The reasons for the surface chemistry-dependent difference in the AuNP distributions are not clear at this point, but it is likely that AuNP 3 is coated with an immune-competent protein. Previous work with functionalized NPs having varying PEG chain lengths suggested that the protein corona around these NPs was formed by the immune-competent proteins IgG and fibrinogen.[27] In contrast, the positively-charged AuNPs 1 and 2 are almost certainly interacting with negatively charged proteins such as serum albumin, which do not elicit an immune response. Perhaps the negatively-charged

NPs are coated to a lesser extent with immune-competent proteins, causing them appear to a lesser extent in the white pulp than the neutral NP.

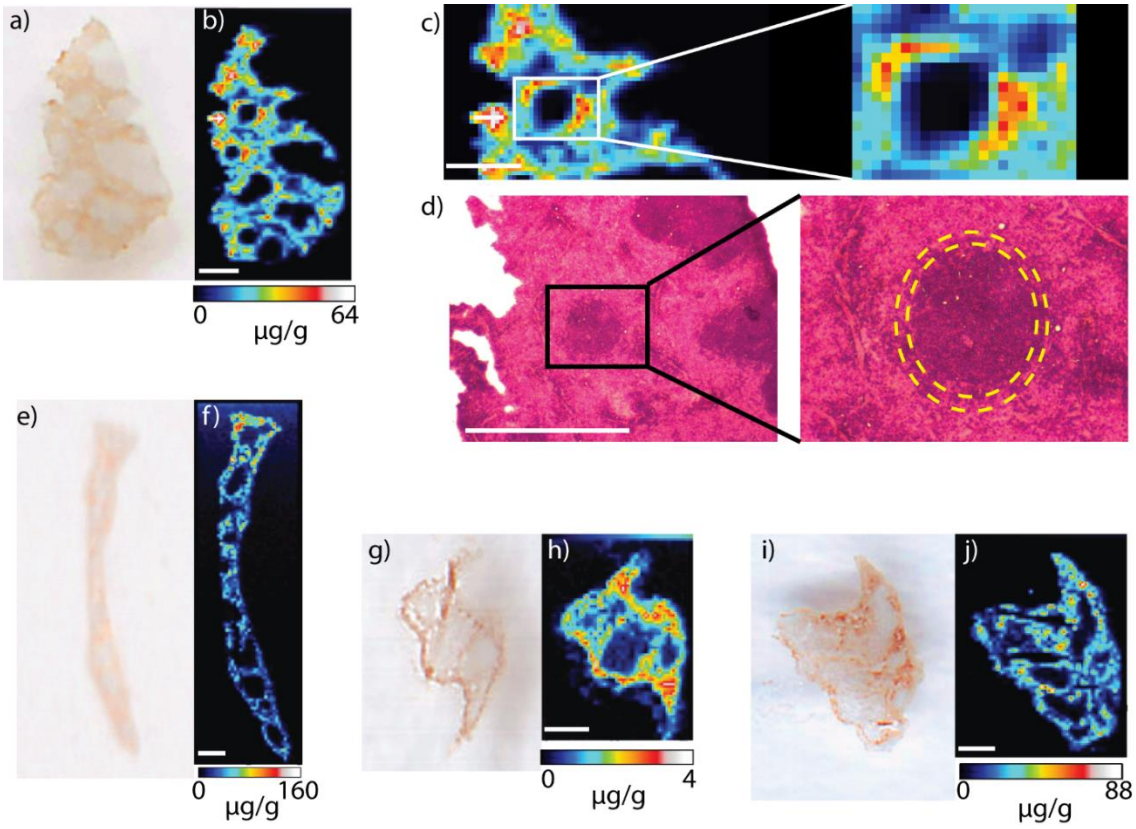

Figure 4.5. Imaging results for spleen tissues. (a) optical and (b) quantitative LA-ICP-MS images of AuNP 1; c) zoomed-in area illustrating the amount of AuNP 1 around a selected white pulp region of the spleen; d) optical image after H&E staining of the same region shown in (c), indicating the white pulp region in dark purple, the red pulp region in light purple and the marginal zone (region circled by the yellow dashed lines). (e) optical and (f) quantitative LA-ICP-MS images of AuNP 2; (g) optical and (h) quantitative LA-ICP-MS images of AuNP 3 (i) optical and (j) quantitative LA-ICP-MS images of AuNP 4. All scale bars correspond to 0.5 mm.

Table 4.1. Percent accumulation of each AuNPs in different regions of the spleen with data averaged from three images for each AuNP.

	Red pulp[a*]	**Marginal zone[b*]**	**White pulp[c*]**
AuNP 1	79 ± 8 %	17 ± 5 %	2.1 ± 0.8 %
AuNP 2	75 ± 3 %	21 ± 2 %	3 ± 1 %
AuNP 3	60 ± 15 %	30 ± 10 %	10 ± 5 %
AuNP 4	70 ± 9 %	27 ± 9%	5 ± 2 %

[a] The red pulp regions in each image were identified from the H&E stains, optical images, and the ^{57}Fe LA-ICP-MS images of the spleen (Figure 4.6).

[b] The marginal zone is the ~ 40 µm thick region between the red pulp and white pulp, and in the LA-ICP-MS images, this corresponds to a single pixel area surrounding each white pulp region.

[c] The white pulp regions in each image were identified from the H&E stains, optical images, and the ^{57}Fe LA-ICP-MS images of the spleen (Figure 4.6).

[*]Average values are calculated based on three images obtained from three separate tissue slices (n=3). See experimental section for details about how the gold percentages were determined in each case.

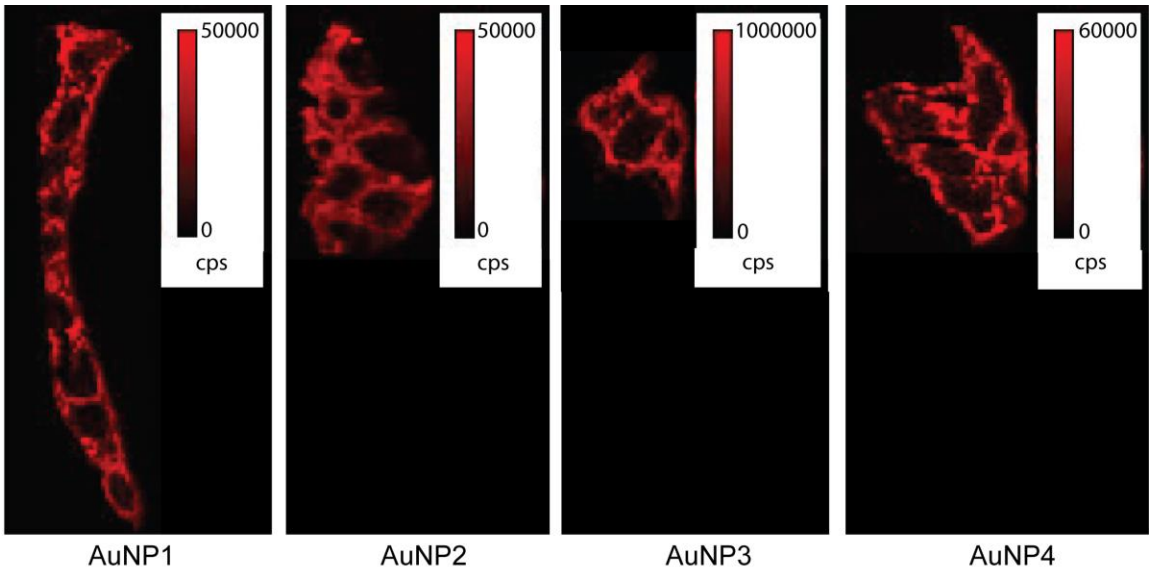

Figure 4.6. ^{57}Fe images of the spleen tissues. Higher concentrations of Fe are found in the red pulp as this region is infused with blood, whereas lower Fe concentrations are found in the white pulp.

A comparison of LA-ICP-MS liver images reveals that the positively-charged NPs distribute themselves in a more heterogeneous fashion than the neutral or negatively-charged NPs (Figure 4.7). AuNPs 1 and 2 accumulate in the hepatocytes and endothelial regions of the tissue that comprise a large percentage of the liver[46] and accumulate very little in the Kupffer cells (*e.g.* Figure 5c and d). In contrast, AuNP 3 (Figure 4.7h) and AuNP 4 (Figure 4.7j) distribute more broadly in the liver. In particular, AuNP 3 seems to be equally distributed through the hepatocytes and Kupffer cells. A quantitative basis for this conclusion can be found by counting the number of pixels in the LA-ICP-MS images that show no detectable gold signal. For AuNP 3, only 7.3% of the pixels are found without gold, whereas 26.3%, 44.1%, and 23.5% of the pixels are found without gold for AuNPs 1, 2, and 4, respectively.

Another interesting observation is that the positively-charged AuNPs do not appear in the blood vessels that transverse the liver. This conclusion is based upon comparisons of the Au and ^{57}Fe distributions from the LA-ICP-MS imaging results (*e.g.* Figure 4.7b and 4.7f vs. Figure 4.8). The blood vessels in the Au images for AuNP 1 and 2 have no gold, whereas the blood vessels in the images of AuNPs 3 and 4 have significant levels of gold. These data are consistent with the low levels of AuNPs 1 and 2 and the relatively high levels of AuNP 3 measured in the blood by ICP-MS (Figure 4.2).

Just as with the spleen data, the AuNP distributions in the liver suggest that AuNP 3 is interacting to a greater extent with the immune system than the positively-charged AuNPs. This conclusion comes from the homogeneous distribution of AuNP 3, including with the Kupffer cells, and the corresponding absence of AuNPs 1 and 2 in these cells (Figure 4.7c and d). Kupffer cells have endocytic activity against blood-borne materials entering the liver and act as part of the host immune system to clear pathogens and waste materials.[47] Kupffer cells are effective at removing foreign material from circulation, and particular matter and microorganisms are known to adhere to Kupffer cells.[48] As speculated earlier in the context of the spleen images, it is possible that differential protein corona formation around the AuNPs leads to different biodistributions in liver. Another interesting conclusion from the liver images is that the positively-charged AuNPs are removed from circulation more quickly than neutral and negatively-charged AuNPs as revealed by the absence of AuNPs 1 and 2 in the blood vessels 24 h after injection.

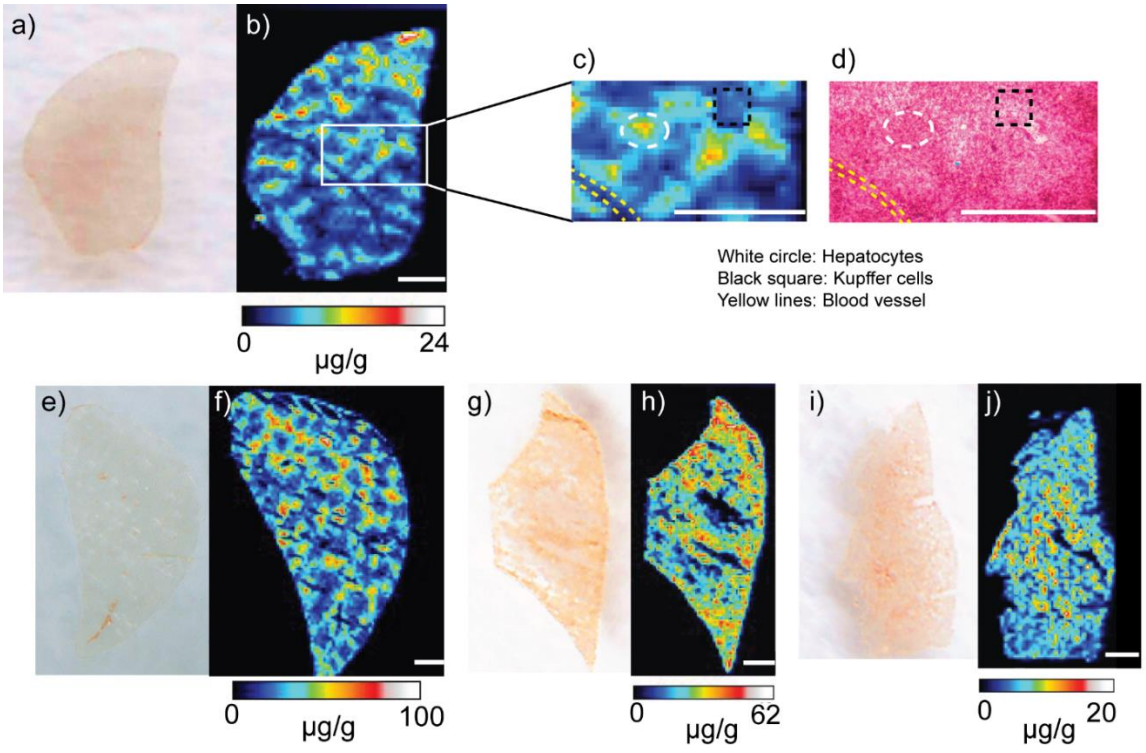

Figure 4.7. Imaging results for the liver tissues. (a) optical and (b) quantitative LA-ICP-MS images of AuNP 1; c) zoomed-in area illustrating the amount of AuNP 1 in a selected area of the liver tissue with a blood vessel, hepatoctyes and Kupffer cells indicated in yellow, white and black dotted lines, respectively; (d) optical image after H&E staining of the same region shown in (c), indicating the blood vessel, hepatoctyes and Kupffer cells in yellow, white and black dotted lines. (e) optical and (f) quantitative LA-ICP-MS images of AuNP 2; (g) optical and (h) quantitative LA-ICP-MS images of AuNP 3 (i) optical and (j) quantitative LA-ICP-MS images of AuNP 4. All scale bars correspond to 0.5 mm.

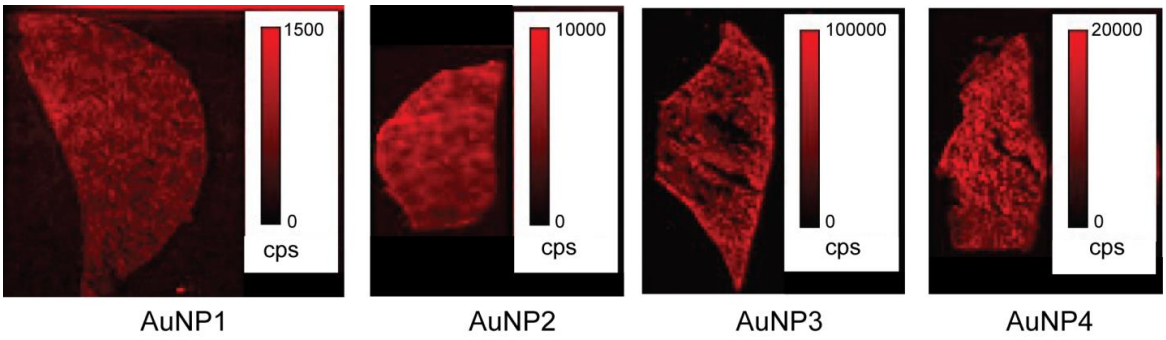

Figure 4.8. ^{57}Fe images of the liver tissues.

4.3. Conclusion

In conclusion, surface charge has a notable effect on NP biodistributions *in vivo*, specifically their sub-organ distributions. LA-ICP-MS images of the kidney show that the positively charged AuNPs concentrate in the glomeruli, whereas the neutral and negatively-charged AuNPs do not. This observation suggests that the NPs might be excreted at different rates that depend on their surface chemistry. Future work will explore this finding in greater detail. LA-ICP-MS imaging results also suggest that neutral AuNPs are more likely to interact with the immune system, as evidenced by their greater relative accumulation in the marginal zone and white pulp regions of the spleen and with the

Kupffer cells of the liver. Positively-charged NPs, on the other hand, are found more extensively in the filtering regions of the spleen and the detoxifying hepatocytes of the liver. In addition, because no measurable gold is found in the liver blood vessels 24 h after injection of the positively-charged AuNPs, it is likely that these AuNPs are rapidly cleared from circulation, whereas the neutral and negatively-charged NPs circulate longer. The negatively-charged AuNPs are cleared more slowly than the positively-charged AuNPs, but they do not interact with the immune system as extensively as the neutral AuNPs, as suggested by their distributions in the spleen and liver. Overall, LA-ICP-MS imaging gives quantitative sub-organ information that can provide a deeper understanding of how NP properties affect the biological responses to the injected NPs. Moreover, observations about the effect of NP surface functionality on sub-organ biodistribution may provide additional valuable information to improve the design of nanotherapeutics for both passive and active targeting strategies. For example, some surface coatings may cause NPs to interact with the immune system to a greater or lesser extent, and understanding this effect is essential for realizing the full implications of a NP-based delivery system.

4.4. Experimental

4.4.1. Material

All the reagents required for the AuNPs syntheses were purchased from Fisher Scientific or Sigma-Aldrich, with the exception of chloroauric acid, which was obtained from Strem Chemicals Inc. The 8-10 weeks old Balb/C type mice required for the animal experiments were obtained from Jackson Laboratory (Bar Harbor, ME). Animals were housed in the University of Massachusetts Amherst Animal Care facility. All of the animal

experiments were conducted in accordance with the guidelines of the Institutional Animal Care and Use Committee (IACUC) at the university. Food and water intake of the mice were assessed. Chicken breast and beef liver were purchased from a local market (Big Y). The H&E staining kit, nitric acid, hydrochloric acid and hydrogen peroxide were purchased from Fisher Scientific. The daily performance solution and Au standard were purchased from Perkin Elmer.

4.4.2. Gold nanoparticle synthesis and characterization

Using the Brust-Schiffrin two-phase synthesis method, 2 nm core AuNPs were synthesized.[49] The AuNPs are initially synthesized with pentanethiols as the capping monolayer. Once these AuNPs were synthesized, the Murray place exchange method was used to functionalize the AuNPs with desired ligand functionality.[50,51] Detailed syntheses of the ligands that were used in this work can be found in previous work.[52] The place exchange reaction involved taking 10 mg of the pentanethiol-conjugated AuNPs and mixing with 30 mg of the ligand of interest in a mixture of dry dichloromethane (3 mL) and methanol (1 mL). This mixture was stirred under nitrogen (N_2) for 3 days at 25 °C. Then, the precipitate was collected (place-exchanged particles precipitate out) and dissolved in distilled water and dialyzed for three days to remove excess ligands, pentanethiol, and other salts present in the nanoparticle solution. The products of the synthesis, including the ligands and the final nanoparticles, were characterized using NMR and mass spectrometry. Figure 1 represents the structure of the AuNPs used in the study. For the characterization of AuNPs, the core sizes of the NPs were measured by transmission electron microscopy (TEM) on a JEOL100S electron microscope and were found to have core diameters of 2.1 ± 0.2 nm (AuNP 1), 2.0 ± 0.1 nm (AuNP 2), 1.8 ± 0.2

nm (AuNP 3) and 2.0 ± 0.4 nm (AuNP 4) (Figure 4.9). The AuNPs were also characterized by laser-desorption/ionization mass spectrometry (LDI-MS) to confirm the monolayer coating.[53] Hydrodynamic size and the zeta potential of the particles were measured with Malvern NanoZetaSizer (1μM NP concentration in 5 mM phosphate buffer pH=7.4).

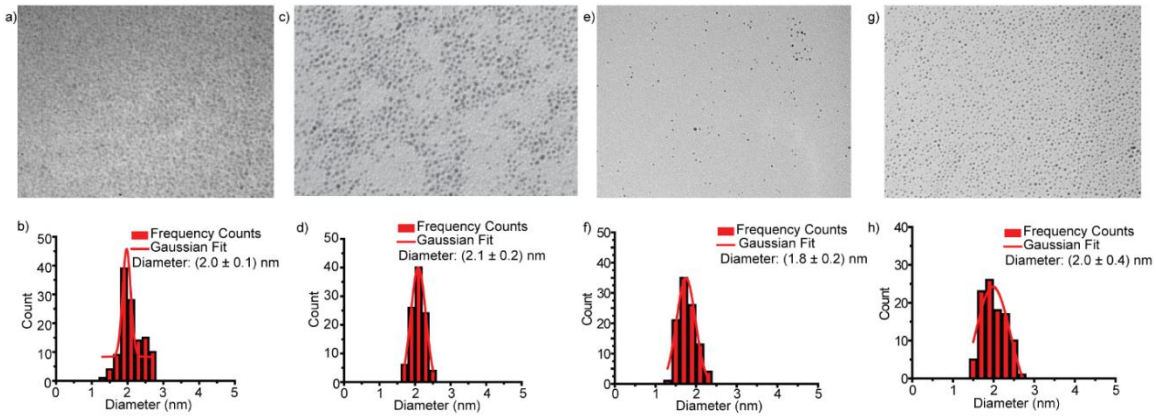

i)

	AuNP 1	AuNP 2	AuNP 3	AuNP 4
TEM (nm)	2.0 ± 0.1	2.1 ± 0.2	1.8 ± 0.2	2.0 ± 0.4
Hydrodynamic size(nm)	10.0 ± 0.7	9.2 ± 0.8	13.5 ± 4.3	7.0 ± 0.2
ζ-potential (mV)	21.1 ± 0.5	16.6 ± 0.6	-0.8 ± 7.6	-41.2 ± 1.7

Figure 4.9. TEM images of the AuNPs studied in this work and summary of the TEM, DLS and zeta potential measurements of the particles.

4.4.3. Intravenous administration of AuNPs in normal mice

Solutions of individual AuNPs were prepared at concentrations of 2 μM, and 50 μL of each AuNP solution was injected into Balb/c mice *via* the tail vein. After 24 h, the mice were sacrificed *via* inhalation of carbon dioxide and cervical dislocation. Organs were then collected and prepared for analysis. Each organ that was collected was cut into two parts, except the kidneys and lungs which are present as a pair in the body. One of the two organs, in the case of the kidneys and lungs, or one part of the organs was homogenized and

analyzed by ICP-MS for total gold amount. The remaining organ or part of the organ was then used for LA-ICP-MS imaging analysis.

4.4.4. Tissue preparation for imaging

Liver and spleen tissue samples were sliced to a thickness of 12 μm at -20 °C using a LEICA CM1850 cryostat microtome instrument. The sliced tissues were then attached to regular glass slides and stored at room temperature until they were analyzed.

4.4.5. Hematoxylin & Eosin Y (H&E) staining

Tissue slices were stained using a kit that was obtained from Thermo Fisher Scientific. Adjacent slices of the tissues were taken and fixed onto a glass slide. Following fixation, the tissues were immersed into distilled water, hematoxylin, bluing reagent, 95% ethanol, eosin-y, 100% ethanol and xylene in the order described by the kit's manual.

4.4.6. ICP-MS sample preparation and measurements

Tissue homogenates of the organs were prepared using a 3:1 (v:v) mixture of nitric acid (68%) and hydrogen peroxide (30%) to digest each organ overnight. The next day, 0.5 mL of aqua regia [3:1 (v:v) mixture of nitric acid and hydrochloric acid] was added and the sample was then diluted to 10 mL using de-ionized water. (**Aqua regia is highly corrosive and must be handled with extreme caution.**) Gold standard solutions (gold concentrations: 20, 10, 5, 2, 1, 0.5, 0.2 and 0 ppb) were prepared prior to each experiment. A Perkin Elmer NEXION 300X ICP mass spectrometer (Waltham, MA) was used to analyze these samples. Prior to the analysis, daily performance measurements were done to ensure the instrument was operating under optimum conditions. The ^{197}Au signals were

obtained using the standard operating mode. The ICP-MS conditions can be found in Chapter 2.

4.4.7. LA-ICP-MS measurement conditions and imaging

A CETAC LSX-213 G2 laser ablation system (Photon Machines, Omaha, NE) that was attached to the ICP mass spectrometer *via* a 2 m length of tubing was used to image the tissue samples. Optimization of the laser ablation conditions was first performed using pure AuNP samples on glass slides. The optimal conditions can be found in Chapter 2. The mass spectrometer was operated using the kinetic energy discrimination mode, which was especially important for measurements of ^{57}Fe.

4.4.8. Data analysis and image generation

ICP-MS data was analyzed using Excel and Origin 9.0 (from OriginLab, Northampton, MA). Images of the analyzed LA-ICP-MS data were generated using the software ImageJ. Optical images of the tissues were processed with Adobe Photoshop.

4.4.9. Matrix-matched standard preparation for ICP-MS

This information can be found in experimental section of Chapter 2.

4.4.10. Gold percentage determination in spleen tissue regions

The gold concentration in each pixel of the red pulp was determined after comparison to a calibration curve as described in the experimental section. The concentrations from each pixel were then summed to obtain the total gold concentration in the red pulp region, and the percentage was calculated after summing the total gold from

each of the three parts of the spleen. We determined the amount in each marginal zone by summing the gold concentrations in a single pixel area surrounding each white pulp region. The gold concentrations were obtained *via* comparison to a calibration curve, and the reported percentage was calculated in the same manner as with the red pulp. The gold concentrations were obtained *via* comparison to a calibration curve, and the reported percentage was calculated in the white pulp in the same manner as with the red pulp and marginal zone.

4.6. References

[1] Ando, J.; Yano, T.; Fujita, K.; Kawata, S. *Phys. Chem. Chem. Phys.* **2013**, *15*, 13713-13722.

[2] Bera, D.; Qian, L.; Tseng, T. K.; Holloway, P. H. *Materials* **2010**, *3*, 2260-2345.

[3] Rana, S.; Bajaj, A.; Mout, R.; Rotello, V. M. *Adv. Drug Deliver. Rev.* **2012**, *64*, 200-216.

[4] Sun, T.; Zhang, Y. S.; Pang, B.; Hyun, D. C.; Yang, M.; Xia, Y. *Angew. Chem. Int. Ed.* **2014**, *53*, 12320-12364.

[5] Kim, C. S.; Duncan, B.; Creran, B.; Rotello, V. M. *Nano Today* **2013**, *8*, 439-447.

[6] Choi, H. S.; Liu, W.; Liu, F.; Nasr, K.; Misra, P.; Bawendi, M. G.; Frangioni, J. V. *Nat. Nanotechnol.* **2009**, *5*, 42-47.

[7] Kreyling, W. G.; Abdelmonem, A. M.; Ali Z.; Alves, F.; Geiser, M.; Haberl, N.; Hartmann, R.; Hirn, S.; de Aberasturi, D. J.; Kantner, K.; Khadem-Saba, G.; Montenegro, J. M.; Rejman, J.; Rojo, T.; de Larramendi, I. R.; Ufartes, R.; Wenk, A.; Parak, W. J. *Nat. Nanotechnol.* **2015,** *10*, 619-623.

[8] Sinha, R.; Kim, G. J.; Nie, S.; Shin, D.M. *Mol. Cancer Ther.* **2006**, *5*, 1909-1917.

[9] De Jong, W. H.; Hagens, W. I.; Krystek, P.; Burger, M. C.; Sips, A. J.A.M.; Geertsma, R. E. *Biomaterials* **2008**, *29*, 1912-1919.

[10] Duan, X.; Li, Y. *Small* **2013**, *9*, 1521-1532.

[11] García, K. P.; Zarschler, K.; Barbaro, L.; Barreto, J. A.; O'Malley, W.; Spiccia, L.; Stephan, H.; Graham, B. *Small* **2014**, *10*, 2516–2529.

[12] Townson, J. L.; Lin, Y.-S.; Agola, J. O.; Carnes, E. C.; Leong, H. S.; Lewis, J. D.; Haynes, C. L.; Brinker, C. J. *J. Am. Chem. Soc.* **2013**, *135*, 16030-16033.

[13] Ernsting, M. J.; Murakami, M.; Roy, A.; Li, S.-H. *J. Control. Release* **2013**, *172*, 782-794.

[14] Khlebtsov, N.; Dykman, L. *Chem. Soc. Rev.* **2011**, *40*, 1647-1671.

[15] Longmire, M.; Choyke, P.; Kobayashi, H. *Nanomedicine* **2008**, *3*, 703-717.

[16] Simone, E. A.; Dziubla, T. D.; Muzykantov, V. R. *Expert Opin. Drug Deliv.* **2008**, *5*, 1283-1300.

[17] Decuzzi, P.; Godin, B.; Tanaka, T.; Lee, S. Y.; Chiappini, C.; Liu, X.; Ferrari, M. *J. Control. Release* **2010**, *141*, 320-327.

[18] Cho, E. C.; Xie, J. W.; Wurm, P. A.; Xia, Y. N. *Nano Lett.* **2009**, *9*, 1080-1084.

[19] Xiao, K.; Li, Y.; Luo, J.; Lee, J. S.; Xiao, W.; Gonik, A. M.; Agarwal, R. G.; Lam, K. S. *Biomaterials* **2011**, *32*, 3435-3446.

[20] Saha, K.; Kim, S. T.; Yan, B.; Miranda, O. R.; Alfonso, F.; Schlosman, D.; Rotello, V. M. *Small* **2013**, *9*, 300-305.

[21] Moyano, D. F.; Goldsmith, M.; Solfiell, D. J.; Landesman-Milo, D.; Miranda, O. R.; Peer, D.; Rotello, V. M. *J. Am. Chem. Soc.*, **2012**, *134*, 3965-3967.

[22] Walkey, C. D.; Chan, W. C. *Chem. Soc. Rev.* **2012**, *41*, 2780.

[23] Fleischer, C. C.; Payne, C. K. *Acc. Chem. Res.* **2014**, *47*, 2651-2659.

[24] Pelley, J. L.; Daar A. S.; Saner, M. A. *Toxicol. Sci.* **2009**, *112*, 276-296.

[25] Lynch, I.; Dawson, K. A. *Nanotoday* **2008**, *3*, 40-47.

[26] Pelaz, B.; Del Pino, P.; Maffre, P.; Hartmann, R.; Gallego, M.; Rivera-Fernández, S.; De la Fuente, J. M.; Nienhaus, G. U.; Parak, W. J. *ACS Nano*, **2015,** *9*, 6996-7008.

[27] Aggarwal, P.; Hall, J. B.; McLeland, C.B.; Dobrovolskaia, M. A.; McNeil, S. E. *Adv. Drug Deliver. Rev.* **2009**, *61*, 428-437.

[28] Walkey, C. D.; Olsen, J. B.; Guo, H.; Emili, A.; Chan, W. C. *J. Am. Chem. Soc.* **2012**, *134*, 2139-2147.

[29] Shah, N. B.; Vercellotti, G. M.; White, J. G.; Fegan, A.; Wagner, C. R.; Bischof, J. C. *Mol. Pharmaceutics* **2012**, *9*, 2146-2155.

[30] Albanese, A.; Tang, P. S.; Chan, W. C. W. *Annu. Rev. Biomed. Eng.* **2012**, *14*, 1-16.

[31] Gessner, A.; Lieske, A.; Paulke, B.; Muller, R. *Eur. J. Pharm. Biopharm.* **2002**, *54*, 165-170.

[32] Gessner, A.; Lieske, A.; Paulke, B.; Muller, R. *J. Biomed. Mater. Res. A* **2003**, *65*, 319-326.

[33] Cheng, X.; Tian, X.; Wu, A.; Li, J.; Tian, J.; Chong, Y.; Chai, Z.; Zhao, Y.; Chen, C.; Ge, C. *ACS Appl. Mater. Interfaces* **2015**, *7*, 20568-20575.

[34] Chen, S.; Xiong, C.; Liu, H.; Wan, Q.; Hou, J.; He, Q.; Badu-Tawiah, A.; Nie, Z. *Nat. Nanotechnol.* **2015**, *10*, 176-182.

[35] Kourtis, I. C.; Hirosue, S.; De Titta, A.; Kontos, S.; Stegmann, T.; Hubbell, J. A.; Swartz, M. A. *PLoS One* **2013**, *8*, e61646.

[36] Zhu, Z.-J.; Posati, T.; Moyano, D. F.; Tang, R.; Yan, B.; Vachet, R. W.; Rotello, V. M. *Small* **2012**, *8*, 2659-2663.

[37] Arvizo, R. R.; Miranda, O. R.; Moyano, D. F.; Walden, C. A.; Giri, K.; Bhattacharya, R.; Robertson, J. D.; Rotello, V. M.; Reid, J. M.; Mukherjee, P. *Plos One* **2011**, *6*, e24374.

[38] Zhu, Z. J.; Carboni, R.; Quercio, M. J.; Yan, B.; Miranda, O. R.; Anderton, D. L.; Vachet, R. W. *Small* **2010**, *6*, 2261-2265.

[39] Kim, S. T.; Saha, K.; Kim, C.; Rotello, V, M. *Acc. Chem. Res.* **2013**, *46*, 681-691.

[40] Yan, B.; Kim, S. T.; Kim, C. S.; Saha, K.; Moyano, D. F.; Xing, Y.; Vachet, R. W. *J. Am. Chem. Soc.* **2013**, *135*, 12564-12567.

[41] Liang, X.; Wang, H.; Zhu, Y.; Zhang, R.; Cogger, V. C.; Liu, X.; Xu, Z. P.; Grice, J. E.; Roberts, M. S. *ACS Nano* **2016**, *10*, 387-395.

[42] Choi, H. S.; Liu, W.; Misra, P.; Tanaka, E.; Zimmer, J. P.; Ipe, B. I.; Bawendi, M. G.; Frangioni, J. V. *Nat. Biotechnol.* **2007**, *25*, 1165-1170.

[43] Mebius, R. E.; Kraal, G. *Nat. Rev. Immunol.* **2005**, *5*, 606-616.

[44] Demoy, M.; Gibaud, S.; Andreux, J. P.; Weingarten, C.; Gouritin, B.; Couvreur, P. *Pharm. Res.* **1997**, *14*, 463-468.

[45] Aoshi, T.; Zinselmeyer, B. H.; Konjufca, V.; Lynch, J. N.; Zhang, X.; Koide, Y.; Miller, M. J. *Immunity* **2008,** *29*, 476–486.

[46] Baratta, J. L.; Ngo, A.; Lopez, B.; Kasabwalla, N.; Longmuir, K. J.; Robertson, R. T. *Histochem Cell Biol.* **2009**, *131*, 713-726.

[47] Naito, M.; Hasegawa, G.; Ebe, Y.; Yamamoto, T. *Med. Electron Microsc.* **2004**, *37*, 16-28.

[48] Bilzer, M.; Roggel, F.; Gerbes, A. L. *Liver International* **2006**, *26*, 1175-1186.

[49] Brust, M.; Walker, M.; Bethell, D.; Schiffrin, D. J.; Whyman, R. *J. Chem. Soc., Chem. Commun.* **1994**, 801-802.

[50] Hong R.; Emrick T.; and Rotello V. M. *J. Am. Chem. Soc.* **2004**, *126*, 13572-13583.

[51] Jiang, Y.; Huo, S.; Mizuhara, T.; Das, R.; Lee, Y.-W.; Hou, S.; Moyano, D. F.; Duncan, B.; Liang, X.-J.; Rotello V. M. *ACS Nano* **2015**, *9*, 9986–9993.

[52] Miranda, O. R.; Chen, H.-T.; You, C.-C.; Mortenson, D. E.; Yang, X.-C.; Bunz, U. H. F.; Rotello, V. M. *J. Am. Chem. Soc.* **2010,** *132*, 5285-5289.

[53] Yan, B.; Zhu, Z. J.; Miranda, O. R.; Chompoosor, A.; Rotello, V. M.; Vachet, R. W. *Anal. Bioanal. Chem.* **2010,** *396*, 1025-1035.

CHAPTER 5

NANOPARTICLE STABILITY MONITORING IN TISSUES USING DUAL MODE MASS SPECTROMETRIC IMAGING

5.1. Introduction

Monolayer-protected nanoparticles (NPs), which are composed of an inorganic core and an organic monolayer, are used in a variety of biological applications including delivery[1,2] and imaging.[3,4] For example, functionalized gold NPs (AuNPs) have been investigated for siRNA and DNA delivery applications in which the oligonucleotides are attached either covalently or *via* physisorption.[5] Similarly, quantum dots (QDs) with different surface coatings have been explored for their use in imaging applications *in vivo*.[6] Effective use of NPs for these applications requires an accurate assessment of monolayer stability[7] especially *in vivo* as aggregation and/or degradation of the core, due to monolayer instability, can compromise the intended purpose of the NP.[8-10] In addition to protecting the NP from aggregation and degradation, the monolayer provides additional control over NP physical and chemical properties, particularly when interacting with biomolecules.[11-14] The integrity of the monolayer is also crucial because it is known to dictate a particle's fate, including its uptake,[15] corona formation,[16-18] distribution,[19] interactions with the biomolecules,[20] and clearance.

Because the application of monolayer-protected NPs depends on the presence of the monolayer, the release and/or exchange of these surface molecules must be considered to optimally use them in biological settings.[21] For example, a robust monolayer is a prerequisite for quantum dots (QDs)[22,23] to prevent aggregation that deteriorates their

fluorescence emission properties. In addition, unstable monolayers lead to direct exposure of the core materials to a biological system, which can trigger cell toxicity.[24] Semi-stable monolayers, however, are desirable for certain applications. For instance, NP monolayers can be tailored to respond to stimuli such as biogenic thiols or other biomolecules to release cargo for delivery applications, and these stimuli work through destabilization of the monolayer.[24-26] Hence, monolayer stability control is crucial to fully exploit the potential of monolayer-protected NPs in biological applications.

Characterization of monolayer exchange and release has relied on a variety of techniques, including nuclear magnetic resonance (NMR), fluorescence microscopy, dynamic light scattering (DLS) and high performance liquid chromatography (HPLC).[26-28] These tools have provided valuable insight into the chemical and structural factors that influence NP monolayer stability,[29,30] but they are limited to relatively pure samples of NPs. Applying these techniques to more complex samples such as cells or tissues is considerably more challenging. Gaining insight into the chemical and biochemical factors that influence NP stability *in vivo* is essential for NPs with diagnostic or therapeutic potential. Moreover, information about how different tissues influence NP stability is important to more deeply understand the biological effects of NPs *in vivo*.

Here, using monolayer functionalized AuNPs as a testbed, we describe a dual-mode imaging approach that can reveal NP monolayer stability in a site-specific manner. We use laser ablation inductively-coupled plasma mass spectrometry (LA-ICP-MS) imaging to report on the distributions of Au,[31,32] while using laser desorption/ionization (LDI) MS imaging to report on the distributions of AuNPs that have intact monolayers.[33] A site-specific comparison of the two images then reveals the extent to which the NPs are still

intact. Previously, we demonstrated that ICP-MS and LDI-MS could be used to determine the monolayer stability of AuNPs and QDs in cell culture.[3,34] The combined imaging approach described in the current chapter goes much further, allowing us to reveal how different organs and sub-organ cell types influence NP stability *in vivo*.

5.2. Results and Discussion

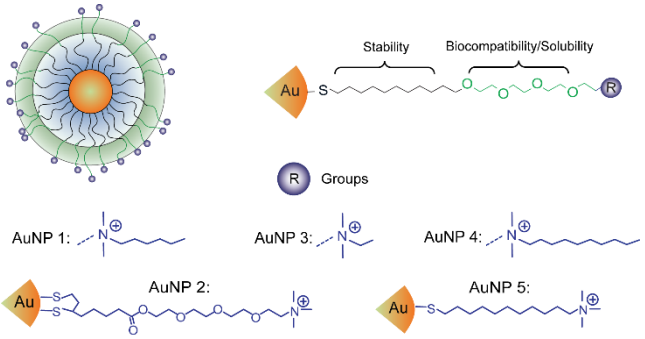

Figure 5.1. Structure of the AuNPs used in this study.

AuNPs (Figure 5.1) with 2 nm cores that were synthesized and characterized as described in experimental section were injected into mice intravenously. After certain time points the mice were sacrificed and their organs were collected. To demonstrate the ability of the combined imaging approach to report on NP stability, we first investigated the stability of selected AuNPs in the liver and spleen. These organs are known to accumulate IV-injected NPs to a significant extent due to their role in blood clearance and filtration.[32,33,35] The liver and spleen differ substantially in their thiol content[36,37] and the cell types involved in blood clearance, however, meaning that they will influence the stability of AuNPs to different extents. The liver has a much higher thiol content than the spleen, so one would expect that AuNPs with thiol-linked monolayers would be less stable in the liver. To test this idea, we compared the LDI-MS and LA-ICP-MS images of spleen

and liver slices from mice injected with AuNP 1 (Figure 5.2). A comparison of these images demonstrates that the monolayer stability of AuNP 1 is low in the liver but is relatively high in the spleen 24 h after injection. We arrive at this conclusion by comparing the signal associated with the monolayer ligand in the LDI-MS images (Figure 5.2b and e) with the signal from Au in the LA-ICP-MS images (Figure 5.2c and f). Previously we had shown that monolayer ligands are only detected by LDI-MS when they are attached to the NP core,[34] so the absence of ligand signal in the LDI-MS image of the liver indicates that the ligands have been displaced in this organ, presumably by the high concentration of thiols. An alternate explanation is that LDI-MS does not work in liver tissue, but this possibility is ruled out by control experiments in which AuNPs that are added to liver tissue slices give rise to significant ligand ion signal (Figure 5.3). Interestingly, AuNPs with dithiol linkers (AuNP 2), which were previously found to be very stable in cell culture, including liver cells,[34] are also not stable in the liver after 4 h *in vivo* (Figure 5.4).

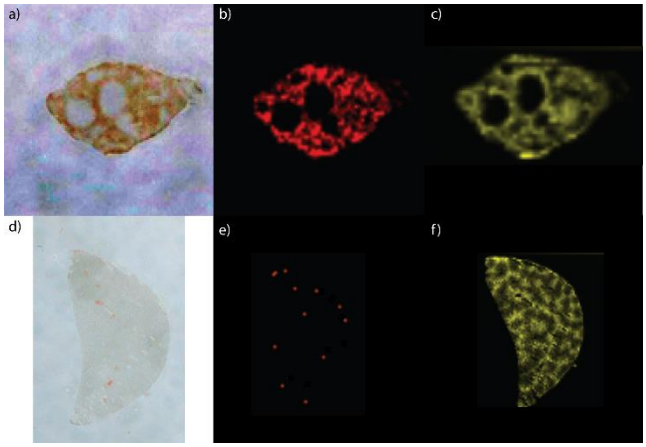

Figure 5.2. Comparison of the stability of AuNPs in spleen and liver slices from mice IV-injected with AuNP 1. Optical images of the spleen (a) and liver (d). LDI-MS images of AuNP 1 that report on the monolayer signal for the spleen (b) and liver (e). LA-ICP-MS

images that report on the Au signal for the spleen (c), and liver (f). See the experimental section and Chapter 2 for instrument parameters and measurement details.

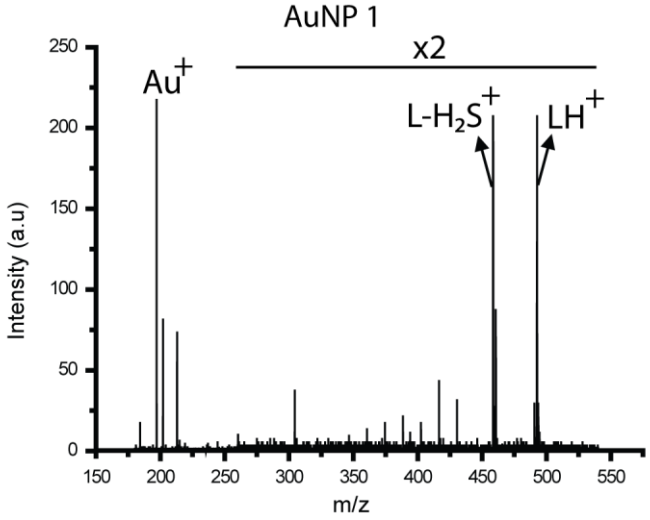

Figure 5.3. LDI mass spectrum of a selected spot in a 12 µm thick liver tissue after pipette spotting 1 µL of a 0.5 µM solution of AuNP 1. LH^+ = molecular ion signal of the ligand attached to AuNP 1 and $L\text{-}H_2S^+$ = fragment ion signal arising from the loss of H_2S from the intact ligand.

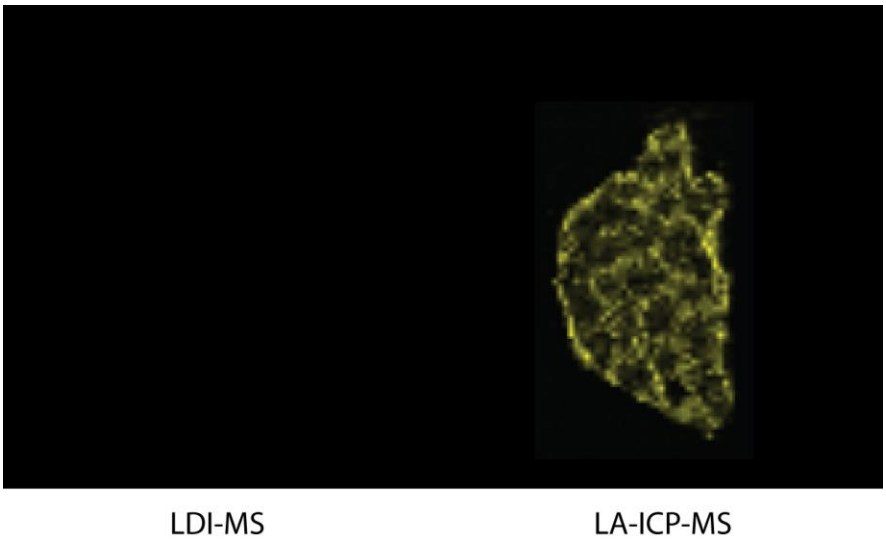

Figure 5.4. LDI-MS and LA-ICP-MS images of liver tissue slices from a mouse injected with AuNP 2.

We next investigated the stability of the particles at different time points (4, 24, and 48 h) after their injection into the mice. AuNPs 1, 3, and 4 were simultaneously injected, and LDI-MS images for each NP's monolayer signal were generated. We predicted that the ligand signal in the LDI-MS images would decrease after longer time points as the AuNPs are degraded over time. Similar to other data from the liver, no significant monolayer signal is observed during LDI-MS (data not shown) even at the shortest time point (i.e. 4 h). This finding suggests that the elevated levels of biogenic thiols in the liver rapidly degrade AuNPs in this organ. The Au distributions from LA-ICP-MS images (e.g. Figure 5.5) indicate that the Au amounts first increase and then decrease over time, which may indicate some early accumulation of Au despite loss of monolayer stability; however, it is difficult to fully conclude this because the data comes from different mice.

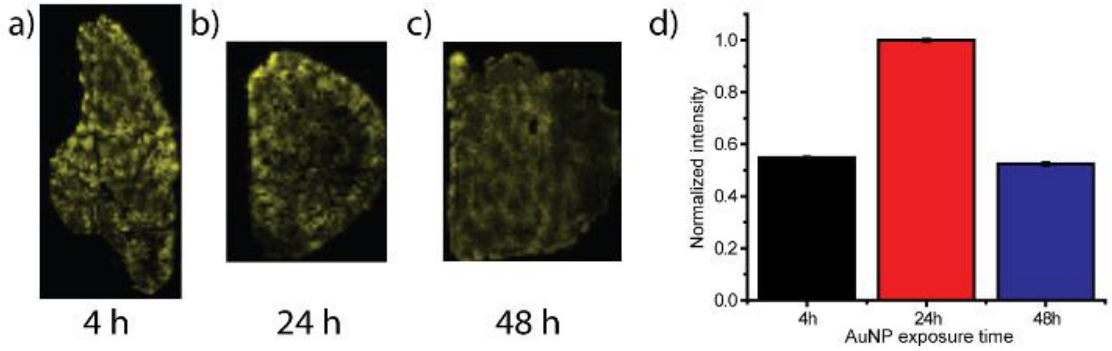

Figure 5.5. Time dependent LA-ICP-MS images of the liver tissue slices from three separate mice. a), b), and c) are images of Au distributions in the liver slices obtained from LA-ICP-MS. d) Bar plots indicating the normalized Au intensity. The normalized intensity is calculated by summing the relative pixel intensity for each image (see calculation below), dividing this sum by the size of each tissue slice and further normalizing by the

total gold amounts in these organs as determined by ICP-MS of partial homogenates. For easier comparison of the three time points, the resulting value for the 24 h time point was set to 1.

LDI-MS images of the spleen reveal that the monolayer signal for each AuNP decreases over time as expected (Figure 5.6a). An evaluation of the ion intensities in these images (Figure 5.6b), after normalizing for the size of the tissue, confirms this observation and further indicates that the signal drop for each AuNP is similar. In contrast, the Au distributions in the spleen, as determined by LA-ICP-MS imaging, indicates that the Au amounts remain somewhat constant when the data is properly normalized for mouse-to-mouse variations (e.g. Figure 5.7 and 5.8). Taken together, the LDI-MS and LA-ICP-MS imaging results suggest that greater than 50% of the monolayer stability is lost in the spleen over a 48 h time period.

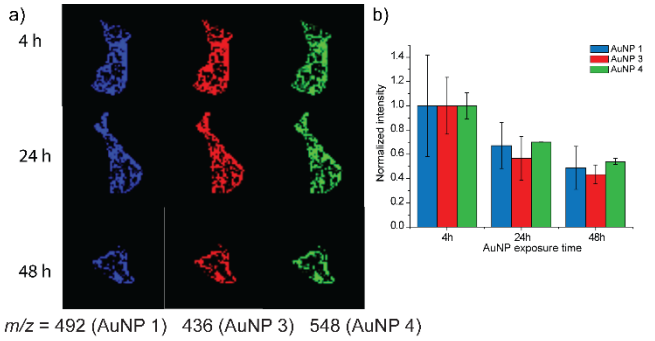

Figure 5.6. a) Time-dependent LDI-MS images of spleen tissue slices for AuNPs 1, 3, and 4. b) Bar plot of the normalized ion intensities for AuNPs 1, 3, and 4, calculated from relative pixel intensities as described in the experimental section.

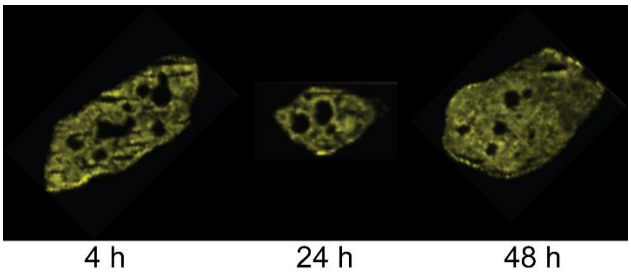

Figure 5.7. An example data set showing the changes in the total Au amount over time in the spleen of 3 different mice after IV injection of AuNPs 1, 3 and 4.

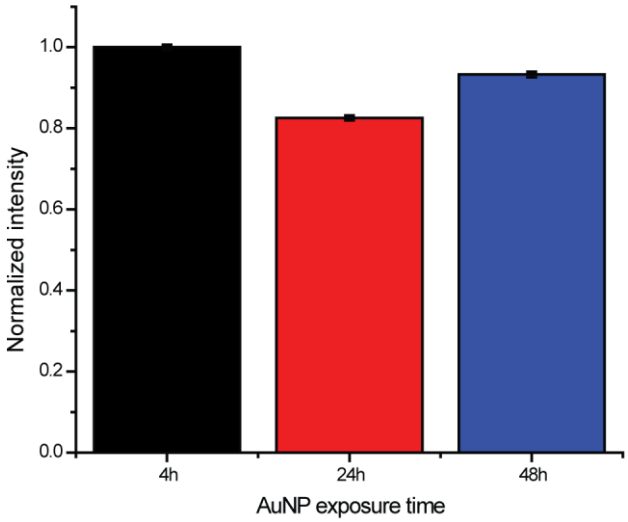

Figure 5.8. Comparison of time dependent LA-ICP-MS images of the spleen tissues (Error bars represent pixel to pixel deviation.) The normalized ion intensity is calculated by summing the relative pixel intensity for each image, dividing this sum by the size of each tissue slice and further normalizing by the total gold amounts in these organs as determined by ICP-MS of partial homogenates. For easier comparison of the three time points, the resulting value for the 4 h time point was set to a value of 1.

We next examined the effect of monolayer structure on NP stability *in vivo*. AuNP 1 and AuNP 5 were compared because we had previously demonstrated in cells that AuNPs without the tetraethyleneglycol (TEG) group are less stable.[34] NPs with slightly different headgroups had to be chosen because the slides used to mount the tissues gave an isobaric interference for the monolayers containing a TEG group and a tri-methyl ammonium headgroup. LDI-MS and LA-ICP-MS images of the spleen are consistent with our previous *in vitro* work in that the TEG-containing AuNP 1 is found to be more stable than AuNP 5, which is missing the TEG group (Figure 5.9). To best compare the two sets of images so that this conclusion can be made, we imaged two sets of tissues that had similar total gold amounts based on ICP-MS measurements of tissue homogenates (Figure 5.13). In separate experiments we found that the relative LDI ionization efficiencies of the two ligands are similar (Figure 5.10), allowing for a better comparison of the ion abundances in the LDI-MS images. Upon comparing the images in Figure 5.9 (left), the LDI-MS signals (shown in green) are brighter for AuNP 1, which indicate higher ligand signals, whereas the gold signals (shown in yellow) in the LA-ICP-MS images are similar for the two AuNPs. A more quantitative comparison can be made by summing the ion abundances in each pixel and dividing this value by the total area of the image (Figure 5.9 (right)), while also correcting for the slight differences in ionization efficiencies of the two monolayers (Figure 5.10). From such an analysis, both AuNPs are found to have similar abundances per unit area in the LA-ICP-MS images but quite different ion abundances are observed per unit area in the LDI-MS images (Figure 5.9 (right)). These comparisons indicate that the monolayer of AuNP 5 is less stable than the monolayer of AuNP 1.

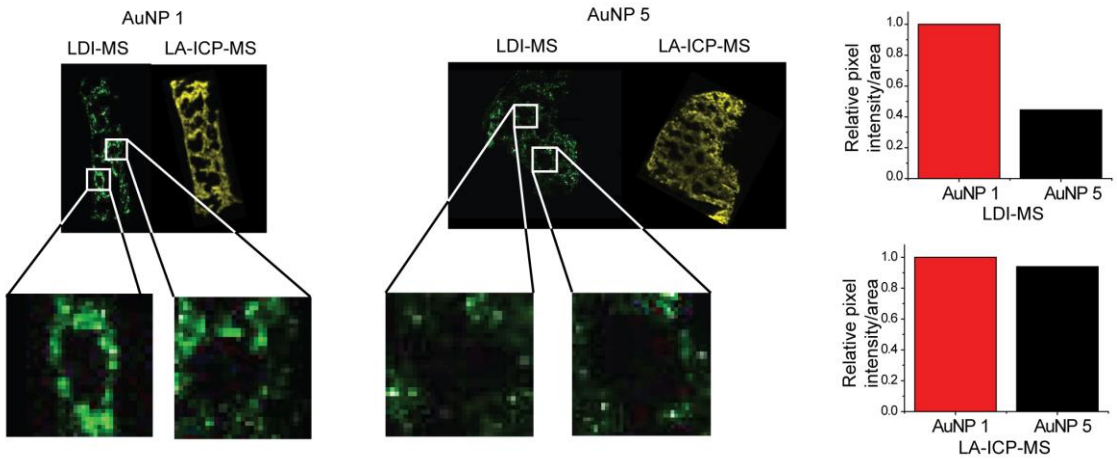

Figure 5.9. Comparison of the stability of AuNP 1 and AuNP 5 in the spleen. (Left) LDI-MS and LA-ICP-MS images showing the intact NP and Au distributions, respectively, in the spleens of mice IV-injected with either AuNP 1 or AuNP 5. The expanded zoomed-in regions illustrate the signal differences observed for AuNP 1 and AuNP 5 in the marginal zones of the spleen. (Right) Summed relative ion abundances of the Au and ligand ions from the LA-ICP-MS and LDI-MS images in the top part of the figure. The relative pixel intensity calculations are described in experimental section.

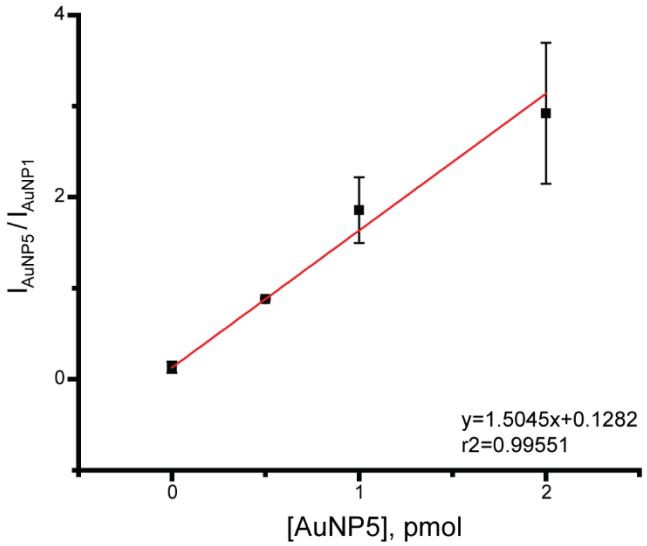

Figure 5.10. Comparison of the LDI-MS ionization efficiencies of AuNP 1 and AuNP 5. As described in our previous work,[11] cell lysate samples were used to determine the ionization efficiencies. A mixture of AuNPs (AuNP 1 = 1 pmol; AuNP 5 = various amounts) were spiked into HeLa cell lysate, and the mixture was transferred into a centrifuge tube to be centrifuged at 14000 rpm to obtain the pellet. The obtained pellet then was transferred onto the MALDI target. The slope of the graph indicates the ratio of the ionization efficiencies, and this value was used to modify the images of the spleen to enable an accurate comparison of the results.

More intriguing insight is obtained upon comparing the stability of AuNP 1 and 5 in different regions of the spleen. The stabilities of the AuNPs are different in two of the three regions of the spleen. H&E staining and Fe images from the LA-ICP-MS experiments identify these three regions of the spleen (Figure 5.11).

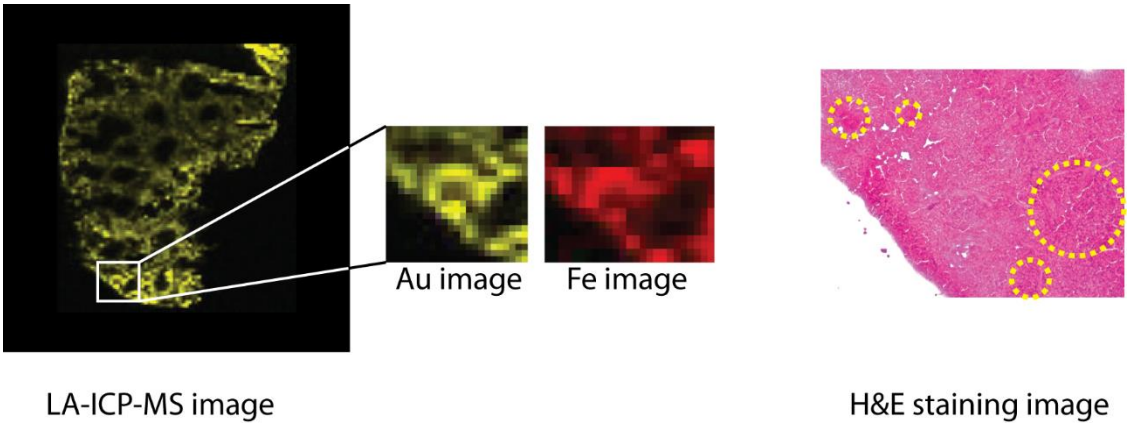

Figure 5.11. Example LA-ICP-MS and H&E staining images of a spleen tissue slice from a mouse injected with AuNP 5. The Fe image reflects the presence of the blood in the organ and can be used to readily distinguish between the red pulp and white pulp regions. The red pulp and marginal zone regions of the spleen filter the blood and therefore contain the highest concentration of Fe. Less Fe is found in the white pulp because the blood does not flow through this region of the spleen. The black regions in the Fe image represent the white pulp, and red regions indicate the red pulp. The marginal zone is the interface between the red and white pulp regions and extends ~ 40 μm from the white pulp. In the H&E stains, the pale pink color indicates the red pulp region, while the dark purple regions indicate the white pulp regions. Again, the marginal zone surrounds the white pulp regions but also can be seen in the H&E stains as a region with less dense coloring.

To compare NP stability in these different regions, the average ligand and gold signals for each spleen region were determined, as described in experimental section. From the comparison of the signals from AuNP 1 and AuNP 5, we observe that the ligand signals are different in certain spleen regions, while the gold signals are similar. Since ligand loss indicates the stability loss, we compared the ligand signals in each of the spleen regions in

reference to the gold levels. Analysis of the data in this way indicates that AuNP 1 and AuNP 5 have similar stability in the red pulp and white pulp, but AuNP 1 is slightly more stable in the marginal zone (Figure 5.12). The reason for the differences in AuNP stability in the different regions of the spleen can be somewhat explained by how blood is filtered in the spleen. Blood primarily flows through and is filtered in the red pulp, and not surprisingly relatively high levels of IV-injected NPs are found here.[38,39] In mice, there are monocytes in the red pulp that might act to phagocytose and thus destroy some of the filtered NPs,[40] but evidently both NPs have similar stability in this region. As for the marginal zone, only a portion of blood transits this region, where antigen-presenting cells are present and the exchange of the blood between the red and white pulp occurs. The immune response that can occur in this region might explain why the less stable AuNP 5 shows greater instability in this region. The similar stability in the white pulp may be due to the fact that both AuNPs are somewhat unstable in this region where high concentrations of lymphocytes are present that could equally degrade both NPs.

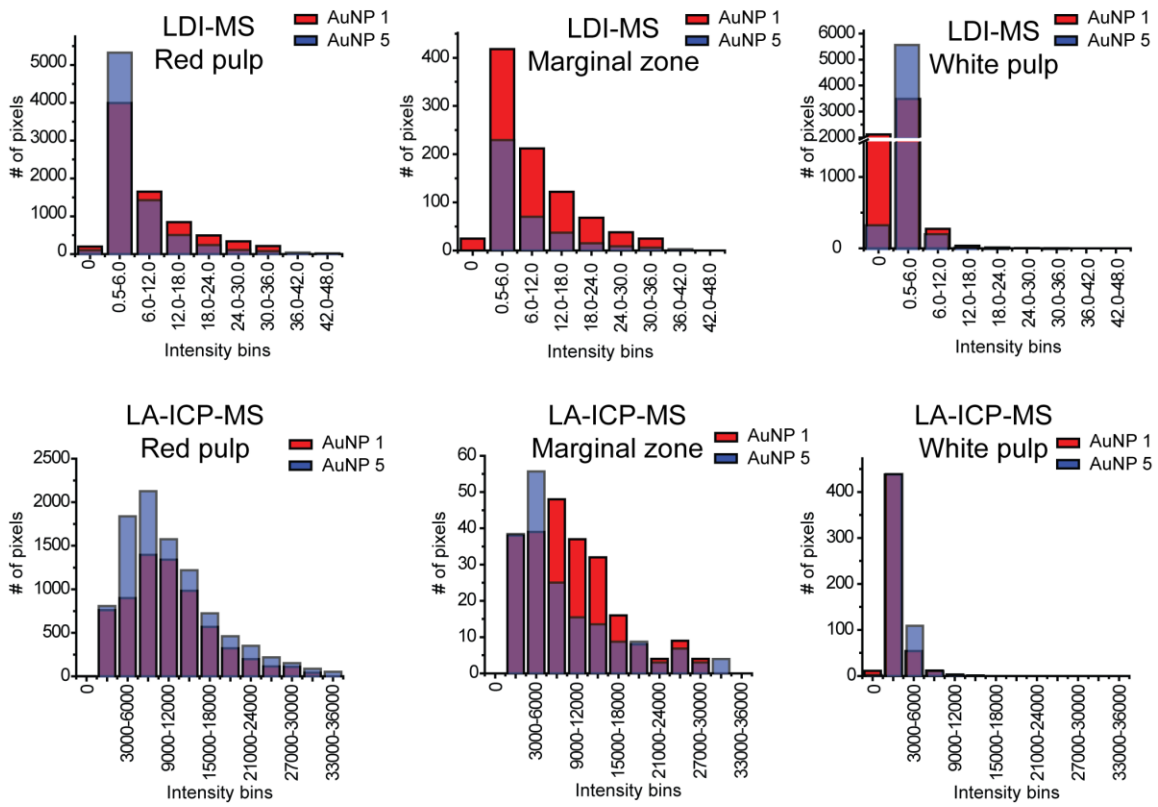

Figure 5.12. Overlayed LDI-MS and LA-ICP-MS histograms for the site specific regions of AuNP 1 and AuNP 5, indicating the signal intensity distributions of the ligands and Au, respectively, for AuNP 1 and AuNP 5. The larger bin numbers represent higher ion intensities. The most significant differences between the two AuNPs are found in the marginal zone, where the monolayer ligand signals for AuNP 1 have notably higher LDI-MS signal intensities.

5.3. Conclusion

In summary, we have demonstrated that LA-ICP-MS and LDI-MS imaging can be used together to monitor NP monolayer stability *in vivo*. In our approach, LA-ICP-MS imaging reports on the distribution of Au in tissues, and LDI-MS images reports on the

distributions of AuNPs containing intact monolayers. A comparison of the two images from adjacent tissue slices indicates whether or not the AuNPs are intact. The validity of this comparison was demonstrated first by observing the expected differences in the relative Au and monolayer ligand signals in the spleen and liver and then by observing the expected decrease of the ligand signal over time. The utility of obtaining site-specific stability information was then demonstrated by comparing the stability of two AuNPs in the spleen, where we find that NP stability is most different in the marginal zone of this organ, which is consistent with the biological makeup of this region. In future work we will develop quantitative imaging protocols that will enable a more quantitative measure of the site-specific stability of NPs *in vivo*. Such methods will provide critical insight into how to design NPs of the desired stability, from semi-stable materials used in drug delivery to more stable materials that are required in commercial products.

5.4. Experimental

5.4.1. Synthesis and characterization of the AuNPs

Using the Burst-Schiffrin two-phase synthesis method, 2 nm core AuNPs were synthesized.[41] Briefly, the Brust-Schiffrin two-phase synthesis method was used to synthesize pentanethiol-coated AuNPs with core diameters around 2 nm by reducing the Au salt. Once these AuNPs were synthesized, the Murray place exchange method was used to functionalize the AuNPs with the desired functionality.[42,43] Previously synthesized ligands were mixed in excess with the pentanethiol-coated AuNPs and allowed to place-exchange. After the place exchange reaction, the sample was filtered and dialyzed for three days to remove the excess ligand/pentanethiol mix.

The structures of the AuNPs used in the study can be found in Figure 5.1. The AuNP sizes were determined by transmission electron microscopy (TEM) and dynamic light scattering (DLS), and their surface charges were obtained from zeta potential measurements as previously described.[33,34] Table 5.1 shows the TEM, DLS and zeta potential measurements of all the AuNPs studied in this work. All AuNPs were also characterized by laser-desorption/ionization mass spectrometry (LDI-MS) to confirm the identity of the monolayer coating.[44]

Table 5.1. Summary of the TEM, DLS, and zeta potential results for the studied AuNPs.

	TEM (nm)	**DLS (nm)**	**Zeta potential**
AuNP 1	2.0 ± 0.1	14 ± 4	+ 21± 6
AuNP 2	2.2 ± 0.3	8 ± 2	+ 26 ± 9
AuNP 3	1.9 ± 0.2	11 ± 2	+ 24 ± 9
AuNP 4	1.9 ± 0.2	13 ± 2	+ 22 ± 8
AuNP 5	2.2 ± 0.3	8 ± 1	+ 24 ± 4

5.4.2. Animal experiments

Solutions of individual AuNPs were prepared at concentrations of 2 μM, and 50 μL of each AuNP solution was injected into Balb/c mice *via* the tail vein. After certain time points, the mice were sacrificed *via* inhalation of carbon dioxide and cervical dislocation. Organs were then collected and prepared for analysis. Each organ that was collected was flash-frozen using liquid N_2. These frozen tissues were then sliced to 12 μm using a LEICA CM1850 cyrostat and placed on either an ITO glass slide (for AuNP 1-4 containing samples) or a metal slide (for AuNP 1 and AuNP 5 for the spleen comparison) for LDI-MS

imaging. Adjacent slices were placed on a regular glass slide for LA-ICP-MS imaging and H&E staining.

5.4.3. H&E staining

Tissue slices were stained using a kit that was obtained from ThermoFisher Scientific. Adjacent slices of the tissues were used by immersing the tissues into distilled water, hematoxylin, bluing reagent, 95% ethanol, eosin-y, 100% ethanol and xylene in the order described by the kit's manual.

5.4.4. LDI-MS instrument parameters

LDI-MS imaging was done using a Bruker Autoflex III MALDI-TOF mass spectrometer (Bruker Daltonics, Bremen, Germany), which is equipped with a Smartbeam 2 Nd:YAG laser. LDI-MS images were constructed using the FlexImaging 2.1 software package. LDI-MS operating conditions were as follows: ion source 1 = 19.00 kV, ion source 2 = 16.60 kV, lens voltage = 8.44 kV, reflector voltage = 20.00 kV, reflector voltage 2 = 9.69 kV, and positive reflectron mode with a mass range of 100−1200 Da. A total of 50 laser shots were measured per position. In almost all cases, the step width between laser shots was 25 μm. The laser energy was optimized to ~ 61 μJ/pulse.

5.4.5. LA-ICP-MS instrumental parameters

A Perkin Elmer Nexion 300 X ICP-MS (Perkin Elmer, Shelton, CT, USA) and a CETAC LSX-213 G2 laser ablation system (Photon Machines, Omaha, NE, USA) were used for the LA-ICP-MS imaging experiments. The optimum parameters for the imaging are given in Chapter 2.

5.4.6. Relative pixel intensity calculation

Using ImageJ for each tissue image, a histogram of the pixel intensity distribution was obtained in the RGB mode (RGB corresponds to the red green blue color channels present in a given image). These histogram values were then copied to Excel into corresponding two columns; one with the RGB value and the second one with the intensity count. The relative pixel intensities were then calculated by multiplying the RGB value with the pixel count and divided by the total number of pixel count. Using ImageJ, the areas of the tissues were obtained and used to calculate the relative pixel intensity per area. The relative pixel intensity calculation is given below.

$$Relative\ pixel\ intensity = \frac{\Sigma(pixel\ intensity)x\ (pixel\ number)}{\Sigma\ pixel\ number}$$

5.4.7. ICP-MS sample preparation and measurements

The organs were dissolved using a 3:1 (v:v) mixture of nitric acid (68%) and hydrogen peroxide (30%) to digest each organ overnight. The next day, 0.5 mL of aqua regia [3:1 (v:v) mixture of nitric acid and hydrochloric acid] was added and the sample was then diluted to 10 mL using de-ionized water. (**Aqua regia is highly corrosive and must be handled with extreme caution.**) Gold standard solutions (gold concentrations: 20, 10, 5, 2, 1, 0.5, 0.2 and 0 ppb) were prepared prior to each experiment. A Perkin Elmer NEXION 300X ICP mass spectrometer (Waltham, MA) was used to analyze the samples. Prior to the analysis, daily performance measurements were done to ensure the instrument was operating under optimum conditions. The ^{197}Au signals were obtained using the standard operating mode.

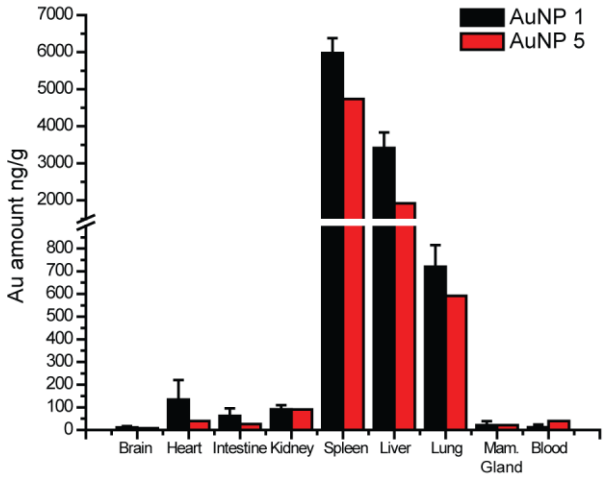

Figure 5.13. Total gold amounts in ng/g in mouse tissue homogenates from ICP-MS measurements. Mice were IV injected with 50 µL of a 2 µM solution of the indicated AuNP. (n = 3 for AuNP 1, but n = 1 for AuNP 5 because of two unsuccessful injections of the NPs into the three mice).

5.5. References

[1] Rana, S.; Bajaj, A.; Mout, R.; Rotello, V. M. *Adv. Drug Deliver. Rev.* **2012**, *64*, 200-216.

[2] Verma, A.; Uzun, O.; Hu, Y.; Hu, Y.; Han, H.-S.; Watson, N.; Chen, S.; Irvine, D. J.; Stellacci, F. *Nat. Mater.* **2008**, *7*, 588-595.

[3] Zhu, Z.-J.; Yeh, Y.-C.; Tang, R.; Yan, B.; Tamayo, J.; Vachet, R. W.; Rotello, V. M. *Nat. Chem.* **2011**, *3*, 963-968.

[4] Park, Y. Il.; Lee, K. T.; Suh, Y. D.; Hyeon, T. *Chem. Soc. Rev.* **2015**, *44*, 1302-1317.

[5] Malmsten, M. *Curr. Opin. Colloid Interface Sci.* **2013**, *18*, 468-480.

[6] Ballou, B.; Lagerholm, B. C.; Ernst, L. A.; Bruchez, M. P.; Waggoner, A. S. *Bioconjug. Chem.* **2004**, *15*, 79-86.

[7] Hong, R.; Fernandez, J. M.; Nakade, H.; Arvizo, R.; Emrick, T.; Rotello, V. M. *Chem. Commun.* **2006**, 2347-2349.

[8] Lia, D.; Lia, G.; Guoa, W.; Lia, P.; Wanga, E.; Wang, J. *Biomaterials* **2008**, *29*, 2776-2782.

[9] Han, G.; Chari, N. S.; Verma, A.; Hong, R.; Martin, C. T.; Rotello, V. M. *Bioconjug. Chem.* **2005**, *16*, 1356–1359.

[10] Chompoosor, A.; Han, G.; Rotello, V. M. *Bioconjug. Chem.* **2008**, *19*, 1342–1345.

[11] Zhu, Z.-J.; Ghosh, P. S.; Miranda, O. R.; Vachet, R. W.; Rotello, V. M. *J. Am. Chem. Soc.* **2008**, *130*, 14139−14143.

[12] Jiang, Y.; Huo, S.; Mizuhara, T.; Das, R.; Lee, Y.-W.; Hou, S.; Moyano, D. F.; Duncan, B.; Liang, X.-J.; Rotello, V. M. *ACS Nano* **2015**, *9*, 9986-9993.

[13] You, C. C.; De, M.; Rotello, V. M. *Curr. Opin. Chem. Biol.* **2005**, *9*, 639-646.

[14] Lin, J.; Zhang, H.; Chen, Z.; Zheng, Y. *ACS Nano* **2010**, *4*, 5421-5429.

[15] Chithrani, B. D.; Chan, W. C. W. *Nano Lett.* **2007**, *7*, 1542-1550.

[16] Lesniak, A.; Fenaroli, F.; Monopoli, M. P.; Åberg, C.; Dawson, K. A.; Salvati, A. *ACS Nano* **2012**, *6*, 5845-5857.

[17] Saha, K.; Rahimi, M.; Yazdani, M.; Kim, S. T.; Moyano, D. F.; Hou, S.; Das, R.; Mout, R.; Rezaee, F.; Mahmoudi, M.; Rotello V. M. *ACS Nano* **2016**, *10*, 4421-4430.

[18] Monopoli, M. P.; Åberg, C.; Salvati, A.; Dawson K. A. *Nat. Nanotechol.* **2012**, *7*, 779-786.

[19] Jong, W. H. D.; Hagens, W. I.; Krystek, P.; Burger, M. C.; Sips, A. J.A.M.; Geertsma, R. E. *Biomaterials* **2008**, *29*,1912-1919.

[20] Mahon, E.; Salvati, A.; Bombelli, F. B.; Lynch, I.; Dawson K. A. *J. Control. Release* **2012**, *161*, 164-174.

[21] Hinterwirth, H.; Kappel, S.; Waitz, T.; Prohaska, T.; Lindner, W.; Lämmerhofer, M. *ACS Nano* **2013**, *7*, 1129-1136.

[22] Medintz, I. L.; H. T. Uyeda, Goldman E. R.; Mattoussi H. *Nat. Mater.* **2005**, *4*, 435-446.

[23] Soenen, S. J.; Parak, W. J.; Rejman, J.; Manshian, B. *Chem. Rev.* **2015**, *115*, 2109-2135.

[24] Pace, H. E.; Lesher, E. K.; Ranville, J. F. *Environ. Toxicol. Chem.* **2010**, *29*, 1338-1344.

[25] Hong, R.; Han, G.; Fernandez, J. M.; Kim, B. J.; Forbes, N. S.; Rotello, V. M. *J. Am. Chem. Soc.* **2006**, *128*, 1078-1079.

[26] Hostetler, M. J.; Templeton, A. C.; Murray, R. W. *Langmuir* **1999**, *15*, 3782-3789.

[27] Donkers, R. L.; Song, Y.; Murray, R. W. *Langmuir* **2004**, *20*, 4703-4707.

[28] Montalti, M.; Prodi, L.; Zaccheroni, N.; Baxter, R.; Teobaldi, G.; Zerbetto, F. *Langmuir* **2003**, *19*, 5172-5174.

[29] Stewart, M. H.; Susumu, K.; Mei, B. C.; Medintz, I. L.; Delehanty, J. B.; Blanco-Canosa, J. B.; Dawson, P. E.; Mattoussi, H. *J. Am. Chem. Soc.* **2010**, *132*, 9804-9813.

[30] Wu, L.; Zhang, J.; Watanabe, W. *Adv. Drug Deliver. Rev.* **2011**, *63*, 456-469.

[31] Elci, S. G.; Jiang, Y.; Yan, B.; Kim, S. T.; Saha, K.; Moyano, D. F.; Yesilbag Tonga, G.; Jackson, L. C.; Rotello, V. M.; Vachet, R. W. *ACS Nano* **2016**, *10*, 5536-5542.

[32] Elci, S. G.; Yan, B.; Kim, S. T.; Saha, K.; Jiang, Y.; Klemmer, G. A.; Moyano, D. F.; Yesilbag Tonga, G.; Rotello V. M.; Vachet, R. W. *Analyst* **2016**, *141*, 2418-2425.

[33] Yan, B.; Kim, S. T.; Kim, C. S.; Saha, K.; Moyano, D. F.; Xing, Y.; Jiang, Y.; Roberts, A. L.; Alfonso, F. S.; Rotello, V. M.; Vachet, R. W. *J. Am. Chem. Soc.* **2013**, *135*, 12564-12567.

[34] Zhu, Z. J.; Tang, R.; Yeh, Y. C.; Miranda, O. R.; Rotello, V. M.; Vachet, R. W. *Anal. Chem.* **2012**, *84*, 4321-4326.

[35] Arvizo, R. R.; Miranda, O. R.; Moyano, D. F.; Walden, C. A.; Giri, K.; Bhattacharya, R.; Robertson, J. D.; Rotello, V. M.; Reid, J. M.; Mukherjee, P. *Plos One* **2011**, *6*, e24374.

[36] Yook, S.; Lu, Y.; Jeong, J. J.; Cai, Z.; Tong, L.; Alwarda, R.; Pignol, J.-P, Winnik, M. A.; Reilly, R. M. *Biomacromolecules* **2016**, *17*, 1292-1302.

[37] Al-Turk, W. A.; Stohs, S. J. *Drug Chem. Toxicol.* **1981**, *4*, 37-48.

[38] Cesta, M. F. *Toxicol. Pathol.* **2006**, *34*, 455-465.

[39] Mebius, R. E.; Kraal, G. *Nat. Rev. Immunol.* **2005**, *5*, 606-616.

[40] Swirski, F. K.; Nahrendorf, M.; Etzrodt, M.; Wildgruber, M.; Cortez-Retamozo, V.; Panizzi, P.; Figueiredo, J. L.; Kohler, R. H.; Chudnovskiy, A.; Waterman, P.; Aikawa, E.; Mempel, T. R.; Libby, P.; Weissleder, R.; Pittet, M. J. *Science* **2009**, *325*, 612-616.

[41] Burst, M.; Walker, M.; Bethell, D.; Schiffrin, D. J.; Whyman, R. *J. Chem. Soc., Chem. Commun.* **1994**, 801-802.

[42] Hong R.; Emrick T.; Rotello V. M. *J. Am. Chem. Soc.* **2004**, *126*, 13572-13583.

[43] Jiang, Y.; Huo, S.; Mizuhara, T.; Das, R.; Lee, Y.-W.; Hou, S.; Moyano, D. F.; Duncan, B.; Liang, X.-J.; Rotello V. M. *ACS Nano* **2015**, *9*, 9986-9993.

[44] Yan, B.; Zhu, Z. J.; Miranda, O. R.; Chompoosor, A.; Rotello, V. M.; Vachet, R. W. *Anal. Bioanal. Chem.* **2010,** *396*, 1025-1035.

[45] Arnon, T. I.; Horton, R. M.; Grigorova, I. L.; Cyster, J. G. *Nature* **2013**, *493*, 684-688.

CHAPTER 6

SUMMARY AND FUTURE WORK

6.1 Dissertation Summary

In this dissertation, the mass spectrometric imaging of AuNPs investigated to reveal their sub-organ biodistribution and stability *in vivo*. Using elemental imaging technique ICP-MS and its hyphenation with a laser ablation system provided sub-organ biodistribution information about AuNPs. Using this method, the quantities of AuNPs in sub-organ regions were also assessed. In addition, the dual mode imaging of AuNPs provided by LA-ICP-MS and LDI-MS allowed us to monitor the stability of the AuNPs in a site-specific manner.

First, using LA-ICP-MS imaging, quantitative images of the AuNPs were obtained. The matrix-matched quantification approach was investigated to select an appropriate matrix that could be used to quantify AuNPs in tissue. Chicken breast and beef liver were found to be appropriate for obtaining accurate quantification. During these analyses, differences were observed in the biodistribution of AuNPs with varying surface functionalities and these findings were further investigated. Our approach provides useful insight into not only how NPs distribute but also how they are processed *in vivo*. In addition, proper matrix selection is essential for accurate quantification of AuNPs in tissues.

Second, inkjet printing as an alternative quantification approach was studied for LA-ICP-MS imaging. Initial findings show no variation in the day-to-day printing and demonstrate that linear calibration curves can be obtained. Printing of the standard pattern

and imaging with a AuNP free mouse tissue also showed linearity in calibration curve. Application towards its use with AuNP injected mouse tissues will be investigated in the future. In addition to be an alternative quantification strategy for the LA-ICP-MS imaging, this method will also provide a standard addition like approach, which will be adding standards to the tissue that is being imaged. By doing so, the "matrix matching" will be ideal.

Third, the initial observation of the differences in the biodistribution of AuNPs in mouse tissues was further investigated. Different AuNP surface functionalities lead to differences in the biodistribution of the AuNPs. With the help of H&E staining, the sub-organ regions were located, and the amounts of AuNPs in these sub-organ levels were determined using the quantitative images obtained.

Finally, a dual mode imaging approach that combined both elemental and molecular imaging was used to investigate the stability of AuNPs. Organ biocomposition, time of exposure, and NP surface chemistry, were examined to determine the stability of the particles *in vivo*. A comparison of the stability in liver and spleen revealed that different biochemical compositios of the organ can substantially affect the stability of NPs in vivo. NPs slowly lose their stability over time within the same organ, indicating degradation of AuNPs. Different surface monolayer attached to the AuNPs also caused changes in their stability within same organ biocomposition.

Overall, the findings obtained in this dissertation should improve our understanding of the *in vivo* fate of AuNPs. It also opens up new areas of research that could help us design better monolayers for AuNPs used in drug delivery applications. Possible areas of future work are described in the next section.

6.2 Future directions

In the following sections, potential new applications and improvements for mass spectrometric imaging of AuNPs will be described to understand more about the interaction of AuNPs with biosystems.

6.2.1 Quantitative dual mode imaging for stability of AuNPs *in vivo*

Qualitative results demonstrate that the stability of NPs are affected by three parameters. Although it was concluded that NP stability differed under these parameters, it is important to quantify the stability of the NPs. Chapters 2 and 3 demonstrated the quantitative ability and methods that can be applied for LA-ICP-MS imaging. These same strategies could also be applied for obtaining quantitative images of the AuNPs in LDI-MS imaging. Matrix-matched quantification standards or inkjet-printed standards could be prepared, and they could be used for quantification of both the surface monolayer and the core of the AuNPs. One of the biggest challenge for the applicability of these methods is to accurately obtain the monolayer amount that is present in the standard samples. That can be done by digesting the AuNPs with KI/I_2 solution and then analyzing the resulting solution by HPLC to find the quantity of the monolayer present on the AuNPs.

6.2.2 Dual mode imaging to track nanocapsules *in vivo*

For the delivery of the drug molecules, nanocapsules can be used to effectively encapsulate the therapeutic cargo.[1-3] Nanocapsules encapsulate the drug molecules, which can then carry the cargo to the desired location in the biosystem. Among various types of

nanocapsules, nanoparticle-stabilized nanocapsules (NPSCs) provide better stability compared their microcapsule counterparts and the oil-in-water emulsion created is ideal for delivery of hydrophobic drugs.[3] Dual mode imaging could be used to both track the delivery of the drug molecules and to understand the effects of the remaining nanoparticles *in vivo*. Elemental imaging of the AuNP core using LA-ICP-MS would provide the location of the AuNPs, while, the molecular imaging using LDI-MS would reveal the location of the drug molecules and it would allow us to track and obtain information pertaining to the success of the delivery.

6.2.3 Modulation of the design of the NPs for immune response

Investigating the sub-organ biodistribution of AuNPs demonstrated that the NPs surface charge dictates the biodistribution. One of the findings showed us that AuNPs with a neutral charge accumulate more in the immunogenic parts of the tissues. This information can be used to modulate AuNPs surfaces to control the immune response generated.[4] These newly designed AuNPs could then be used in therapeutic applications. Previously, hydrophobic surface functionalities were investigated for their immune response capability and findings demonstrated that a linear relationship between the immune response generated and the hydrophobicity of the AuNPs exists.[5] Although these results are promising, one of the concerns with the hydrophobic AuNPs are their cytotoxicity. Since our results demonstrated that the neutral surface functionalities can also trigger the immune response, design of new particles that having both of these monolayers to modulate the immune response generated could overcome this problem. For initial design, mixed monolayer AuNPs with neutral and hydrophobic ligands could be synthesized readily and used as a testbed.

6.2.4. 3D imaging of whole tissue using LA-ICP-MS

A 3D imaging approach would be beneficial since the 2D representation of the tissues are limited to a certain section of the tissue and the tissue inhomogeneity may result in an uncharacteristic representation of small scale features within individual 2D sections. In addition, 3D imaging could reveal isolated hotspots in larger volumes within the organ that might not be seen in a single cross-section. Consecutive sections of the tissue samples can be obtained by carefully slicing the tissue samples and images of the tissues can be generated using LA-ICP-MS. With a house built software (e.g MATLAB script), the images obtained from LA-ICP-MS analysis would compiled to form the 3D image of the whole tissue. Developments in the LA system and ICP-MS instrumentation would also help reduce the time required for the analysis of the samples.

6.3. References

[1] Somiyaa, M.; Kurodaa, S. *Adv. Drug Deliv. Rev.* **2015**, *95*, 77-89.

[2] Crespy, D.; Lv, L. P.; Landfester, K. *Nanoscale Horiz.* **2016**, *1*, 268-271.

[3] Yang, X.-C.; Samanta, B.; Agasti, S. S.; Jeong, Y.; Zhu, Z.; Rana, S.; Miranda, O. R.; Rotello, V. M. *Angew. Chem. Int. Ed.* **2011**, *50*, 477-481.

[4] Luo, Y.-H.;Chang, L. W.; Lin, P. *Biomed Res Int.* **2015**, *2015*, 143720.

[5] Moyano, D. F.; Goldsmith, M.; Solfiell, D. J.; Landesman-Milo, D.; Miranda, O. R.; Peer, D.; Rotello, V. M. *J. Am. Chem. Soc.* **2012**, *134*, 3965-3967.

APPENDIX

CHANGES MAY OCCUR IN LIVER BIOCOMPOSITION AFTER THE LOSS OF AUNPS STABILITY

AuNP stability in the liver is low even only 4 hours after injection. It is known that liver has a high concentration of biogenic thiols, such as glutathione (GSH), cysteine (Cys) and homocycteine (Hcys).[1,2] The main role of these biomolecules are to detoxify the liver and remove the reactive oxygen species (ROS). GSH is one of the most common and abundant biogenic thiol in the liver and it takes places in oxidative detoxification, especially the removal of the peroxidation products.[3,4] Biogenic thiols, such as GSH, are likely to compete with the monolayers for binding to the surface of the Au core.[5] The stability loss of the AuNPs in liver indicates that the biogenic thiols successfully displace the monolayers. As a result of these stability loss, it is possible that the concentration of active biogenic thiols is decreased due to the presence of the AuNPs. To confirm this hypothesis further analysis would be required. If the biogenic thiols in liver do decrease in concentration, then less thiols would be available for scavenging ROS,[6] an associated increase in ROS levels could lead to the cell and organ dysfunction. The extent to which this occurs, however, would depend upon the levels of biogenic thiols that are recruited to destabilize the AuNPs. One might also predict that oxidative damage to the liver would increase, and this occurrence could be confirmed by measuring the extent of protein oxidation in this tissue.

References

[1] Prakash, M.; Shetty, M. S.; Tilak, P.; Anwar, N. *Online J. Health Allied Scs.* **2009**, *8*, 2-9.

[2] Lu, S. C. *Biochim. Biophys. Acta* **2013**, *1830*, 3143-3153.

[3] Dalle-Donne, I.; Aldini, G.; Carini, M.; Colombo, R.; Rossi, R.; Milzani, A. *J. Cell. Mol. Med.* **2006**, *10*, 389-406.

[4] Griffiths, H. R.; Møller, L.; Bartosz, G.; Bast, A.; Bertoni-Freddari, C.; Collins, A.; Cooke, M.; Coolen, S.; Haenen, G.; Hoberg, A.-M. *J. Mol. Asp. Med.* **2002**, *23*, 101-208.

[5] Hong, R.; Han, G.; Fernandez, J. M.; Kim, B. J.; Forbes, N. S.; Rotello, V. M. *J. Am. Chem. Soc.*, **2006**, *128*, 1078-1079.

[6] Martinez-Chantar, M. L.; Corrales, F. J.; Martinez-Cruz, L. A.; Garcia-Trevijano, E. R.; Huang, Z.-Z.; Chen, L.; Kanel G.; Avila, M. A.; Mato, J. M.; Lu, S. C. *FASEB J.* **2002**, *16*, 1292-1294.

BIBLIOGRAPHY

Aggarwal, P.; Hall, J. B.; McLeland, C.B.; Dobrovolskaia, M. A.; McNeil, S. E. *Adv. Drug Deliver. Rev.* **2009**, *61*, 428-437.

Albanese, A.; Tang, P. S.; Chan, W. C. W. *Annu. Rev. Biomed. Eng.* **2012**, *14*, 1-16.

Allabashi, R.; Stach, W.; De La Escosura-Muñiz, A.; Liste-Calleja, L.; Merkoçi, A. *J. Nanopart. Res.* **2009**, *11*, 2003-2011.

Al-Turk, W. A.; Stohs, S. J. *Drug Chem. Toxicol.* **1981**, *4*, 37-48.

Ando, J.; Yano, T.; Fujita, K.; Kawata, S. *Phys. Chem. Chem. Phys.* **2013**, *15*, 13713-13722.

Ando, J.; Fujita, K.; Smith, N.I.; Kawata, S. *Nano Lett.* **2011**, *11*, 5344-5348.

Angel, L. A.; Majors, L. T.; Dharmaratne, A. C.; Dass, A. *ACS Nano* **2010**, *4*, 4691-4700.

Aoshi, T.; Zinselmeyer, B. H.; Konjufca, V.; Lynch, J. N.; Zhang, X.; Koide, Y.; Miller, M. J. *Immunity* **2008,** *29*, 476–486.

Arnon, T. I.; Horton, R. M.; Grigorova, I. L.; Cyster, J. G. *Nature* **2013**, *493*, 684-688.

Arvizo, R. R.; Miranda, O. R.; Thompson, M. A.; Pabelick, C. M.; Bhattacharya, R.; Robertson, J. D.; Rotello, V. M.; Prakash, Y. S.; Mukherjee, P. *Nano Lett.* **2010**, *10*, 2543-2548.

Arvizo, R. R.; Miranda, O. R.; Moyano, D. F.; Walden, C. A.; Giri, K.; Bhattacharya, R.; Robertson, J. D.; Rotello, V. M.; Reid, J. M.; Mukherjee, P. *Plos One*, **2011**, *6*, e24374.

Ballou, B.; Lagerholm, B. C.; Ernst, L. A.; Bruchez, M. P.; Waggoner, A. S. *Bioconjug. Chem.* **2004**, *15*, 79-86.

Baratta, J. L.; Ngo, A.; Lopez, B.; Kasabwalla, N.; Longmuir, K. J.; Robertson, R. T. *Histochem Cell Biol.* **2009**, *131*, 713-726.

Becker, J. S.; Matusch, A.; Wu, B. *Anal. Chim. Acta* **2014**, *835*, 1-18.

Becker, J. S.; Becker, J. S. *Biomed. Spectrosc. Imaging* **2012**, *1*, 187-204.

Becker, J. S. *Int. J. Mass Spectrom.* **2010**, *289*, 65-75.

Becker, J. S.; Zoriy, M. V.; Pickhardt, C.; Palomero-Gallagher, N.; Zilles, K. *Anal. Chem.* **2005**, *77*, 3208-3216.

Behra, R.; Krug, H. *Nat. Nanotechnol.* **2008**, *3*, 253-254.

Bera, D.; Qian, L.; Tseng, T. K.; Holloway, P. H. *Materials* **2010**, *3*, 2260-2345.

Berry, K. A. Z.; Li, B. L.; Reynolds, S. D.; Barkley, R. M.; Gijon, M. A.; Hankin, J. A.; Henson, P. M.; Murphy, R. C. *J. Lipid Res.* **2011**, *52*, 1551-1560.

Bilzer, M.; Roggel, F.; Gerbes, A. L. *Liver International* **2006**, *26*, 1175-1186.

Boisselier, E.; Astruc, D. *Chem. Soc. Rev*. **2009**, *38*, 1759-1782.

Bonta, M.; Lohninger, H.; Marchetti-Deschmanna, M.; Limbeck, A. *Analyst* **2014**, *139*, 1521-1531.

Brust, M.; Walker, M.; Bethell, D.; Schiffrin, D.J.; Whyman, R.J. *Chem. Soc. Chem. Comm.* **1994**, 801-802.

Büchner, T.; Drescher, D.; Traub, H.; Schrade, P.; Bachmann, S.; Jakubowski, N.; Kneipp, J. *Anal. Bioanal. Chem.* **2014**, *406*, 7003-7014.

Castellana, E. T.; Russell, D. H. *Nano Lett.* **2007**, *7*, 3023-3025.

Cha, S. W.; Song, Z. H.; Nikolau, B. J.; Yeung, E. S. *Anal. Chem.* **2009**, *81*, 2991-3000.

Cesta, M. F. *Toxicol. Pathol.* **2006**, *34*, 455-465.

Chen, S.; Xiong, C.; Liu, H.; Wan, Q.; Hou, J.; He, Q.; Badu-Tawiah, A.; Nie, Z. *Nat. Nanotechnol.* **2015**, *10*, 176-182.

Cheng, Y.; Meyers, J. D.; Broome, A. M.; Kenney, M. E.; Basilion, J. P.; Burda, C. *J. Am. Chem. Soc.* **2011**, *133*, 2583-2591.

Cheng, X.; Tian, X.; Wu, A.; Li, J.; Tian, J.; Chong, Y.; Chai, Z.; Zhao, Y.; Chen, C.; Ge, C. *ACS Appl. Mater. Interfaces* **2015**, *7*, 20568-20575.

Chithrani, B. D.; Chan, W. C. W. *Nano Lett.* **2007**, *7*, 1542-1550.

Cho, E. C.; Xie, J. W.; Wurm, P. A.; Xia, Y. N. *Nano Lett.* **2009**, *9*, 1080-1084.

Choi, H. S.; Liu, W.; Liu, F.; Nasr, K.; Misra, P.; Bawendi, M. G.; Frangioni, J. V. *Nat. Nanotechnol.* **2009**, *5*, 42-47.

Choi, H. S.; Liu, W.; Misra, P.; Tanaka, E.; Zimmer, J. P.; Ipe, B. I.; Bawendi, M. G.; Frangioni, J. V. *Nat. Biotechnol.* **2007**, *25*, 1165-1170.

Chompoosor, A.; Han, G.; Rotello, V. M. *Bioconjug. Chem.* **2008**, *19*, 1342–1345.

Claverie, F.; Malherbe, J.; Bier, N.; Molloy, J. L.; Long, S. E. *Anal. Chem.* **2013**. *85*, 3584-3591.

Cobley, C. M.; Chen, J.; Cho, E. C.; Wang, L. V.; Xia, Y. *Chem. Soc. Rev.* **2011**, *40*, 44-56.

Colvin, V. L. *Nat. Biotechnol.* **2003**, *21*, 1166-1170.

Crespy, D.; Lv, L. P.; Landfester, K. *Nanoscale Horiz.*, **2016**, *1*, 268-271.

Creran, B.; Yan, B.; Moyano, D. F.; Gilbert, M. M.; Vachet, R. W.; Rotello, V. M. *Chem. Comm.* **2012**, *48*, 4543-4545.

Daniel, M. C.; Astruc, D. *Chem. Rev.* **2004**, *104*, 293-346.

Dass, A.; Stevenson, A.; Dubay, G. R.; Tracy, J. B.; Murray, R. W. *J. Am. Chem. Soc.* **2008**, *130*, 5940-5946.

Dass, A.; Holt, K.; Parker, J. F.; Feldberg, S. W.; Murray, R. W. *J. Phys. Chem. C* **2008**, *112*, 20276-20283.

Dalle-Donne, I.; Aldini, G.; Carini, M.; Colombo, R.; Rossi, R.; Milzani, A. *J. Cell. Mol. Med.* **2006**, *10*, 389-406.

De, M.; Ghosh, P. S.; Rotello, V. M. *Adv. Mater.* **2008**, *20*, 4225-4241.

De Jong, W. H.; Hagens, W. I.; Krystek, P.; Burger, M. C.; Sips, A. J.A.M.; Geertsma, R. E. *Biomaterials* **2008**, *29*, 1912-1919.

Decuzzi, P.; Godin, B.; Tanaka, T.; Lee, S. Y.; Chiappini, C.; Liu, X.; Ferrari, M. *J. Control. Release* **2010**, *141*, 320-327.

Demoy, M.; Gibaud, S.; Andreux, J. P.; Weingarten, C.; Gouritin, B.; Couvreur, P. *Pharm. Res.* **1997**, *14*, 463-468.

Donkers, R. L.; Song, Y.; Murray, R. W. *Langmuir* **2004**, *20*, 4703-4707.

Drescher, D.; Kneipp, J. *J. Chem. Soc. Rev*. **2012**, *41*, 5780-5799.

Drescher, D.; Giesen, C.; Traub, H.; Panne, U.; Kneipp, J.; Jakubowski, N. *Anal. Chem.* **2012**, *84*, 9684-9688.

Dreaden, E. C.; Alkilany, A. M.; Huang, X.; Murphy, C. J.; El-Sayed, M. A. *Chem. Soc. Rev.* **2012**, *41*, 2740-2779.

Duan, X.; Li, Y. *Small* **2013**, *9*, 1521-1532.

Duncan, B.; Kim, C.; Rotello, V. M. *J. Control. Release* **2010**, *148*, 122-127.

Dwivedi, A. D.; Dubey, S. P.; Sillanpää, M.; Kwon, Y.-N.; Lee, C.; Varma, R. S. *Coord. Chem. Rev.* **2015**, *287*, 64-78.

Dykman, L. A.; Khlebtsov, N. G. *Chem. Rev.* **2014**, *114*, 1258-1288.

Elci, S. G.; Jiang, Y.; Yan, B.; Kim, S. T.; Saha, K.; Moyano, D. F.; Yesilbag Tonga, G.; Jackson, L. C.; Rotello, V. M.; Vachet, R. W. *ACS Nano* **2016**, *10*, 5536-5542.

Elci, S. G.; Yan, B.; Kim, S. T.; Saha, K.; Jiang, Y.; Klemmer, G. A.; Moyano, D. F.; Yesilbag Tonga, G.; Rotello V. M.; Vachet, R. W. *Analyst* **2016**, *141*, 2418-2425.

Ernsting, M. J.; Murakami, M.; Roy, A.; Li, S.-H. *J. Control. Release* **2013**, *172*, 782-794.

Faraday, M. *Philos. Trans. R. Soc. London* **1857**, *147*, 145-181.

Farre, M.; Sanchis, J.; Barcelo, D. *Trend. Anal. Chem.* **2011**, *30*, 517-527.

Fields-Zinna, C. A.; Sardar, R.; Beasley, C. A.; Murray, R. W. *J. Am. Chem. Soc.* **2009**, *131*, 16266-16271.

Fleischer, C. C.; Payne, C. K. *Acc. Chem. Res.* **2014**, *47*, 2651-2659.

García, K. P.; Zarschler, K.; Barbaro, L.; Barreto, J. A.; O'Malley, W.; Spiccia, L.; Stephan, H.; Graham, B. *Small* **2014**, *10*, 2516–2529.

Gessner, A.; Lieske, A.; Paulke, B.; Muller, R. *J. Biomed. Mater. Res. A* **2003**, *65*, 319-326.

Gessner, A.; Lieske, A.; Paulke, B.; Muller, R. *Eur. J. Pharm. Biopharm.* **2002**, *54*, 165-170.

Gong, W.; Elitzin, V. I.; Janardhanam, S.; Wilkins, C. L.; Fritsch, I. *J. Am. Chem. Soc.* **2001**, *123*, 769-770.

Gray, T.; Mann, N. *The Elements: A Visual Exploration of Every Known Atom in the Universe*; Black Dog & Leventhal Publishers, Inc.: New York, 2012.

Griffiths, H. R.; Møller, L.; Bartosz, G.; Bast, A.; Bertoni-Freddari, C.; Collins, A.; Cooke, M.; Coolen, S.; Haenen, G.; Hoberg, A.-M. *J. Mol. Asp. Med.* **2002**, *23*, 101-208.

Han, G.; Chari, N. S.; Verma, A.; Hong, R.; Martin, C. T.; Rotello, V. M. *Bioconjug. Chem.* **2005**, *16*, 1356–1359.

Hardesty, W. M.; Caprioli, R. M. *Anal. Bioanal. Chem.* **2008**, *391*, 899-903.

Hare, D.; Austin, C.; Doble, P. *Analyst* **2012**, *137*, 1527-1537.

Hare, D. J.; Lear, J.; Bishop, D.; Beavis, A.; Doble, P. A. *Anal. Methods* **2013**, *5*, 1915-1921.

Harkness, K. M.; Fenn, L. S.; Cliffel, D. E.; McLean, J. A. *Anal. Chem.* **2010**, *82*, 3061-3066.

Harper, S.; Usenko, C.; Hutchison, J. E.; Maddux, B. L. S.; Tanguay, R. L. *J. Exp. Nanosci.* **2008**, *3*, 195-206.

Heaven, M. W.; Dass, A.; White, P. S.; Holt, K. M.; Murray, R. W. *J. Am. Chem. Soc.* **2008**, *130*, 3754-3755.

Hernandez-Viezcasa, J. A.; Castillo-Michel, H.; Servin, A.D.; Peralta-Videa, J. R.; Gardea-Torresdey, J. L. *Chem. Eng. J.* **2011**, *170*, 346-352.

Hinterwirth, H.; Kappel, S.; Waitz, T.; Prohaska, T.; Lindner, W.; Lämmerhofer, M. *ACS Nano* **2013**, *7*, 1129-1136.

Hong, R.; Emrick, T.; Rotello, V. M. *J. Am. Chem. Soc.* **2004**, *126*, 13572-13573.

Hong, R.; Fernandez, J. M.; Nakade, H.; Arvizo, R.; Emrick, T.; Rotello, V. M. *Chem. Commun.* **2006**, 2347-2349.

Hong, R.; Han, G.; Fernandez, J. M.; Kim, B. J.; Forbes, N. S.; Rotello, V. M. *J. Am. Chem. Soc.*, **2006**, *128*, 1078-1079.

Hostetler, M. J.; Templeton, A. C.; Murray, R. W. *Langmuir* **1999**, *15*, 3782-3789.

Hsieh, Y.-K.; Hsieh, H.-A.; Hsieh, H.-F.; Wang, T.-H.; Ho, C.-C.; Lin, P.-P.; Wang, C.-F. *J. Anal. At. Spectrom.* **2013**, *28*, 1396-1401.

Hoesl, S.; Neumann, B.; Techritz, S.; Sauter, G.; Simon, R.; Schluter, H.; Michael W.; Linscheid, M.W.; Theuring, F.; Jakubowskia, N.; Muellera, L. *J. Anal. At. Spectrom*. **2016**, *31*, 801-808.

Hostetler, M. J.; Wingate, J. E.; Zhong, C.-J.; Harris, J. E.; Vachet, R. W.; Clark, M. R.; Londono, J. D.; Green, S. J.; Stokes, J. J.; Wignall, G. D.; Glish, G. L.; Porter, M. D.; Evans, N. D.; Murray, R. W. *Langmuir* **1998**, *14*, 17-30.

Jackson, A. M.; Hu, Y.; Silva, P. J.; Stellacci, F. *J. Am. Chem. Soc.* **2006**, *128*, 11135-11149.

Jain, P. K.; Huang, X.; El-Sayed, I. H.; El-Sayed, M. A. *Accounts Chem. Res.* **2008**, *41*, 1578-1586.

Jensen, T. R.; Malinsky, M. D.; Haynes, C. L.; Van Duyne, R. P. *J. Phys. Chem. B* **2000**, *104*, 10549-10556.

Jiang, Y.; Huo, S.; Mizuhara, T.; Das, R.; Lee, Y.-W.; Hou, S.; Moyano, D. F.; Duncan, B.; Liang, X.-J.; Rotello V. M. *ACS Nano* **2015**, *9*, 9986–9993.

Jong, W. H. D.; Hagens, W. I.; Krystek, P.; Burger, M. C.; Sips, A. J.A.M.; Geertsma, R. E. *Biomaterials* **2008**, *29*,1912-1919.

Kamaly, N.; Pugh, J. A.; Kalber, T. L.; Bunch, J.; Miller, A. D.; McLeod, C. W.; Bell, J. D. *Mol. Imaging Biol.* **2010**, *12*, 361-366.

Kang, S.; Mauter, M. S.; Elimelech, M. *Environ. Sci. Technol.* **2009**, *43*, 2648-2653.

Khlebtsov, N.; Dykman, L. *Chem. Soc. Rev.* **2011**, *40*, 1647-1671.

Kim, C. S.; Duncan, B.; Creran, B.; Rotello, V. M. *Nano Today* **2013**, *8*, 439-447.

Kim, S. T.; Saha, K.; Kim, C.; Rotello, V, M. *Acc. Chem. Res.* **2013**, *46*, 681-691.

Koelmel, J.; Leland, T.; Wang, H.; Amarasiriwardena, D.; Xing, B. *Environ. Pollut.* **2013**, *174*, 222-228.

Konz, I.; Fernández, B.; Fernández, M. L.; Pereiro, R.; Sanz-Medel, A. *Anal. Bioanal. Chem.* **2012**, *403*, 2113-2125.

Kourtis, I. C.; Hirosue, S.; De Titta, A.; Kontos, S.; Stegmann, T.; Hubbell, J. A.; Swartz, M. A. *PLoS One* **2013**, *8*, e61646.

Köppen, C.; Reifschneider, O.; Castanheira, I.; Sperling, M.; Karst, U.; Ciarimboli, G. *Metallomics*, **2015**, *7*, 1595-1603.

Kreyling, W. G.; Abdelmonem, A. M.; Ali Z.; Alves, F.; Geiser, M.; Haberl, N.; Hartmann, R.; Hirn, S.; de Aberasturi, D. J.; Kantner, K.; Khadem-Saba, G.; Montenegro, J. M.; Rejman, J.; Rojo, T.; de Larramendi, I. R.; Ufartes, R.; Wenk, A.; Parak, W. J. *Nat. Nanotechnol.* **2015,** *10*, 619-623.

Liu, X.; Atwater, M.; Wang, J.; Huo, Q. *Colloids Surf., B* **2007**, *58*, 3-7.

Lee, D.-E.; Koo, H.; Sun, I-C.; Ryu, J. H.; Kim, K.; Kwon, I.C. *Chem. Soc. Rev.* **2012**, *41*, 2656-2672.

Lee, J. H.; Huh, Y. M.; Jun, Y.; Seo, J.; Jang, J.; Song, H. T.; Kim, S.; Cho, E. J.; Yoon, H. G.; Suh, J. S.; Cheon, J. *Nat. Med.* **2007**, *13*, 95-99.

Lesniak, A.; Fenaroli, F.; Monopoli, M. P.; Åberg, C.; Dawson, K. A.; Salvati, A. *ACS Nano* **2012**, *6*, 5845-5857.

Li, Z.-P.; Wang, Y.-C.; Liu, C.-H.; Li, Y.-K. *Anal. Chim. Acta* **2005**, *551*, 85-89.

Li, Z.; Barnes, J. C.; Bosoy, A.; Stoddart, J. F.; Zink, J. I. *Chem. Soc. Rev.* **2012**, *41*, 2590-2605.

Lia, D.; Lia, G.; Guoa, W.; Lia, P.; Wanga, E.; Wang, J. *Biomaterials* **2008**, *29*, 2776-2782.

Limbeck, A.; Galler, P.; Bonta, M.; Bauer, G.; Nischkauer, W.; Vanhaecke, F. *Anal. Bioanal. Chem.* **2015**, *407*, 6593-6617.

Linscheid, M.W.; Theuring, F.; Jakubowskia, N.; Muellera, L. *J. Anal. At. Spectrom*. **2016**, *31*, 801-808.

Liang, X.; Wang, H.; Zhu, Y.; Zhang, R.; Cogger, V. C.; Liu, X.; Xu, Z. P.; Grice, J. E.; Roberts, M. S. *ACS Nano* **2016**, *10*, 387-395.

Lin, J.; Zhang, H.; Chen, Z.; Zheng, Y. *ACS Nano* **2010**, *4*, 5421-5429.

Lin, S.; Reppert, J.; Hu, Q.; Hudson, J. S.; Reid, M. L.; Ratnikova, T. A.; Rao, A. M.; Luo, H.; Ke, P. C. *Small* **2009**, *5*, 1128-1132.

Lindfors, K.; Kalkbrenner, T.; Stoller, P.; Sandoghdar, V. *Phys. Rev. Lett.* **2004**, *93*, 037401.

Love, J. C.; Estroff, L. A.; Kriebel, J. K.; Nuzzo, R. G.; Whitesides, G. M. *Chem. Rev.* **2005**, *105*, 1103-1169.

Longmire, M.; Choyke, P.; Kobayashi, H. *Nanomedicine* **2008**, *3*, 703-717.

Lu, S. C. *Biochim. Biophys. Acta* **2013**, *1830*, 3143-3153.

Luo, Y.-H.;Chang, L. W.; Lin, P. *Biomed Res Int.* **2015**, *2015*, 143720.

Lynch, I.; Dawson, K. A. *Nanotoday* **2008**, *3*, 40-47.

Mahon, E.; Salvati, A.; Bombelli, F. B.; Lynch, I.; Dawson K. A. *J. Control. Release* **2012**, *161*, 164-174.

Mahmoudi, M.; Hosseinkhani, H.; Hosseinkhani, M.; Boutry, S.; Simchi, A.; Journeay, W. S.; Subramani, K.; Laurent, S. *Chem. Rev.* **2011**, *111*, 253-280.

Mappes, T.; Jahr, N.; Csaki, A.; Vogler, N.; Popp, J.; Fritzsche, W. *Angew. Chem. Int. Ed.* **2012**, *51*, 11208-11212.

Malmsten, M. *Curr. Opin. Colloid Interface Sci.* **2013**, *18*, 468-480.

Martinez-Chantar, M. L.; Corrales, F. J.; Martinez-Cruz, L. A.; Garcia-Trevijano, E. R.; Huang, Z.-Z.; Chen, L.; Kanel G.; Avila, M. A.; Mato, J. M.; Lu, S. C. *FASEB J.* **2002**, *16*, 1292-1294.

Marsico, A. L. M.; Creran, B.; Duncan, B.; Elci, S. G.; Jiang, Y.; Onasch, T. B.; Wormhoudt, J.; Rotello, V. M.; Vachet R. W. *J. Am. Soc. Mass Spectrom.* **2015**, *26*, 1931-1937.

Maynard, A. D.; Aitken, R. J.; Butz, T.; Colvin, V.; Donaldson, K.; Oberdorster, G.; Philbert, M. A.; Ryan, J.; Seaton, A.; Stone, V.; Tinkle, S. S.; Tran, L.; Walker, N. J.; Warheit, D. B. *Nature* **2006**, *444*, 267-269.

McLean, J. A.; Stumpo, K. A.; Russell, D. H. *J. Am. Chem. Soc.* **2005**, *127*, 5304-5305.

Minerva, L.; Boonen, K.; Menschaert, G.; Landuyt, B.; Baggerman, G.; Arckens, L. *Anal. Chem.* **2011**, *83*, 7682-7688.

Miranda, O. R.; Chen, H. -T.; You, C.-C.; Mortenson, D. E.; Yang, X. -C.; Bunz, U. H. F.; Rotello, V. M. *J. Am. Chem. Soc.* **2010**, *132*, 5285-5289.

Miranda, O. R.; Li, X. N.; Garcia-Gonzalez, L.; Zhu, Z. J.; Yan, B.; Bunz, U. H. F.; Rotello, V. M. *J. Am. Chem. Soc.* **2011**, *133*, 9650-9653.

Mebius, R. E.; Kraal, G. *Nat. Rev. Immunol.* **2005**, *5*, 606-616.

Medintz, I. L.; Uyeda, H. T.; Goldman, E. R.; Mattoussi, H. *Nat. Mater.* **2005**, *4*, 435-446.

Monopoli, M. P.; Åberg, C.; Salvati, A.; Dawson K. A. *Nat. Nanotechol.* **2012**, *7*, 779-786.

Montalti, M.; Prodi, L.; Zaccheroni, N.; Baxter, R.; Teobaldi, G.; Zerbetto, F. *Langmuir* **2003**, *19*, 5172-5174.

Moraleja, I.; Esteban-Fernández, D.; Lázaro, A.; Humanes, B.; Neumann, B.; Tejedor, A.; Luz Mena, M.; Jakubowski, N.; Gómez-Gómez, M. M. *Anal. Bioanal. Chem.* **2016**, 408, 2309-2318.

Moyano, D. F.; Goldsmith, M.; Solfiell, D. J.; Landesman-Milo, D.; Miranda, O. R.; Peer, D.; Rotello, V. M. *J. Am. Chem. Soc.* **2012**, *134*, 3965-3967.

Naito, M.; Hasegawa, G.; Ebe, Y.; Yamamoto, T. *Med. Electron Microsc.* **2004**, *37*, 16-28.

Nie, S.; Emory, S. R. *Science* **1997**, *275*, 1102-1106.

Nutting, J.; Nuttall, J. L. *Gold Bull.* **1977**, *10*, 2-8.

Ocsoy, I.; Gulbakan, B.; Shukoor, M. I.; Xiong, X.; Chen, T.; Powell, D. H.; Tan, W. *ACS Nano* **2013**, *7*, 417-427.

Pace, H. E.; Lesher, E. K.; Ranville, J. F. *Environ. Toxicol. Chem.* **2010**, *29*, 1338-1344.

Park, Y. Il.; Lee, K. T.; Suh, Y. D.; Hyeon, T. *Chem. Soc. Rev.* **2015**, *44*, 1302-1317.

Paul, S.; Paul, D.; Fern, G. R.; Ray, A. K. *J. R. Soc. Interface* **2011**, *8*, 1204-1211.

Pelaz, B.; Del Pino, P.; Maffre, P.; Hartmann, R.; Gallego, M.; Rivera-Fernández, S.; De la Fuente, J. M.; Nienhaus, G. U.; Parak, W. J. *ACS Nano* **2015,** *9*, 6996-7008.

Pelley, J. L.; Daar A. S.; Saner, M. A. *Toxicol. Sci.* **2009**, *112*, 276-296.

Petros, R.; DeSimone, J. *Nat. Rev. Drug Discovery* **2010**, *9*, 615-627.

Pilolli, R.; Palmisano, F.; Cioffi, N. *Anal. Bioanal. Chem.* **2012**, *402*, 601-623.

Polito, L.; Colombo, M.; Monti, D.; Melato, S.; Caneva, E.; Prosperi, D. *J. Am. Chem. Soc.* **2008**, *130*, 12712-12724.

Prakash, M.; Shetty, M. S.; Tilak, P.; Anwar, N. *Online J. Health Allied Scs.* **2009**, *8*, 2-9.

Priester, J. H.; Ge, Y.; Mielke, R. E.; Horst, A. M.; Cole Moritz, S.; Espinosa, K.; Gelb, J.; Walker, S. L.; Nisbet, R. M.; An, Y.-J.; Schimel, J. P.; Palmer, R. G.; Hernandez-Viezcas, J. A.; Zhao, L.; Gardea-Torresdey, J. L.; Holden, P. A. *Proc. Natl. Acad. Sci.* **2012**, *109*, 2451-2456.

Puddephatt, R. J. *The Chemistry of Gold*; Elsevier Scientific:Amsterdam, 1978.

Qian, X. M.; Nie, S. M. *Chem. Soc. Rev*. **2008**, *37*, 912-920.

Rana, S.; Bajaj, A.; Mout, R.; Rotello, V. M. *Adv. Drug Deliver. Rev.* **2012**, *64*, 200-216.

Reyzer, M. L.; Caprioli, R. M. *Int. J. Biol. Marker* **2007**, *22*, 56.

Ricketts, K.; Guazzoni, C.; Castoldi, A.; Gibson, A.P.; Royle, G.J. *Phys. Med. Biol.* **2013**, *58*, 7841-7855.

Rojas, S.; Gispert, J. D.; Martin, R.; Abad, S.; Menchon, C.; Pareto, D.; Victor, V. M.; Alvaro, M.; Garcia, H.; Herance, J. R. *ACS Nano* **2011**, *5*, 5552-5559.

Saha, K.; Agasti, S. S.; Kim, C.; Li, X.; Rotello, V. M. *Chem. Rev*. **2012**, *112*, 2739-2779.

Saha, K.; Rahimi, M.; Yazdani, M.; Kim, S. T.; Moyano, D. F.; Hou, S.; Das, R.; Mout, R.; Rezaee, F.; Mahmoudi, M.; Rotello V. M. *ACS Nano* **2016**, *10*, 4421-4430.

Saha, K.; Kim, S. T.; Yan, B.; Miranda, O. R.; Alfonso, F.; Schlosman, D.; Rotello, V. M. *Small* **2013**, *9*, 300-305.

Savage, N. *Nature* **2013**, *495*, S2-S3.

Schaaff, T. G. *Anal. Chem.* **2004**, *76*, 6187-6196.

Sendroiu, I. E.; Gifford, L. K.; Luptak, A.; Corn, R. M. *J. Am. Chem. Soc.* **2011**, *133*, 4271-4273.

Service, R. F. *Science* **2005**, *310*, 1609.

Shah, N. B.; Vercellotti, G. M.; White, J. G.; Fegan, A.; Wagner, C. R.; Bischof, J. C. *Mol. Pharmaceutics* **2012**, *9*, 2146-2155.

Simone, E. A.; Dziubla, T. D.; Muzykantov, V. R. *Expert Opin. Drug Deliv.* **2008**, *5*, 1283-1300.

Sinha, R.; Kim, G. J.; Nie, S.; Shin, D.M. *Mol. Cancer Ther.* **2006**, *5*, 1909-1917.

Soenen, S. J.; Parak, W. J.; Rejman, J.; Manshian, B. *Chem. Rev.* **2015**, *115*, 2109-2135.

Somiyaa, M.; Kurodaa, S. *Adv. Drug Deliv. Rev.*, **2015**, *95*, 77-89.

Sun, S.; Murray, C. B.; Weller, D.; Folks, L.; Moser, A. *Science* **2000**, *287*, 1989-1992.

Sun, T.; Zhang, Y. S.; Pang, B.; Hyun, D. C.; Yang, M.; Xia, Y. *Angew. Chem. Int. Ed.* **2014**, *53*, 12320-12364.

Subramani, K.; Laurent, S. *Chem. Rev.* **2011**, *111*, 253-280.

Stewart, M. H.; Susumu, K.; Mei, B. C.; Medintz, I. L.; Delehanty, J. B.; Blanco-Canosa, J. B.; Dawson, P. E.; Mattoussi, H. *J. Am. Chem. Soc.* **2010**, *132*, 9804-9813.

Swirski, F. K.; Nahrendorf, M.; Etzrodt, M.; Wildgruber, M.; Cortez-Retamozo, V.; Panizzi, P.; Figueiredo, J. L.; Kohler, R. H.; Chudnovskiy, A.; Waterman, P.; Aikawa, E.; Mempel, T. R.; Libby, P.; Weissleder, R.; Pittet, M. J. *Science* **2009**, *325*, 612-616.

Tai, L.-A.; Kang, Y.-T.; Chen, Y.-C.; Wang, Y.-C.; Wang, Y.-J.; Wu, Y.-T.; Liu, K.-L.; Wang, C.-Y.; Ko, Y.-F.; Chen, C.-Y.; Huang, N.-C.; Chen, J.-K.; Hsieh, Y.-F.; Yew, T.-R.; Yang, C.-S. *Anal. Chem.* **2012**, *84*, 6312-6316.

Templeton, A. C.; Wuelfing, M. P.; Murray, R. W. *Acc. Chem. Res.* **2000**, *33*, 27-36.

Tilling, R. I.; Gottfried, D.; Rowe, J. J. *Econ. Geol. Bull. Soc. Econ. Geol.* **1973**, *68*, 168-186.

Townson, J. L.; Lin, Y.-S.; Agola, J. O.; Carnes, E. C.; Leong, H. S.; Lewis, J. D.; Haynes, C. L.; Brinker, C. J. *J. Am. Chem. Soc.* **2013**, *135*, 16030-16033.

Tracy, J. B.; Crowe, M. C.; Parker, J. F.; Hampe, O.; Fields-Zinna, C. A.; Dass, A.; Murray, R. W. *J. Am. Chem. Soc.* **2007**, *129*, 16209-16215.

Tracy, J. B.; Kalyuzhny, G.; Crowe, M. C.; Balasubramanian, R.; Choi, J. P.; Murray, R. W. *J. Am. Chem. Soc.* **2007**, *129*, 6706-6707.

Trisha, E.; James, F. L. *Int. J. Nanomed.* **2012**, *7*, 5625-5639.

Ulf Leonhardt *Nature Photonics* **2007**, *1*, 207-208.

Veiseh, O.; Gunn, J. W.; Zhang, M. Q. *Adv. Drug Deliv. Rev.* **2010**, *62*, 284-304.

Verma, A.; Stellacci, F. *Small* **2010**, *6*, 12-21.

Verma, A.; Uzun, O.; Hu, Y.; Hu, Y.; Han, H.-S.; Watson, N.; Chen, S.; Irvine, D. J.; Stellacci, F. *Nat. Mater.* **2008**, *7*, 588-595.

Walkey, C. D.; Olsen, J. B.; Guo, H.; Emili, A.; Chan, W. C. *J. Am. Chem. Soc.* **2012**, *134*, 2139-2147.

Walkey, C. D.; Chan, W. C. *Chem. Soc. Rev.* **2012**, *41*, 2780.

Wang, L.; Li, Y.-F.; Zhou, L.; Liu, Y.; Meng, L.; Zhang, K.; Wu, X.; Zhang, L.; Li, B.; Chen, C. *Anal. Bioanal. Chem.* **2010**, *396*, 1105-1114.

Wang, M.; Zheng, L.-N.; Wang, B.; Chen, H.-Q.; Zhao, Y.-L.; Chai, Z.-F.; Reid, H. J.; Sharp, B. L.; Feng, W.-Y. *Anal. Chem.* **2014**, *86*, 10252-10256.

Wang, T.; Hsieh, H.; Hsieh, Y.; Chiang, C.; Sun, Y.; Wang, C. *Anal. Bioanal. Chem.* **2012**, *404*, 3025-3036.

Whetten, R. L.; Khoury, J. T.; Alvarez, M. M.; Murthy, S.; Vezmar, I.; Wang, Z. L.; Stephens, P. W.; Cleveland, C. L.; Luedtke, W. D.; Landman, U. *Adv. Mater.* **1996**, *8*, 428-433.

Whitesides, G. M.; Laibinis, P. E. *Langmuir* **1990**, *6*, 87-96.

Wiesner, M. R.; Lowry, G. V.; Alvarez, P.; Dionysiou, D.; Biswas, P. *Environ. Sci. Technol.* **2006**, *40*, 4336-4345.

Wu, Z. W.; Gayathri, C.; Gil, R. R.; Jin, R. C. *J. Am. Chem. Soc.* **2009**, *131*, 6535-6542.

Wu, L.; Zhang, J.; Watanabe, W. *Adv. Drug Deliver. Rev.* **2011**, *63*, 456-469.

Xiang Li, X.; Anton, N.; Zuber, G.; Vandamme, T. *Adv. Drug Delivery Rev*. **2014**, *76*, 116-133.

Xiao, K.; Li, Y.; Luo, J.; Lee, J. S.; Xiao, W.; Gonik, A. M.; Agarwal, R. G.; Lam, K. S. *Biomaterials* **2011**, *32*, 3435-3446.

Yan, B.; Kim, S. T.; Kim, C. S.; Saha, K.; Moyano, D. F.; Xing, Y.; Jiang, Y.; Roberts, A. L.; Alfonso, F. S.; Rotello, V. M.; Vachet, R. W. *J. Am. Chem. Soc.* **2013**, *135*, 12564-12567.

Yan, B.; Zhu, Z. J.; Miranda, O. R.; Chompoosor, A.; Rotello, V. M.; Vachet, R. W. *Anal. Bioanal. Chem.* **2010,** *396*, 1025-1035.

Yang, X.; Yang, M.; Pang, B.; Vara, M.; Xia, Y. *Chem. Rev.* **2015**, *115*, 10410-10488.

Yang, X.-C.; Samanta, B.; Agasti, S. S.; Jeong, Y.; Zhu, Z.; Rana, S.; Miranda, O. R.; Rotello, V. M. *Angew. Chem. Int. Ed.* **2011**, *50*, 477-481.

Yeh, Y.-C.; Creran, B.; Rotello, V. M. *Nanoscale* **2012**, *4*, 1871-1880.

Yesilbag Tonga, G.; Moyano, D. F.; Kim, C. S.; Rotello, V. M. *Curr. Opin. Colloid Interface Sci.* **2014**, *19*, 49-55.

Yook, S.; Lu, Y.; Jeong, J. J.; Cai, Z.; Tong, L.; Alwarda, R.; Pignol, J.-P, Winnik, M. A.; Reilly, R. M. *Biomacromolecules* **2016**, *17*, 1292-1302.

You, C. C.; De, M.; Rotello, V. M. *Curr. Opin. Chem. Biol.* **2005**, *9*, 639-646.

You, C. C.; Miranda, O. R.; Gider, B.; Ghosh, P. S.; Kim, I. B.; Erdogan, B.; Krovi, S. A.; Bunz, U. H. F.; Rotello, V. M. *Nat. Nanotechnol.* **2007**, *2*, 318-323.

Zhu, Z.-J.; Carboni, R.; Quercio, M. J.; Yan, B.; Miranda, O. R.; Anderton, D. L.; Arcaro, K.F.; Rotello, V. M.; Vachet, R. W. *Small* **2010**, *6*, 2261-2265.

Zhu, Z. -J.; Tang, R.; Yeh, Y.-C.; Miranda, O. R.; Rotello, V. M.; Vachet, R. W. *Anal. Chem.* **2012**, *8*, 4321-4326.

Zhu, Z.-J.; Wang, H.; Yan, B.; Zheng, H.; Jiang, Y.; Miranda, O.R.; Rotello, V. M.; Xing, B.; Vachet, R. W. *Environ. Sci. Technol.* **2012**, *46*, 12391-12398.

Zhu, Z.-J.; Posati, T.; Moyano, D. F.; Tang, R.; Yan, B.; Vachet, R. W.; Rotello, V. M. *Small*, **2012**, *8*, 2659-2663.

Zhu, Z.-J.; Ghosh, P. S.; Miranda, O. R.; Vachet, R. W.; Rotello, V. M. *J. Am. Chem. Soc.* **2008**, *130*, 14139−14143.

Zhu, Z.-J.; Yeh, Y.-C.; Tang, R.; Yan, B.; Tamayo, J.; Vachet, R. W.; Rotello, V. M. *Nat. Chem.* **2011**, *3*, 963-968.

Zimmerman, T. A.; Rubakhin, S. S.; Romanova, E. V.; Tucker, K. R.; Sweedler, J. V. *Anal. Chem.* **2009**, *81*, 9402-9409.

Zolnik, B. S.; Sadrieh, N. *Adv. Drug Deliver. Rev.* **2009**, *61*, 422-427.